Functional Organization of Entorhinal Cortex Layer V Neurons: electrophysiological and morphological characterization

Bassam Hamam

Department of Neurology and Neurosurgery
McGill University, Montreal

A thesis submitted to the Faculty of Graduate Studies and Research in partial fulfillment of the requirements of the degree of
Doctorate of Philosophy.

April 2002

National Library
of Canada

Acquisitions and
Bibliographic Services

395 Wellington Street
Ottawa ON K1A 0N4
Canada

Bibliothèque nationale
du Canada

Acquisisitons et
services bibliographiques

395, rue Wellington
Ottawa ON K1A 0N4
Canada

Your file Votre référence
ISBN: 0-612-85711-5
Our file Notre référence
ISBN: 0-612-85711-5

Abstract

The entorhinal cortex occupies an important anatomical position in the temporal lobe as the interface between the hippocampus and the neocortex. Its superficial cell layers funnel the cortical input into the hippocampus while the deep layer V is the major target of hippocampal output, which it then directs back to the cortex. This connectivity alone makes the entorhinal cortex a crucial element in what is known as the neocortical-hippocampal-neocortical circuit, a system involved in the long-term storage of "declarative" memories. However, the detailed analysis of the morphological and electrophysiological characteristics of cells in entorhinal cortex layer V had not been carried out; information that is necessary to understand how this cortical layer may participate in the processing of cortically directed hippocampal information. The main goal of the present study was thus to carry out by means of intracellular recording and labelling in a "in vitro" rat entorhinal cortex slice preparation an extensive characterization of the intrinsic electrophysiological characteristics of entorhinal cortex layer V principal neurons in correlation with their morphological attributes. Our main working hypothesis was that electrophysiologically, similar to the neocortex, layer V principal neurons in both the medial and lateral subdivisions of the entorhinal cortex would constitute a heterogeneous population comprised of regularly spiking cells and intrinsically bursting neurons.

We found layer V of the entorhinal cortex to be comprised of three main cellular subtypes, pyramidal, horizontal and polymorphic neurons, that were electrophysiologically non distinguishable. Cells in both medial and lateral entorhinal areas had similar morphological and electrophysiological properties. No intrinsically

bursting neurons were encountered; instead, cells were classified as regular spiking neurons with varying spike-frequency adaptation. We also found that most layer V neurons displayed persistent Na^+ current (I_{Nap}) dependent subthreshold membrane potential oscillations; a mechanism that might endow layer V cells with a functional contribution to network rhythmicity.

Résumé

Le cortex entorhinal occupe une position anatomique importante dans le lobe temporal où il agit comme interface entre d' l'hippocampe et le néocortex. Les cellules de la couche superficielle dirigent l'entrée d'information provenant du cortex vers l'hippocampe tandis que la couche profonde V est la cible principale de la sortie d'information de l'hippocampe qu'elle dirige de nouveau au cortex. Cette connectivité fait du cortex entorhinal un élément essentiel dans ce qui est connu comme le circuit néocortical-hippocampal-néocortical, un système impliqué dans l'entreposage à long terme des mémoires déclaratives. Cependant, l'analyse détaillée des caractéristiques morphologiques et électrophysiologiques des cellules de la couche V du cortex entorhinal n'avait pas été effectuée; une information nécessaire pour comprendre comment cette couche corticale peut participer au traitement de l'information hippocampale dirigée vers le cortex. Le but principal de la présente étude est ainsi d'effectuer, au moyen d'enregistrement de marquage intracellulaire dans une préparation de tranche de cortex entorhinal de rat "in vitro", une caractérisation étendue des caractéristiques électrophysiologiques intrinsèques des neurones principaux de la couche V du cortex entorhinal en corrélation avec leurs attributs morphologiques. Notre hypothèse principale était qu'au niveau de leur électrophysiologie, comme le néocortex, les neurones principaux de la couche V des les subdivisions médiales et latérales du cortex entorhinal constitueraient une population hétérogène formée de cellules à décharge régulière et de neurones à décharge en boufeé.

Nous avons trouvé que la couche V du cortex entorhinal est composée de trois sous-types de cellules principales, pyramidaux, horizontaux et polymorphes, qui étaient

non distingables par rapport à leur électrophysiologie. Les cellules dans les secteurs entorhinaux médiaux et latéraux ont eu des propriétés semblables. En outre, aucun neurone avec décharge en boufeé n'a été détecté; par contre, des cellules ont été classifiées avec décharge régulière avec une adaptation de fréquence de décharge variable. Cependant, nous avons constaté que la plupart des neurones de la couche V ont montré des oscillations du potentiel de membrane subliminal dépendant du courant persistant de Na^+ (I_{Nap}), un mécanisme qui pourrait permette aux cellules de la couche V de contribuen fonctionnellement à la rythmicité du réseau.

Statement of Originality and Contributions of Authors

The results described in this thesis are presented in four studies and correspond to a novel understanding of the properties of layer V neurons of the entorhinal cortex, the target of much of the hippocampal output. These studies are presented in manuscript format and have been either published or submitted for publication. In addition, some of the results included here have been presented as posters at the 1997, 1998 and 2000 Society for Neuroscience meetings.

The first study, which is presented in chapter two, describes a novel histochemical technique to process biocytin injected neurons in the thick slices (400 μm), that are typically employed in *in vitro* electrophysiological recordings, without further re-sectioning. I performed all the experimentations that led to the full function of this technique under the supervision of Dr. Angel Alonso in collaboration with Dr. Timothy E. Kennedy. The manuscript was written by myself and co-edited by Dr. Timothy E. Kennedy before being submitted for publication.

The second and third studies presented here provided an original and comprehensive study of the electrophysiological in conjunction with the morphological properties of layer V neurons of the medial and lateral entorhinal cortex, respectively. I carried out all the experiments and subsequent analysis under the supervision of Dr. Angel Alonso in collaboration with Dr. David G. Amaral. The manuscript was written by myself and co-edited by Dr. Alonso and Dr. Amaral before being submitted for publication.

The fourth and final study presented in this thesis dealt with characterizing the current underlying the subthreshold membrane potential oscillations and the low

threshold firing mechanism in entorhinal layer V neurons. I performed the current-clamp analysis on the sodium dependency of the mentioned phenomena and the subsequent analysis under the supervision of Dr. Alonso. The voltage clamp recordings and the noise analysis were carried out by Newton Agrawal under the supervision of Dr. Angel Alonso and Dr. David S. Ragsdale. My contribution to the writing of the manuscript was restricted to the sections regarding the current-clamp studies.

This is a manuscript-based thesis and the results chapters represent either submitted for publication or already published manuscripts, as follows:

Chapter 2: Submitted for publication to Journal of Neuroscience Methods, 2002, Hamam BN and Kennedy TE: "Visualization of the Dendritic Arbor of Single Neurons in Intact Brain Slices".

Chapter 3: Reprinted from Journal of Comparative Neurology, 2000, Hamam BN, Kennedy TE, Alonso A, Amaral DG: "Morphological and electrophysiological characteristics of layer V neurons of the rat medial entorhinal cortex", 418:457-472, Copyright (2000), with permission from Wiley-Liss.

Chapter 4: Submitted for publication to Journal of Comparative Neurology, 2002, Hamam BN, Amaral DG and Alonso A: "Morphological and electrophysiological characteristics of layer V neurons of the rat lateral entorhinal cortex".

Chapter 5: Reprinted from Neuroscience, 2001, Agrawal N, Hamam BN, Magistretti J, Alonso A, Ragsdale DS: "Persistent sodium channel activity mediates subthreshold membrane potential oscillations and low-threshold spikes in

rat entorhinal cortex layer V neurons", 102:53-64, Copyright (2001), with permission from Elsevier Science.

Acknowledgements

Firstly, it is appropriate to thank my thesis supervisor Dr. Angel Alonso for all the help and support he has given me throughout my stay at his laboratory. In addition, thanks go to those who went through Dr. Alonso's Lab while I was there: Drs. Clayton Dickson, Jacopo Magestretti, Ruby Klink and Li Ma, and the soon to be Dr. Mark Shalinsky, as well as Armando Rene Mena and Adriana Galue. I also want to thank the members of my advisory committee Dr. David S. Ragsdale and Dr. Timothy E. Kennedy for their help and support. In addition, I would like to thank Dr. David G. Amaral for all the help he gave me during my visits to his Lab.

Also, special thanks go to Dr. Heather Durham for her kindness and understanding. I would also like to thank Naomi Takeda and Monique Ledermann for all the help they provided.

Last but not least, I would like to thank my family for all the encouragement and support they gave me; and for their patience while I compled this work.

Table of Contents

List of Figures and Tables

List of Abbreviations

Ab, angular bundle
AD, Alzheimer's disease
AHP, afterhyperpolarization
DAB, diaminobenzidine
d.c., direct current
DG, dentate gyrus
EC, entorhinal cortex
FB, Fast Blue
HC, horizontal cells
HRP, horseradish peroxidase
I/V, current intensity/voltage plots
IB, intrinsically bursting
I_h, hyperpolarization-induced depolarizing current
I_{Na}, transient sodium current
I_{NAP}, voltage-sensitive persistent sodium current
IR, inward rectification
LEA, lateral entorhinal area
LY, lucifer yellow
NT, Neurofibrillary tangles
MEA, medial entorhinal area
MTL, medial temporal lobe
NaPB, sodium-phosphate buffer
PC, polymorphic cells
PFA, paraformaldehyde
PHT, heat inactivated normal goat serum
PP, perforant path
PY, pyramidal cells
Rin, input resistance
RMP, resting membrane potential
RS, regular spiking
SAG%, sag percentage
Sub, subiculum
TBS, tris buffered saline
TLE, Temporal lobe epilepsy
Vr, Resting membrane potential

Chapter One

1. Introduction

1.1 General Background

The entorhinal cortex, as part of the parahippocampal region, is intimately related to the hippocampal formation, all together representing an integral part of the limbic system (reviewed in Lopes da Silva et al., 1990). Although its constituents are not perfectly defined, the term "limbic system" refers to a functional entity that originally was linked to olfactory functions and later to emotional behavior. More recently, components of the limbic system, especially the hippocampal formation and the parahippocampal region, are thought to make a major contribution towards learning and memory. Evidence for this stems from the original observations of Scoville and Milner (1957) on the patient HM and a multitude of subsequent neuropsychological and lesioning studies in humans

and animal models (reviewed in Squire and Zola, 1996). The fact that loss of function in this system leads to anterograde amnesia has lead to the definition of the "medial temporal lobe memory system" (MTL; Zola-Morgan et al., 1994; Witter et al., 2000). The evidence that the entorhinal cortex is an essential part of the MTL system has grown stronger over the years, and this evidence includes the finding that in Alzheimer's dementia (AD) pathological alterations are always seen in this structure (Braak and Braak, 1991; Van Hoesen et al., 1991).

Synchronized neuronal activity and synaptic plasticity are general properties of the nervous system which are particularly prominent in limbic structures and, especially, in the MTL (Lopes da Silva et al., 1990). EEG studies in limbic structures have shown that the limbic system generates a variety of population rhythms the most prominent of which is the so called "theta" rhythm that appears to dominate the activity of the hippocampus and the entorhinal cortex (Lopes da Silva et al., 1990; Bland and Colom, 1993; Vinogradova, 1995). Though oscillatory activities in general, and the "theta" rhythm in particular, have been regarded of importance in learning and memory processes (Greenstein et al., 1988; Staubli and Xu, 1995, Oddie and Bland, 1998) in pathological conditions oscillatory processes may contribute to hypersynchronicity and lead to an epileptic state. As mentioned above, synaptic plasticity is also a prominent feature of limbic circuits (Bliss and Lomo, 1973; Andersen et al., 1980; Commins et al., 1998; Alonso et al., 1990; Malenka, 1991; Moser et al., 1994). This plasticity, while certainly relevant to learning and memory (Bliss and Collingridge, 1993; Laroche et al., 2000), also predisposes the system to hyperexcitability (Schwartzkroin, 2001). The more plastic the system is, the more potentially excitable it may become. This fact, combined with

synchronous population activity may play an important role in the generation and propagation of the most common form of epilepsy (Kalynchuk, 2000), temporal lobe epilepsy.

The entorhinal cortex (EC) is closely interrelated with many fields of the hippocampal formation and it is equally reciprocally connected with the rest of the cortical mantle (reviewed in Amaral and Witter, 1995). The superficial cell layers of the EC are the targets of converging inputs from unimodal and polymodal sensory cortices (Van Hoesen and Pandya, 1975; Amaral et al., 1983; Insausti et al., 1987; Burwell and Amaral, 1998b; Burwell and Amaral, 1998a), which are funnelled to the hippocampus via the perforant path (Steward and Scoville, 1976). In turn, the hippocampus projects back to the deep layers of the entorhinal cortex (Beckstead, 1978; Kohler, 1985; Witter et al., 1989), which send feed-back projections to the cortex that reciprocate the input channels. As a relay station in the neocortical-hippocampal-neocortical circuitry, the EC was initially thought to play a rather passive role (that of an "interface") in the functions of the MTL (Lopes da Silva et al., 1990). However, new pieces of evidence suggest that the entorhinal cortex also plays an active and independent role to that of the hippocampus in memory processing (Mishkin et al., 1997; Milner et al., 1997). This evidence has emerged from experimental studies of memory tasks in behaving animals (Levisohn and Isacson, 1991; Leonard et al., 1995), as well as from the detailed "in vitro" analysis of the cellular and synaptic properties of entorhinal neurons and circuits. For example, the electrophysiological and morphological analysis of neurons in layer II of the entorhinal cortex, which have been classically viewed as simple relays of cortical input to the hippocampus, has demonstrated that these neurons display a very rich intrinsic

electroresponsiveness. One of their most dominant active properties is their ability to generate subthreshold membrane potential oscillations in the "theta" range of frequencies (Alonso and Klink, 1993). This oscillatory activity appears to present the required element to implement a very effective synchronizing device that, as suggested (Alonso and Klink, 1993), may facilitate the binding of sensory information relevant to a memory event. Moreover, it has also been shown that the intrinsic activation of entorhinal layer II neurons at their intrinsic oscillatory range can lead to a non-hebbian type of synaptic plasticity (Alonso et al., 1990). Finally, the morphological analysis of layer II cells has also revealed that these neurons give rise to an extensive net of recurrent collaterals that expands throughout layer II thus providing the circuit basis for an associational network (Lingenhöhl and Finch, 1991; Klink and Alonso, 1997). Hence, the mechanisms by which the entorhinal cortex may participate in memory processes and in pathologies such as epilepsy, may be better understood by characterizing the functional organization of its neurons and circuits.

On the basis of primarily anatomical and also electrophysiological studies, layer V of the entorhinal cortex is considered the output layer of the structure. It receives the bulk of the hippocampal feed-back (Swanson and Cowan, 1977; Sorensen and Shipley, 1979; Finch et al., 1986; Van Groen and Lopes da Silva, 1986; Naber et al., 2001) and projects extensively to the cortical mantle (Swanson and Kohler, 1986; Insausti et al., 1997; Lavenex and Amaral, 2000). Similarly to the neocortex (Connors, 1984; Chagnac-Amitai and Connors, 1989; Silva et al., 1991; Telfeian and Connors, 1998), layer V of the entorhinal cortex is highly epileptogenic (Jones and Heinemann, 1988; Bragin et al., 1997; Dickson and Alonso, 1997; Dhillon and Jones, 2000). In order to gain information

on the mechanisms by which layer V neurons may affect the transfer and/or processing of hippocampal encoded information and, also, to clarify the potential cellular basis of the well-established EC layer V hyperexcitable tendency, we undertook an extensive electrophysiological and morphological characterization of the neurons in this cortical layer. Our initial working hypothesis, substantiated by preliminary evidence gathered by other laboratories (Jones and Heinemann, 1988), was that entorhinal layer V would consist of primarily pyramidal neurons with electrophysiological profiles similar to those of neocortical layer V cells and consisting of regular spiking and rhythmic bursting neurons. Our final observations demonstrated that layer V neurons are, in fact, quite distinct from their neocortical counterparts, very diverse and with unique properties that suggest that they may play a more active role in MTL functions than previously recognized. Moreover, the data presented here suggest that the extreme epileptiform tendency of this cortical layer does not depend on intrinsic bursting properties of some layer V cells. Our findings will be discussed in the context of how the cellular properties of entorhinal layer V neurons may contribute to memory function and to the generation of oscillatory activity and hypersynchronicity.

1.2 Anatomy

The entorhinal cortex, along with the hippocampus, belongs to what is known as the limbic cortex. Broca first used the term "limbic lobe" in 1878 to refer to the cortical areas surrounding the brainstem and which included: the subcallosal, cingulate and parahippocampal gyri and the hippocampal (CA areas) and dentate areas. The term "limbic system" later replaced this designation to include an ensemble of areas

functionally involved in emotional behaviour (MacLean, 1952) and that included, in addition to the above mentioned cortical regions, the anterior nuclei of the thalamus, the hypothalamus, the septal nuclei, the amygdala, the preoptic area and nucleus acumbens of the basal ganglia.

The entorhinal cortex can be regarded as part of the parahippocampal region (Witter et al., 1989; Burwell, 2000), however, here we follow the Amaral and Witter (1995) classification in which the hippocampus and the adjacent areas were all combined into one general entity as the "hippocampal formation". The main reason for this classification is the very close anatomical interrelations between the hippocampus and the entorhinal cortex (described below). The entorhinal cortex is bordered medially by the parasubiculum and laterally by the perirhinal cortex. Rostrally, it ends at the amygdaloid complex and the piriform cortex. The caudal limit of the entorhinal cortex is the rhinal fissure (Insausti et al., 1997).

The entorhinal cortex was first annotated as Brodmann's area 28. Broadman (1909) made a distinction between a medial entorhinal area, which he called area 28a, and a lateral entorhinal area, which he called area 28b, reflecting two cytoarchitectonically distinct areas within the mediolateral axis of the entorhinal cortex. Subsequently, a rather large number of studies appeared that subdivided the EC into subregions on the basis of fibre architectonic and cytoarchitectonic analysis (reviewed in Haug, 1976). The bulk of these studies, although might have used different terminologies, described an entorhinal cortex that is divided into a medial and lateral area (Blackstad, 1956; Haug, 1976). In the present study, we used the term medial entorhinal area (MEA) and lateral entorhinal area

(LEA) to reflect the medial and the lateral divisions of the entorhinal area, respectively, following Amaral and Witter (1995) and as described below.

1.2.1 Cytoarchitecture

The entorhinal cortex is a transitional cortex between the isocortex (neocortex) and the three layered allocortex; hence it is regarded as periallocortex (reviewed in Lopes da Silva et al., 1990). Ramon y Cajal (1911) documented seven entorhinal layers: two plexiform layers (layers I and IV), two superficial cellular layers (layers II and III) and three deep cellular layers (layers V-VII). Lorente de Nó (1933) extended Cajal's study on the entorhinal cortex and made some modifications to his nomenclature. The two authors agree about the first and the second layers. Lorente de Nó, however, assigned layer IIIa to represent the superficial layer of pyramidal cells and layer IIIb to represent the cell free layer of Cajal's inner plexiform layer IV. Lorente de Nó's layer IV, V and VI would then represent Cajal's Layer V, VI and VII, respectively (Lorente de Nó, 1933). Throughout this study, we have followed Cajal's classification with the modifications introduced by Amaral and Witter (1995) where layer V was considered to include both layer V and layer VI of the Cajal classification, and Cajal's layer VII become layer VI. Below is a brief description of the entorhinal layers according to this nomenclature:

Layer I: The outer plexiform layer; a cell-free, fiber-rich layer composed mainly of afferent fibres and ascending axons from the deep layers.

Layer II: The layer of the stellate ("star") cells; is mostly comprised of star-shaped cells with thick dendritic plexus reaching layer I.

Layer III: The layer of superficial pyramids; a multi-striated broad layer containing mostly medium-sized pyramidal cells.

Layer IV: The inner plexiform layer (*lamina dissecans*); an extensively fiber-rich layer almost completely devoid of cell bodies.

Layer V: The layer of deep large pyramidal cells; considered to be mostly composed of densely packed pyramidal neurons of variable soma sizes.

Layer VI: Polymorphic layer; contains few sparsely dispersed neurons, mostly big polygonal, spindle or triangular cells.

1.2.2. Anatomical subdivisions

The subdivision of the entorhinal cortex into MEA and LEA mentioned above is mostly based on cytoarchitectural criteria. The comprehensive studies by Blackstad in 1956 and Haug in 1976 provided great detail relating to the basis of this subdivision, which is mostly based on the characteristics of layer II and the *lamina dissecans*. According to these authors, the medial extreme of the MEA is defined by the widening of layer II at the border with the parasubiculum at the expense of layers III and I. Layer II throughout the MEA is also uniformly dense, reflecting the uniform distribution of its neurons and the plexus in which they are embedded. The lateral border of the MEA is then marked by the transition from a densely cell packed layer II to a much less dense structure. In addition, the *lamina dissecans* becomes less demarcated as it progresses into the LEA. In the LEA, layer II actually brakes up into two sublayers; an outer sublayer in which smaller cells are grouped into islands separated by a cell-free zone from an inner sublayer. The rhinal fissure indicates the lateral border of the lateral entorhinal area, which is clearly delimited by a *lamina dissecans* that bends superficially.

1.2.3 Cellular morphology

Until the late 20th century, morphological analysis of neuronal areas was done using techniques that targeted the whole cell population rather than individual neurons. A popular technique was the Golgi method (Luis de la Iglesia and Lopez-Garcia, 1997; Golgi et al., 2001), which was very useful in setting up the basis for the classification and cytoarchitectural distribution of neuronal population in the cortex. However, this technique is limited by the fact that it is quite random and cannot be used to label a specific neuronal subtype of interest. With the development of modern intracellular labelling techniques such as the intracellular injection of horseradish peroxidase (HRP) (Light and Durkovic, 1976) or the most commonly used biocytin (Horikawa and Armstrong, 1988), numerous studies have been undertaken to describe detailed morphological differentiation of neurons within specific areas of the central nervous system. These new techniques carried an added advantage over Golgi methods, which is the ability to perform intracellular electrophysiological recording while delivering the labelling substrate inside the target neuron. This moved the study of cellular morphology to an obviously higher level at which morphological subtypes could be further differentiated based on physiological roles.

The original descriptions of morphological cell types within the entorhinal cortex made by Cajal (1902) and Lorente de Nó (1933) using the Golgi labelling method have been, for the most part, confirmed by subsequent investigation using modern labelling techniques such as retrograde injection (Fast Blue (FB): Germroth et al., 1989; HRP: Schwartz and Coleman, 1981), *in vivo* intracellular labelling (HRP: Lingenhöhl and Finch, 1991; Neurobiotin: Tamamaki and Nojyo, 1993) and *in vitro* intracellular labelling

(Lucifer Yellow (LY): Germroth et al., 1989; Biocytin: Empson and Heinemann, 1995; Gloveli et al., 1997; Klink and Alonso, 1997; Schmitz et al., 1998). Because of the advanced capability of the new labelling and processing techniques, new information has emerged about the fine structure and the details of the soma-dendritic and, particularly, axonal characteristics of these neurons. Following, a summary of the basic morphological profiles of principal (projection) neurons within the different layers of the entorhinal cortex in the rodent that were known prior to our investigation is presented.

Layer II: Briefly, the most abundant cell type in the MEA are the stellate cells which are characterized by a trapezoidal or elongated soma with a number of primary dendrites that branch extensively in layer II and I (Lingenhöhl and Finch, 1991; Klink and Alonso, 1997). The second abundant cell group in this area are the pyramidal-like cells that have a pyramidal shaped soma and a prominent apical dendrite that branches superficially. The basal dendrites typically branch extensively within layers II and III. Layer II of the LEA is populated primarily by horizontal (bi- and tri-polar) cells with stellate cells present in lower proportion (Schwartz and Coleman, 1981; Germroth et al., 1989).

Layer III: classical pyramidal cells are the most abundant cell type in layer III. Most of these cells have a relatively large pyramidal-shaped soma with only few smaller size cells (Lingenhöhl and Finch, 1991; Gloveli et al., 1997). The apical dendrites of the layer III pyramidal cells typically break into two main branches within layer III (Dickson et al., 1997) and bifurcate in layers II and I. All dendrites, apical and basal, are covered with spines (Lingenhöhl and Finch, 1991); however, there are reports of a subset of projection cells in this layer that reportedly have no spines (Gloveli et al., 1997).

Layer V: The most extensive description of layer V morphology as a result of intracellular labelling was the study by Lingenhöhl and Finch (1991) in which they injected HRP into cells in vivo. Although they only looked at layer V cells in the medial entorhinal cortex, the majority of layer V cells they describe belong to the classical pyramidal-type morphology. The layer V pyramids described in that study have a relatively large soma and their basal dendritic tree bifurcates within the deep layers of the entorhinal cortex mainly layer V and then layer VI.

Layer VI: There is scarce information about individually labelled neurons in this layer. For example, in the in vivo study by Lingenhöhl and Finch (1991), only one cell was recovered from this layer and it resembles the spindle type cells described in layer V, with dendrites crossing into the angular bundle and the superficial layers (Lingenhöhl and Finch, 1991).

1.2.4 Entorhinal connectivity

The anatomical connections of the entorhinal cortex have been extensively studied both in primates and non-primates using an array of anatomical methods that included anterograde labelling of nerve terminals, retrograde labelling of cell bodies, degeneration studies and autoradiography (Segal, 1977; Swanson et al., 1978; Kohler, 1986; Kohler, 1988; Naber and Witter, 1998). The connections of the EC can be classified as intra-entorhinal, hippocampal, cortical and subcortical, and they are reviewed below.

1.2.4.1 Intra-Entorhinal Connections

According to Köhler, all layers of the entorhinal cortex in the rat have extensive associational connections that are marked by a more prominent longitudinal than transversal distribution (Kohler, 1986). This author also indicated that the deep layer associational projections that terminate in the superficial layers were more extensive than those of the superficial cell layers, although this point was contended by Dolorfo and Amaral (1998) who recently claimed that superficial cell layers have similarly robust associational connections to those of the deep layers. The inter-laminar organisation of associational fibers is structured so that cells in the deep layers project mainly to all layers superficial to them (Kohler, 1986; Dolorfo and Amaral, 1998). Hence, layers V and VI project to layer III and II, and layer III projects to layer II. Although numerous fibers running from the superficial layers towards the deep layers are found, these fibers are primarily destined for areas outside the ipsilateral entorhinal cortex (Kohler, 1986).

As far as the difference between the MEA and the LEA, Kohler (1986 and 1988) indicated that only associational connection originating from the MEA could reach the LEA; whereas, associational connection originating in the LEA were restricted to this structure. However, Dolorfo and Amaral (1998) described associational fibers originating from specific segments of the LEA, ventromedial portion, which crossed through the MEA border. All the entorhinal areas have commissural connections, the target of which is more restricted to the superficial layers of the contralateral side (Kohler, 1986; Kohler, 1988).

1.2.4.2 Connections with the hippocampus

The entorhinal cortex projects to all the different subfields of the hippocampus, a term that we use to include the dentate gyrus (DG), areas CA1 and CA3 of the hippocampus proper and subiculum (figure 1). The entorhinal-hippocampal projection system, named as the perforant path (PP) by Ramon y Cajal (1902), originates almost exclusively from cells in the superficial cell layers (II and III), each of which having different hippocampal targets (Steward and Scoville, 1976). The most prominent component of the PP originates from cells in layer II and terminates on the molecular layer of the dentate gyrus, the fibers making monosynaptic contact with the dentate granule cells (Steward and Scoville, 1976; Schwartz and Coleman, 1981). This projection is topographically organized so that PP fibers originating in the MEA terminate in the middle 1/3 of the DG molecular layer while PP fibers originating from the LEA terminate in the outer 1/3 of the DG molecular layer (Hjorth-Simonsen, 1972; Steward, 1976; Witter, 1993). Layer II of the EC also gives rise to PP fibers that terminate on the distal apical dendrites of the CA3 pyramidal cells (Steward and Scoville, 1976). Neurons in layer III of the EC give rise to the PP projection that terminates on the distal apical dendritic fields of the CA1 and subicular pyramidal cells (Steward and Scoville, 1976; Amaral and Witter, 1995). The EC-CA1 component of the PP is also topographically organized with MEA fibers terminating in the CA1 subfield proximal to CA3 and LEA fibers terminating in the CA1 subfield proximal to subiculum (Steward, 1976; Naber et al., 2001). The EC-subicular component of the PP is similarly topographically organized to the EC-CA1 component (Steward, 1976; Naber et al., 2001). Within the hippocampus the main flow of information is in the direction of the so-called hippocampal trisynaptic

circuit. DG granule cells give rise to the mossy fibers that terminate on the CA3 pyramidal cells. Then, the CA3 pyramidal cells give rise to the Schaffer collaterals that terminate on the CA1 pyramidal cells. In turn the CA1 pyramidal cells project onto subiculum, which finally projects massively back to the deep layers of the EC (Swanson and Cowan, 1977, Beckstead, 1978; Swanson et al., 1978; Claiborne et al., 1986; Tamamaki and Nojyo, 1995). The CA1 area also projects to the deep EC layers with layer V as the main target (Swanson and Cowan, 1977; van Groen and Wyss, 1990). The EC-hippocampal connections are in fact topographically organized in such a way that the information originating in a particular medio-lateral segment of the EC flows back to the deep EC layers of that segment (Tamamaki and Nojyo, 1995).

1.2.4.3 Cortical Connections

1.2.4.3.1 Afferent Connections

Cortical projections to the entorhinal cortex can be divided, based on their origin, into those that arise from unimodal sensory areas and associational areas; or based on their termination as those that target specific layers (superficial or deep) of the MEA or the LEA. In the rat, the most prominent direct projection from unimodal sensory areas is from the piriform (olfactory) cortex that terminates in layer I and superficial layer II of the MEA and the LEA although the extent of the projection to the latter is stronger (Kosel et al., 1981; Room et al., 1984; Burwell and Amaral, 1998a). This projection in the monkey, however, is less profound (Van Hoesen and Pandya, 1975; Van Hoesen et al., 1975).

Although cortical afferents from associational sensory areas to the entorhinal cortex reach all parts of this structure, there is a differential distribution of terminals between the MEA and LEA (Burwell and Amaral, 1998a; Burwell and Amaral, 1998b). The LEA receives strong input from the insular cortex as compared to the MEA. In contrast, the MEA receives more robust projections from retrosplenial, posterior parietal, and visual association areas. A major source of cortical input to the entorhinal cortex is the projection through the perirhinal and postrhinal cortices (the postrhinal area in the rat is the equivalent of the parahippocampal area in the monkey (Burwell, 2001)), and through the pre and parasubiculum. As the recipients of converging unimodal and multimodal sensory input (Jones and Powell, 1970; Burwell et al., 1995; Burwell and Amaral, 1998a), the prirhinal and postrhinal cortices contribute highly integrated information to the entorhinal cortex (Burwell and Amaral, 1998b). The perirhinal cortex preferentially projects the LEA. This projection is mostly confined to the lateral aspect of the medial and lateral entorhinal areas and terminates as well in the superficial layers (Van Hoesen and Pandya, 1975). Although, the perirhinal and postrhinal termination fields in the entorhinal cortex partially overlap, postrhinal projections to the entorhinal cortex terminate heavily in the MEA in addition to a more restricted termination in the LEA as compared to the perirhinal cortex termination (Burwell and Amaral, 1998b).

In addition, deep layers of the MEA and LEA, although to a varying degree, have also been described to receive cortical projections from the agranular insular cortex, the infralimbic, prelimbic and anterior and posterior cingular cortices, and from the retrosplenial cortex (granular and dysgranular subdivisions) (Wyss and Van Groen,

1992). Finally, a projection form the presubiculum to layer V of the MEA has recently been described (van Haeften et al., 2000).

1.2.4.3.2 Efferent Connections

The entorhinal cortex reciprocates the cortical connections by directly projecting to sensory areas that are the sources of its sensory input in the first place; hence closing a neocortical-hippocampal-neocortical loop. Swanson and Kohler (1986) have originally suggested that the EC-neocortical projection arise from layer V cells throughout the medio-lateral extent of the EC and have widespread termination in much of the cortical mantle (Swanson and Kohler, 1986). Later studies confirmed that both MEA and LEA do project to sensory areas in the cortex; however, the widespread projections, as originally described, have been later found to originate only from a specific segment of layer V of the LEA (Insausti et al., 1997).

In addition, a major output arises from deep layers of the LEA that reciprocate the perirhinal cortex-LEA projections (Insausti et al., 1997). The perirhinal cortex, being reciprocally connected with polymodal sensory areas (Burwell and Amaral, 1998a), hence closes the loop between the entorhinal cortex and the same polymodal sensory areas from which it receives input. These efferent EC-perirhinal projections appear to be, however, weaker than the perirhinal to entorhinal projections (Burwell and Amaral, 1998b). Even though the postrhinal cortex projects to both MEA and LEA, only restricted portions of the LEA reciprocate these connections (Burwell and Amaral, 1998b).

1.2.4.4 Subcortical Connections

The entorhinal cortex receives input from a number of subcortical areas that project to all layers in the MEA and LEA. One of the most prominent subcortical afferents is from the medial septal complex of the basal forebrain that terminate predominantly in layer V and to a lesser extent in layer II (Beckstead, 1978; Alonso and Kohler, 1984; Milner and Amaral, 1984). In addition, the lateral and basal nuclei of the amygdaloid complex project to layers I-III and layers III-V of the entorhinal cortex, respectively (Beckstead, 1978). Other subcortical efferents arise from the claustrum, nucleus reuniens of the thalamus, the supramammillary nucleus, the tuberomammillary nucleus, the lateral hypothalamic area, the ventral tegmental area, the locus coeruleus of the pontine region and the central and dorsal raphe nuclei (Krettek and Price, 1977; Beckstead, 1978; Kohler and Steinbusch, 1982; Wouterlood et al., 1990). Projections from the supramammillary nucleus, the lateral hypothalamic area and the dorsal raphe nuclei preferentially terminate in and around layer V of the entorhinal cortex.

The entorhinal cortex also projects to subcortical areas. These projections are predominantly mediated through layer V and target the medial and lateral septal areas, the amygdala (mainly the basal nucleus) and the striatum (particularly the nucleus accumbens) (Beckstead, 1978; Ottersen, 1982; Alonso and Kohler, 1984; Phillipson and Griffiths, 1985).

1.3 Electrophysiology

As treated above, there is an extensive amount of data that describes in detail the anatomical connections that the entorhinal cortex has with the different areas in the

central nervous system. However, until recently, very little was known about the intrinsic electrophysiological properties of neurons in this structure. Most of the electrophysiological studies involving the entorhinal cortex were focused on studying and verifying the perceived connections it made (Lopes da Silva et al., 1984; Van Groen and Lopes da Silva, 1985; Finch et al., 1986; Van Groen and Lopes da Silva, 1986; White et al., 1990; Bartesaghi, 1994). This was probably because the functional role of the entorhinal cortex was seen as that of being mainly a "relay" station for the flow of information in and out of the hippocampal formation. Recent studies that focused on the basic electrophysiological characteristics of cells in this area have demonstrated that, as in other cortical areas, entorhinal principal neurons have very complex intrinsic electrogenesis, clearly indicative of tasks well beyond those of acting as a simple relay station (Jones and Heinemann, 1988; Alonso and Llinas, 1989; Alonso and Klink, 1993; Jones, 1994; Empson et al., 1995; Scharfman, 1996; Dickson et al., 1997; Gloveli et al., 1997; Schmitz et al., 1998; van der Linden and Lopes da Silva, 1998; Dugladze et al., 2001; Gloveli et al., 2001).

1.3.1 Electrophysiological Cell Types

Layer II: The two main morphological cell types in this layer, the stellate and pyramidal-like neurons, are each endowed with distinct electrophysiological properties (Alonso and Llinas, 1989; Alonso and Klink, 1993). Stellate cells have non-linear current-voltage (I/V) relationship both in the depolarizing and hyperpolarizing direction that is characteristic of inward rectification. In addition, stellate cells display time dependent inward rectification as reflected by the difference between the early and steady

state voltage in response (early being larger) to current pulse activation. This property always insured the stellate cells firing relatively early in response to current stimulation. However, the main characteristic of stellate cells was the ability to generate membrane potential oscillations in the subthreshold range when depolarized to subthreshold level. These oscillations had a persistent character and a mean frequency of 8.2 Hz at –55 mV, which is in the frequency range of the "theta" rhythm. This is important since EC layer II neurons "in vivo" are generators of theta rhythmicity (Alonso and García-Austt, 1987; Stewart et al., 1992; Chrobak et al., 2000) and implies that the subthreshold oscillations may represent the cellular basis for the theta rhythm in the EC. Because of the functional implications of the subthreshold oscillations, its ionic mechanism of generation has been investigated and the studies have shown that they are dependent on the interplay between a subthreshold persistent Na^+ current known as I_{NaP} and a time-dependent inward rectifier known as I_h (Klink and Alonso, 1993; Dickson et al., 2000).

In contrast to the stellate cells, pyramidal like cells, displayed less pronounced time-dependent inward rectification, delayed firing in response to step membrane depolarizations and the absence of subthreshold membrane potential oscillations. This profile was characteristic in spite of the fact that these cells, like the stellate cells, also appear to express a subthreshold persistent Na^+ current (Alonso and Klink, 1993).

Layer III: This layer constitutes the second contributor to the perforant path and is mainly comprised of pyramidal cells that resemble "regular firing" neurons in the neocortex (Connors and Gutnick, 1990). Basically, layer III cells are described as having little, if any, rectification in the hyperpolarizing direction (Dickson et al., 1997; Gloveli et al., 1997). The mean "sag percentage", which is an indication of this time dependent

rectification, was calculated to be around 6% for the layer III pyramidal cells, a pronounced difference as compared to that of layer II stellate or pyramidal-like cells which is 30 % and 17 %, respectively. However, layer III cells displayed pronounced sodium dependent inward rectification in the depolarizing direction. No subthreshold membrane potential oscillations were described in these cells (Dickson et al., 1997).

Layer V: One of the most extensive studies to address the intrinsic electrophysiological properties of layer V neurons is that of Jones and Heinemann (1988). Following will be a brief summary of their findings. Their description and classification of layer V cells, fairly comparable to layer V cells in the neocortex (Connors and Gutnick, 1990), was mainly based on firing properties. Three main categories of cells were described: non-bursting, to include 88 %, bursting cells, to include 9 %, and fast spiking cells to include 3 % of the total population of recorded neurons. Non-bursting neurons were all regularly spiking cells, as evident by non-decrementing action potential firing with little spike frequency adaptation in response to a depolarising current pulse application. Fast spiking cells were characterized by high frequency firing that also displayed no accommodation. The frequency of firing in this subtype typically increased close to the end of the voltage response. Bursting cells, are characterized by a depolarizing envelope that carries a train of decrementing action potentials in response to positive current injections. In addition, bursting cells display a pronounced after train AHP while exhibiting very little after spike AHP, completely opposite to properties of non-bursting neurons. Cells across the three different subtypes frequently display inward rectification in the hyperpolarizing direction. And the non-bursting cells did not display

bursting behaviour from even when hyperpolarized to more negative than resting membrane potentials.

A more recent report describes most layer V pyramidal cells as having subthreshold membrane potential oscillations, similar to what has been described in layer II of the entorhinal cortex (Schmitz et al., 1998). These oscillations are similar to those in layer II in terms of their frequency and progression. No studies, however, have been aimed at the electrophysiological properties of layer V neurons in the lateral entorhinal cortex.

1.3.2 Neocortical layer V cells

Since the entorhinal layer V cells have been classified in line with the electrophysiological properties of neocortical layer V neurons, this section will briefly review the relevant properties of neurons in layer V of the neocortex.

At least two general groups have been recognised for neocortical (somatosensory, prefrontal and visual cortices) layer V neurons based on firing patterns: regular spiking (RS) and intrinsically bursting (IB) neurons; both groups having distinct morphological attributes (reviewed in: Connors et al., 1982; Agmon and Connors, 1989; Chagnac-Amitai et al., 1990; Connors and Gutnick, 1990; Yang et al., 1996). IB neurons are characterized by a burst response of 3 to 5 action potentials riding on a depolarising envelope to a depolarising current step injection. However, bursting neurons can also display repetitively rhythmic bursting behaviour (Agmon and Connors, 1989; Yang et al., 1996). RS cells never display the typical bursting behaviour, however, in one study, some RS cells displayed a doublet-firing pattern, the closest resemblance to the bursting pattern of

IB cells (Chagnac-Amitai et al., 1990). In IB cells, a calcium conductance is largely responsible for the bursting behaviour (Yang et al., 1996).

1.4 Functional Aspects of The Entorhinal Area

1.4.1 Memory Formation

As mentioned in the first section of this chapter, the role of the entorhinal cortex in what is known as the "medial temporal lobe or hippocampal memory system" (Witter et al., 2000) is well established based on behavioural observations in humans with temporal lobectomy and lesioned animals. Another indication that the entorhinal cortex is playing a role in this system comes from evidence of its involvement in AD. Neurofibrillary tangles (NT), a hallmark of AD, are consistently heavily deposited in the entorhinal cortex especially layers II and V in contrast to all other areas of the cortex where deposits are pretty variable (Van Hoesen et al., 1991). Layers II and V are reported to be the most atrophied (Gomez-Isla et al., 1996). In addition, the entorhinal cortex is also thought to be the area to be targeted early during the onset of this disease (Braak and Braak, 1991, Braak and Braak, 1993). These studies suggested that the entorhinal cortex might be responsible for the early behavioral symptoms of AD patients.

Layer V of the entorhinal cortex, by virtue of its anatomical connections, holds the key to the flow of information from the hippocampus to the different areas of the neocortex (as reviewed previously). Hence, any atrophy or disruption in this layer would effectively mean: first, the loss the "relay" function this layer has between the hippocampus and the sensory areas in the neocortex, and two, the loss of the processing power this layer might have in this memory loop. Electrophysiological studies have

shown that EC layer V can generate very high frequency population oscillations known as "ripples" (Chrobak and Buzsaki, 1994). It has been proposed that these ripples represent a mechanism by which hippocampal coded information is transferred to the cortex for storage (Draguhn et al., 2000).

1.4.2 Epilepsy

Temporal lobe epilepsy (TLE) is the most common form of epilepsy and is particularly resistant to drug treatment (Kalynchuk, 2000). In the most severe cases, removal of the hippocampus would lead to relief from epilepsy and the success is improved if the parahippocampal region, including the entorhinal cortex, is also removed (Siegel et al., 1990). The entorhinal cortex has indeed been implicated in the genesis of temporal lobe epilepsy in numerous studies (Rutecki et al., 1989; Spencer and Spencer, 1994; Bragin et al., 1997; Bernasconi et al., 1999; Bragin et al., 1999). MRI volumetric measurements have revealed that the entorhinal cortex alone could be atrophied in patients with temporal lobe epilepsy and normal hippocampus (Bernasconi et al., 2001). In addition, current source density and unit recordings in the hippocampus and entorhinal cortex revealed that afterdischarges could arise in the EC independent of the hippocampus after epileptic activity was induced by extracellular stimulation (Bragin et al., 1997). Finally, the fact that layer III of the entorhinal cortex is severely atrophied in temporal lobe epilepsy in humans and certain animal models (Du et al., 1993; Du et al., 1995; Du et al., 1998) is a further indication of the involvement of this structure in epileptic processes.

The deep entorhinal layers are considered to have the ability to act as generators and/or promoters of such epileptic activity (Walther et al., 1986; Jones and Heinemann, 1988; Jones and Lambert, 1990a; Jones and Lambert, 1990b; Dickson and Alonso, 1997). In this respect, layer V was thought to have a sub-population of neurons that posses intrinsic bursting properties (Jones and Heinemann, 1988) in addition to strong recurrent collaterals between principal cells (Jones and Lambert, 1990b; Dhillon and Jones, 2000). The combination of intrinsic bursting behavior and synaptic reverberation could facilitate hyperexcitability and epileptogenesis (Traub and Wong, 1982; Traub et al., 1985; Wong et al., 1986; Heineman et al., 1993). In addition, the cholinergic system is implicated in epileptic activity (Wasterlain and Jonec, 1983; Rutecki and Yang, 1997), and layer V is known to receive a strong projection from cholinergic neurones of the basal forebrain (as mentioned previously). Hence, it is not surprising that cholinergic activation of entorhinal cortex slices leads to the generation of epileptiform events (Dickson and Alonso, 1997).

1.5 Objectives of This Study

It is clear from the literature reviewed here that the entorhinal cortex is highly involved in the neocortico-hippocampal memory functions as well as in pathophysiology of epilepsy. It has long been believed that the entorhinal cortex plays the role of a relay station in the hippocampo-neocortical communications. However, studies aimed at understanding the intrinsic properties of cells in this structure, especially those carried out on superficial cell layer neurons, revealed a much higher complexity in the intrinsic cellular excitability than expected for simple relay functions. This prompted us to carry out a study of the basic properties of neurons in layer V of the entorhinal cortex. These neurons are the main source of neocortical efferents from the hippocampal formation. In addition, they also affect the neocortical afferents to the hippocampus by projection to EC superficial layers.

The study was carried out using intracellular recording and labelling techniques in an *in vitro* rat brain slice preparation. The specific aims were to characterize the basic electrophysiological and morphological properties of these neurons and to attempt to categorize different cell types based on differences in both aspects. A new histochemical processing technique for biocytin-injected neurons was developed for the anatomical analysis. This study could help verify whether classification of entorhinal layer V cells could be made in line with what has been described for layer V of the neocortex as well as shed some light onto how neurons in layer V of the entorhinal cortex might participate in the memory functions of the structure as well as in the pathophysiology of epilepsy.

1.6 References

Agmon A, Connors BW. 1989. Repetitive burst-firing neurons in the deep layers of mouse somatosensory cortex. Neurosci Lett 99:137-141.

Alonso A, de Curtis M, Llinas R. 1990. Postsynaptic Hebbian and non-Hebbian long-term potentiation of synaptic efficacy in the entorhinal cortex in slices and in the isolated adult guinea pig brain. Proc. Natl. Acad. Sci. USA 87:9280-9284.

Alonso A, García-Austt E. 1987. Neuronal sources of theta rhythm in the entorhinal cortex of the rat. II. Phase relations between unit discharges and theta field potentials. Exp. Brain Res. 67:502-509.

Alonso A, Klink R. 1993. Differential electroresponsiveness of stellate and pyramidal-like cells of medial entorhinal cortex layer II. J. Neurophysiol. 70:128-143.

Alonso A, Kohler C. 1984. A study of the reciprocal connections between the septum and the entorhinal area using anterograde and retrograde axonal transport methods in the rat brain. J Comp Neurol 225:327-343.

Alonso A, Llinas RR. 1989. Subthreshold Na^+-dependent theta-like rhythmicity in stellate cells of entorhinal cortex layer II. Nature 342:175-177.

Amaral DG, Insausti R, Cowan WM. 1983. Evidence for a direct projection from the superior temporal gyrus to the entorhinal cortex in the monkey. Brain Res. 275:263-277.

Amaral DG, Witter MP (1995) Hippocampal Formation. In: The rat nervous system, 2nd Edition (Paxinos G, ed): Academic Press Inc. London, pp 443-493.

Andersen P, Sundberg SH, Sveen O, Swann JW, Wigstrom H. 1980. Possible mechanisms for long-lasting potentiation of synaptic transmission in hippocampal slices from guinea-pigs. J Physiol 302:463-482.

Bartesaghi R. 1994. Hippocampal-entorhinal relationships: electrophysiological analysis of the ventral hippocampal projections to the ventral entorhinal cortex. Neuroscience 61:457-466.

Beckstead RM. 1978. Afferent connections of the entorhinal area in the rat as demonstrated by retrograde cell-labeling with horseradish peroxidase. Brain Res 152:249-264.

Bernasconi N, Bernasconi A, Andermann F, Dubeau F, Feindel W, Reutens DC. 1999. Entorhinal cortex in temporal lobe epilepsy: a quantitative MRI study. Neurology 52:1870-1876.

Bernasconi N, Bernasconi A, Caramanos Z, Dubeau F, Richardson J, Andermann F, Arnold DL. 2001. Entorhinal cortex atrophy in epilepsy patients exhibiting normal hippocampal volumes. Neurology 56:1335-1339.

Blackstad TW. 1956. Commissural connections of the hippocampal region in the rat, with special reference to their mode of termination. J. Comp. Neurol. 105:417-537.

Bland BH, Colom LV. 1993. Extrinsic and intrinsic properties underlying oscillation and synchrony in limbic cortex. Prog Neurobiol 41:157-208.

Bliss TV, Collingridge GL. 1993. A synaptic model of memory: long-term potentiation in the hippocampus. Nature 361:31-39.

Bliss TVP, Lomo T. 1973. Long-lasting potentiation of synaptic transmission in the dentate area of the anesthetized rabbit following stimulation of the perforant path. J. Physiol. (Lond.) 232:331-356.

Braak H, Braak E. 1993. Entorhinal-hippocampal interaction in mnestic disorders. Hippocampus 3:239-246.

Braak H, Braak E. 1991. Neuropathological stageing of Alzheimer-related changes. Acta Neuropathol 82:239-259.

Bragin A, Csicsvari J, Penttonen M, Buzsaki G. 1997. Epileptic afterdischarge in the hippocampal-entorhinal system: current source density and unit studies. Neuroscience 76:1187-1203.

Bragin A, Engel J, Jr., Wilson CL, Fried I, Mathern GW. 1999. Hippocampal and entorhinal cortex high-frequency oscillations (100--500 Hz) in human epileptic brain and in kainic acid--treated rats with chronic seizures. Epilepsia 40:127-137.

Broca P. 1878. Anatomie comparée des circonvolutions cérébrales. Le grand lobe limbique et la scissure limbique dans la série des mammifères. Rev. Anthrop. 2:285-498.

Burwell RD. 2000. The parahippocampal region: corticocortical connectivity. Ann N Y Acad Sci 911:25-42.

Burwell RD. 2001. Borders and cytoarchitecture of the perirhinal and postrhinal cortices in the rat. J Comp Neurol 437:17-41.

Burwell RD, Amaral DG. 1998a. Cortical afferents of the perirhinal, postrhinal, and entorhinal cortices of the rat. J Comp Neurol 398:179-205.

Burwell RD, Amaral DG. 1998b. Perirhinal and postrhinal cortices of the rat: interconnectivity and connections with the entorhinal cortex. J Comp Neurol 391:293-321.

Burwell RD, Witter MP, Amaral DG. 1995. Perirhinal and postrhinal cortices of the rat: A review of the neuroanatomical literature and comparison with findings from the monkey brain. Hippocampus 5:390-408.

Chagnac-Amitai Y, Connors BW. 1989. Synchronized excitation and inhibition driven by intrinsically bursting neurons in neocortex. J Neurophysiol 62:1149-1162.

Chagnac-Amitai Y, Luhmann HJ, Prince DA. 1990. Burst generating and regular spiking layer 5 pyramidal neurons of rat neocortex have different morphological features. J Comp Neurol 296:598-613.

Chrobak JJ, Buzsaki G. 1994. Selective activation of deep layer (V-VI) retrohippocampal cortical neurons during hippocampal sharp waves in the behaving rat. J. Neurosci. 14:6160-6170.

Chrobak JJ, Lorincz A, Buzsaki G. 2000. Physiological patterns in the hippocampo-entorhinal cortex system. Hippocampus 10:457-465.

Claiborne BJ, Amaral DG, Cowan WM. 1986. A light and electron microscopic analysis of the mossy fibers of the rat dentate gyrus. J Comp Neurol 246:435-458.

Commins S, Gigg J, Anderson M, O'Mara SM. 1998. The projection from hippocampal area CA1 to the subiculum sustains long-term potentiation. Neuroreport 9:847-850.

Connors BW. 1984. Initiation of synchronized neuronal bursting in neocortex. Nature 310:685-687.

Connors BW, Gutnick MJ. 1990. Intrinsic firing patterns of diverse neocortical neurons. Trends Neurosci. 13:99-104.

Connors BW, Gutnick MJ, Prince DA. 1982. Electrophysiological properties of neocortical neurons in vitro. J Neurophysiol 48:1302-1320.

Dhillon A, Jones RS. 2000. Laminar differences in recurrent excitatory transmission in the rat entorhinal cortex in vitro. Neuroscience 99:413-422.

Dickson CT, Alonso A. 1997. Muscarinic induction of synchronous population activity in the entorhinal cortex. J. Neurosci. 17:6729-6744.

Dickson CT, Magistretti J, Shalinsky MH, Fransen E, Hasselmo ME, Alonso A. 2000. Properties and role of I(h) in the pacing of subthreshold oscillations in entorhinal cortex layer II neurons. J Neurophysiol 83:2562-2579.

Dickson CT, Mena AR, Alonso A. 1997. Electroresponsiviness of medial entorhinal cortex layer III neurons *in vitro*. Neuroscience 81:937-950.

Dolorfo CL, Amaral DG. 1998. Entorhinal cortex of the rat: organization of intrinsic connections. J Comp Neurol 398:49-82.

Draguhn A, Traub RD, Bibbig A, Schmitz D. 2000. Ripple (approximately 200-Hz) oscillations in temporal structures. J Clin Neurophysiol 17:361-376.

Du F, Eid T, Schwarcz R. 1998. Neuronal damage after the injection of aminooxyacetic acid into the rat entorhinal cortex: a silver impregnation study. Neuroscience 82:1165-1178.

Du F, Tore E, Kohler C, Lothman EW, Schwarcz R. 1995. Preferential neuronal loss in layer III of the medial entorhinal cortex in rat models of temporal lobe epilepsy. J. Neurosci. 15:8301-8313.

Du F, Whetsell WO, Abou-Khalil B, Blumenkopf B, Lothman EW, Schwarcz R. 1993. Preferential neuronal loss in layer III of the entorhinal cortex in patients with temporal lobe epilepsy. Epilepsy Res. 16:223-233.

Dugladze T, Heinemann U, Gloveli T. 2001. Entorhinal cortex projection cells to the hippocampal formation in vitro. Brain Res 905:224-231.

Empson RM, Gloveli T, Schmitz D, Heinemann U. 1995. Electrophysiology and morphology of a new type of cell within layer II of the rat lateral entorhinal cortex in vitro. Neurosci Lett 193:149-152.

Empson RM, Heinemann U. 1995. The perforant path projection to hippocampal area CA1 in the rat hippocampal-entorhinal cortex combined slice. J. Physiol. 484:707-720.

Finch DM, Wong EE, Derian EL, Babb TL. 1986. Neurophysiology of limbic system pathways in the rat: projections from the subicular complex and hippocampus to the entorhinal cortex. Brain Res 397:205-213.

Germroth P, Schwerdtfeger WK, Buhl EH. 1989. Morphology of identified entorhinal neurons projecting to the hippocampus. A light microscopical study combining retrograde tracing and intracellular injection. Neuroscience 30:683-691.

Gloveli T, Dugladze T, Schmitz D, Heinemann U. 2001. Properties of entorhinal cortex deep layer neurons projecting to the rat dentate gyrus. Eur J Neurosci 13:413-420.

Gloveli T, Schmitz D, Empson RM, Dugladze T, Heinemann U. 1997. Morphological and electrophysiological characterization of layer III cells of the medial entorhinal cortex of the rat. Neurosci 77:629-648.

Golgi C, Bentivoglio M, Swanson L. 2001. On the fine structure of the pes Hippocampi major (with plates XIII-XXIII). 1886. Brain Res Bull 54:461-483.

Gomez-Isla T, Price JL, McKeel DW, Morris JC, Growdon JH, Hyman BT. 1996. Profound loss of layer II entorhinal cortex neurons occurs in very mild Alzheimer's disease. J. Neurosci. 16:4491-4500.

Greenstein YJ, Pavlides C, Winson J. 1988. Long-term potentiation in the dentate gyrus is preferentially induced at theta rhythm periodicity. Brain Res 438:331-334.

Haug FM. 1976. Sulphide silver pattern and cytoarchitectonics of parahippocampal areas in the rat. Special reference to the subdivision of area entorhinalis (area 28) and its demarcation from the pyriform cortex. Adv Anat Embryol Cell Biol 52:3-73.

Heineman U, Zhang CL, Eder C. 1993. Entorhinal cortex-hippocampal interactions in normal and epileptic temporal lobe. Hippocampus 3:88-98.

Hjorth-Simonsen A. 1972. Projection of the lateral part of the entorhinal area to the hippocampus and fascia dentata. J Comp Neurol 146:219-232.

Horikawa K, Armstrong WE. 1988. A versatile means of intracellular labeling: injection of biocytin and its detection with avidin conjugates. J. Neurosci. Methods 25:1-11.

Insausti R, Amaral DG, Cowan WM. 1987. The entorhinal cortex of the monkey: II. Cortical afferents. J. Comp. Neurol. 264:356-395.

Insausti R, Herrero MT, Witter MP. 1997. Entorhinal cortex of the rat: cytoarchitectonic subdivisions and the origin and distribution of cortical efferents. Hippocampus 7:146-183.

Jones EG, Powell TPS. 1970. An anatomical study of convergin sensory pathways within the cerebral cortex of the monkey. Brain 93:793-820.

Jones RS. 1994. Synaptic and intrinsic properties of neurons of origin of the perforant path in layer II of the rat entorhinal cortex in vitro. Hippocampus 4:335-353.

Jones RS, Heinemann U. 1988. Synaptic and intrinsic responses of medial entorhinal cortical cells in normal and magnesium-free medium in vitro. J Neurophysiol 59:1476-1496.

Jones RSG, Lambert JDC. 1990a. The role of excitatory amino acid receptors in the propagation of epileptiform discharges from the entorhinal cortex to the dentate gyrus in vitro. Exp Brain Res 80:310-322.

Jones RSG, Lambert JDC. 1990b. Synchronous discharges in the rat entorhinal cortex *in vitro*: site of initiation and the role of excitatory amino acid receptors. Neuroscience 34:657-670.

Kalynchuk LE. 2000. Long-term amygdala kindling in rats as a model for the study of interictal emotionality in temporal lobe epilepsy. Neurosci Biobehav Rev 24:691-704.

Klink R, Alonso A. 1993. Ionic mechanisms for the subthreshold oscillations and differential electroresponsiveness of medial entorhinal cortex layer II neurons. J. Neurophysiol. 70:144-157.

Klink R, Alonso A. 1997. Morphological characteristics of layer II projection neurons in the rat medial entorhinal cortex. Hippocampus 7:571-583.

Kohler C. 1985. Intrinsic projections of the retrohippocampal region in the rat brain. I. The subicular complex. J. Comp. Neurol. 236:504-522.

Kohler C. 1986. Intrinsic connections of the retrohippocampal region in the rat brain. II. The medial entorhinal area. J. Comp. Neurol. 246:149-169.

Kohler C. 1988. Intrinsic connections of the retrohippocampal region in the rat brain. III. The lateral entorhinal area. J. Comp. Neurol. 271:208-228.

Kohler C, Steinbusch H. 1982. Identification of serotonin and non-serotonin-containing neurons of the mid-brain raphe projecting to the entorhinal area and the hippocampal formation. A combined immunohistochemical and fluorescent retrograde tracing study in the rat brain. Neuroscience 7:951-975.

Kosel KC, Van Hoesen GW, West JR. 1981. Olfactory bulb projections to the parahippocampal area of the rat. J Comp Neurol 198:467-482.

Krettek JE, Price JL. 1977. The cortical projections of the mediodorsal nucleus and adjacent thalamic nuclei in the rat. J Comp Neurol 171:157-191.

Laroche S, Davis S, Jay TM. 2000. Plasticity at hippocampal to prefrontal cortex synapses: dual roles in working memory and consolidation. Hippocampus 10:438-446.

Lavenex P, Amaral DG. 2000. Hippocampal-neocortical interaction: a hierarchy of associativity. Hippocampus 10:420-430.

Leonard BW, Amaral DG, Squire LR, Zola-Morgan S. 1995. Transient memory impairment in monkeys with bilateral lesions of the entorhinal cortex. J. Neurosci. 15:5637-5659.

Levisohn LF, Isacson O. 1991. Excitotoxic lesions of the rat entorhinal cortex. Effects of selective neuronal damage on acquisition and retention of non-spatial reference memory task. Brain Res. 564:230-244.

Light AR, Durkovic RG. 1976. Horseradish peroxidase: an improvement in intracellular staining of single, electrophysiologically characterized neurons. Exp Neurol 53:847-853.

Lingenhöhl K, Finch DM. 1991. Morphological characterization of rat entorhinal neurons in vivo: soma-dendritic structure and axonal domains. Exp. Brain Res. 84:57-74.

Lopes da Silva FH, Arnolds DE, Neijt HC. 1984. A functional link between the limbic cortex and ventral striatum: physiology of the subiculum accumbens pathway. Exp Brain Res 55:205-214.

Lopes da Silva FH, Witter MP, Boeijinga PH, Lohman AH. 1990. Anatomic organization and physiology of the limbic cortex. Physiol Rev 70:453-511.

Lorente de Nó R. 1933. Studies on the structure of the cerebral cortex. I. The area entorhinalis. J. Psychol. Neurol. 45:381-438.

Luis de la Iglesia JA, Lopez-Garcia C. 1997. A Golgi study of the short-axon interneurons of the cell layer and inner plexiform layer of the medial cortex of the lizard Podarcis hispanica. J Comp Neurol 385:565-598.

MacLean P. 1952. Some psychiatric implications of physiological studies on frontotemporal portion of limbic system (visceral brain). Electroencephalogr. Clin. Neurophysiol. 4:407-418.

Malenka RC. 1991. Postsynaptic factors control the duration of synaptic enhancement in area CA1 of the hippocampus. Neuron 6:53-60.

Milner B, Johnsrude I, Crane J. 1997. Right medial temporal-lobe contribution to object-location memory. Philos Trans R Soc Lond B Biol Sci 352:1469-1474.

Milner TA, Amaral DG. 1984. Evidence for a ventral septal projection to the hippocampal formation of the rat. Exp Brain Res 55:579-585.

Mishkin M, Suzuki WA, Gadian DG, Vargha-Khadem F. 1997. Hierarchical organization of cognitive memory. Philos Trans R Soc Lond B Biol Sci 352:1461-1467.

Moser EI, Moser MB, Andersen P. 1994. Potentiation of dentate synapses initiated by exploratory learning in rats: dissociation from brain temperature, motor activity, and arousal. Learn Mem 1:55-73.

Naber PA, Lopes da Silva FH, Witter MP. 2001. Reciprocal connections between the entorhinal cortex and hippocampal fields CA1 and the subiculum are in register with the projections from CA1 to the subiculum. Hippocampus 11:99-104.

Naber PA, Witter MP. 1998. Subicular efferents are organized mostly as parallel projections: a double-labeling, retrograde-tracing study in the rat. J Comp Neurol 393:284-297.

Oddie SD, Bland BH. 1998. Hippocampal formation theta activity and movement selection. Neurosci Biobehav Rev 22:221-231.

Ottersen OP. 1982. Connections of the amygdala of the rat. IV: Corticoamygdaloid and intraamygdaloid connections as studied with axonal transport of horseradish peroxidase. J Comp Neurol 205:30-48.

Phillipson OT, Griffiths AC. 1985. The topographic order of inputs to nucleus accumbens in the rat. Neuroscience 16:275-296.

Room P, Groenewegen HJ, Lohman AH. 1984. Inputs from the olfactory bulb and olfactory cortex to the entorhinal cortex in the cat. I. Anatomical observations. Exp Brain Res 56:488-496.

Ramon y Cajal S. 1902. Studies on the human cerebral cortex IV: Structure of the olfactory cerebral cortex of man and mammals. Trab. del Lab. de invest. Biol. Univ. Madrid 1:1-140.

Ramon y Cajal S. 1911. Histologie du système nerveux de l'homme et des vertébrés. trans. by L. Azoulay. Paris: Maloine 2 vols.

Rutecki PA, Grossman RG, Armstrong D, Irish-Loewen S. 1989. Electrophysiological connections between the hippocampus and entorhinal cortex in patients with complex partial seizures. J. Neurosurg. 70:667-675.

Rutecki PA, Yang Y. 1997. Metabotropic glutamate receptor activation modulates epileptiform activity in the hippocampus. Neuroscience 81:927-935.

Scharfman HE. 1996. Hyperexcitability of entorhinal cortex and hippocampus after application of aminooxyacetic acid (AOAA) to layer III of the rat medial entorhinal cortex in vitro. J Neurophysiol 76:2986-3001.

Schmitz D, Gloveli T, Behr J, Dugladze T, Heinemann U. 1998. Subthreshold membrane potential oscillations in neurons of deep layers of the entorhinal cortex. Neuroscience 85:999-1004.

Schwartz SP, Coleman PD. 1981. Neurons of origin of the perforant path. Exp. Neurol. 74:305-312.

Schwartzkroin PA. 2001. Mechanisms of brain plasticity: from normal brain function to pathology. Int Rev Neurobiol 45:1-15.

Scoville WB, Milner B. 1957. Loss of recent memory after bilateral hippocampal lesions. J. Neurol. Neurosurg. Psychiat. 20:11-21.

Segal M. 1977. Afferents to the entorhinal cortex of the rat studied by the method of retrograde transport of horseradish peroxidase. Exp. Neurol. 57:750-765.

Siegel AM, Wieser HG, Wichmann W, Yasargil MG. 1990. Relationship betwenn MR-imaged total amount of tissue removed, resection scores of specific mediobasal limbic subcompartments and clinical outcome following selective amygdalohippocampectomy. Epilepsy Research 6:55-65.

Silva LR, Amitai Y, Connors BW. 1991. Intrinsic oscillations of neocortex generated by layer 5 pyramidal neurons. Science 251:432-435.

Sorensen KE, Shipley MT. 1979. Projections from the subiculum to the deep layers of the ipsilateral presubicular and entorhinal cortices in the guinea pig. J. Comp. Neurol. 188:313-334.

Spencer SS, Spencer DD. 1994. Entorhinal-hippocampal interactions in medial temporal lobe epilepsy. Epilepsia 35:721-727.

Squire LR, Zola SM. 1996. Structure and function of declarative and nondeclarative memory systems. Proc Natl Acad Sci U S A 93:13515-13522.

Staubli U, Xu FB. 1995. Effects of 5-HT3 receptor antagonism on hippocampal theta rhythm, memory, and LTP induction in the freely moving rat. J Neurosci 15:2445-2452.

Steward O. 1976. Topographic organization of the projections from the entorhinal area to the hippocampal formation of the rat. J Comp Neurol 167:285-314.

Steward O, Scoville SA. 1976. The cells of origin of entorhinal afferents to the hippocampus and fascia dentata of the rat. J. Comp. Neurol. 169:347-370.

Stewart M, Quirk GJ, Barry M, Fox SE. 1992. Firing relations of medial entorhinal neurons to the hippocampal theta rhythm in urethane anesthetized and walking rats. Exp Brain Res 90:21-28.

Swanson LW, Cowan WM. 1977. An autoradiographic study of the organization of the efferent connections of the hippocampal formation in the rat. J. Comp. Neurol. 172:49-84.

Swanson LW, Kohler C. 1986. Anatomical evidence for direct projections from the entorhinal area to the entire cortical mantle in the rat. J Neurosci 6:3010-3023.

Swanson LW, Wyss JM, Cowan WM. 1978. An autoradiographic study of the organization of intrahippocampal association pathways in the rat. J Comp Neurol 181:681-715.

Tamamaki N, Nojyo Y. 1993. Projection of the entorhinal layer II neurons in the rat as revealed by intracellular pressure-injection of neurobiotin. Hippocampus 3:471-480.

Tamamaki N, Nojyo Y. 1995. Preservation of topography in the connections between the subiculum, field CA1, and the entorhinal cortex in rats. J Comp Neurol 353:379-390.

Telfeian AE, Connors BW. 1998. Layer-specific pathways for the horizontal propagation of epileptiform discharges in neocortex. Epilepsia 39:700-708.

Traub RD, Wong RK. 1982. Cellular mechanism of neuronal synchronization in epilepsy. Science 216:745-747.

Traub RD, Wong RK, Miles R, Knowles WD. 1985. Neuronal interactions during epileptic events in vitro. Fed Proc 44:2953-2955.

van der Linden S, Lopes da Silva FH. 1998. Comparison of the electrophysiology and morphology of layers III and II neurons of the rat medial entorhinal cortex in vitro. Eur. J. Neurosci. 10:1479-1489.

Van Groen T, Lopes da Silva FH. 1985. Septotemporal distribution of entorhinal projections to the hippocampus in the cat: electrophysiological evidence. J Comp Neurol 238:1-9.

Van Groen T, Lopes da Silva FH. 1986. Organization of the reciprocal connections between the subiculum and the entorhinal cortex in the cat: II. An electrophysiological study. J Comp Neurol 251:111-120.

van Groen T, Wyss JM. 1990. Extrinsic projections from area CA1 of the rat hippocampus: olfactory, cortical, subcortical, and bilateral hippocampal formation projections. J Comp Neurol 302:515-528.

van Haeften T, Wouterlood FG, Witter MP. 2000. Presubicular input to the dendrites of layer-V entorhinal neurons in the rat. Ann N Y Acad Sci 911:471-473.

Van Hoesen GW, Hyman BT, Damasio AR. 1991. Entorhinal cortex pathology in Alzheimer's disease. Hippocampus 1:1-8.

Van Hoesen GW, Pandya DN. 1975. Some connections of the entorhinal (area 28) and perirhinal (area 35) cortices of the rhesus monkey. I. Temporal lobe afferents. Brain Res. 95:1-24.

Van Hoesen GW, Pandya DN, Butters N. 1975. Some connections of the entorhinal (area 28) and perirhinal (area 35) cortices of the rhesus monkey. II. Frontal lobe afferents. Brain Res. 95:25-38.

Vinogradova OS. 1995. Expression, control, and probable functional significance of the neuronal theta-rhythm. Prog. Neurobiol. 45:523-583.

Walther H, Lambert JDC, Jones RSG, Heinemann U, Hamon B. 1986. Epileptiform activity in combined slices of the hippocampus, subiculum and entorhinal cortex during perfusion with low magnesium medium. Neurosci.Lett. 69:165-161.

Wasterlain CG, Jonec V. 1983. Chemical kindling by muscarinic amygdaloid stimulation in the rat. Brain Res 271:311-323.

White TD, Tan AM, Finch DM. 1990. Functional reciprocal connections of the rat entorhinal cortex and subicular complex with the medial frontal cortex: an in vivo intracellular study. Brain Res 533:95-106.

Witter MP. 1993. Organization of the entorhinal-hippocampal system: a review of current anatomical data. Hippocampus 3 Spec No:33-44.

Witter MP, Groenewegen HJ, Lopes da Silva FH, Lohman AH. 1989. Functional organization of the extrinsic and intrinsic circuitry of the parahippocampal region. Prog Neurobiol 33:161-253.

Witter MP, Naber PA, van Haeften T, Machielsen WC, Rombouts SA, Barkhof F, Scheltens P, Lopes da Silva FH. 2000. Cortico-hippocampal communication by way of parallel parahippocampal- subicular pathways. Hippocampus 10:398-410.

Wong RK, Traub RD, Miles R. 1986. Cellular basis of neuronal synchrony in epilepsy. Adv Neurol 44:583-592.

Wouterlood FG, Saldana E, Witter MP. 1990. Projection from the nucleus reuniens thalami to the hippocampal region: light and electron microscopic tracing study in

the rat with the anterograde tracer Phaseolus vulgaris-leucoagglutinin. J Comp Neurol 296:179-203.

Wyss JM, Van Groen T. 1992. Connections between the retrosplenial cortex and the hippocampal formation in the rat: a review. Hippocampus 2:1-11.

Yang CR, Seamans JK, Gorelova N. 1996. Electrophysiological and morphological properties of layers V-VI principal pyramidal cells in rat prefrontal cortex in vitro. J Neurosci 16:1904-1921.

Zola-Morgan S, Squire LR, Ramus SJ. 1994. Severity of memory impairment in monkeys as a function of locus and extent of damage within the medial temporal lobe memory system. Hippocampus 4:483-495.

1.8 Figures

Figure 1: A schematic representation of the main circuitry in the entorhinal-hippocampal loop. EC, entorhinal cortex; DG, dentate gyrus; CA, cornu ammonis; SUB, subiculum.

Entorhinal - Hippocampal Circuitry

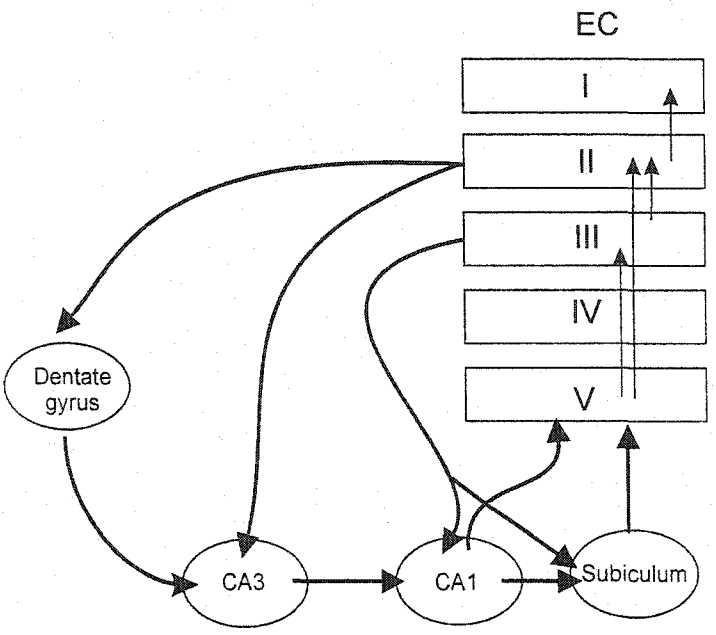

Chapter Two

2. Visualization of the Dendritic Arbor of Single Neurons in Intact Brain Slices

2.1 Preface

As stated in the objectives, a large part of the work in the thesis involved combining electrophysiological and morphological analysis of neurons. The first aspect of the study was done with the use of traditional "sharp electrode" recording techniques. During early experimentation, traditionally used histochemical processing techniques for biocytin-injected neurons were employed. These typically involved resectioning the original slice preparation into slices one-tenth the original thickness. However, this process was very time consuming and fraught with technical difficulties that would make the output reconstruction and analysis of the anatomical data susceptible to error. Therefore, we adapted a technique that is used for histochemical analysis in thick embryos and used it successfully in our preparation. This chapter describes the details of this technique and suggests further use of it beyond the scope of the current study.

2.2 Abstract

Characterizing the structure and electrophysiological properties of single neurons is essential for understanding how individual cells contribute to the function of neuronal networks. After recording from a neuron in a slice of brain tissue, the structure of the recorded cell has been typically examined by serial sectioning the tissue slice and then reconstructing the neuron of interest, a labor intensive and time consuming process. Here, we have adapted a whole-mount immunohistochemical technique and used it to visualize the dendritic arborization of individual neurons in sections of adult CNS tissue up to 500 μm thick. Permeabilization of the slice and extensive washing allow histochemical reagents to penetrate and be washed from the section, generating limited background staining. Using this method, the cell within the slice can be sectioned optically and the optical sections reconstructed. We present images of the intact dendritic trees of neurons in slices of adult rat entorhinal cortex. The resolution obtained is sufficient to visualize details in the structure of dendritic spines. The method is free from artifacts associated with cutting serial sections and is broadly applicable to tasks that require visualization of the fine structure of individual cells in thick slices of CNS tissue.

2.3 Introduction

Many studies aim to understand the relationship between the morphological and electrophysiological properties of single neurons. An important method for revealing the morphological structure of individual neurons has been the Golgi impregnation technique (Golgi, 1886). However, this and related methods (Glaser and Van Der Loos, 1981; McMullen et al., 1984; Uylings et al., 1986) are limited by the fact that the cell staining is stochastic, making it impossible for the investigator to determine beforehand exactly which cells in a tissue will be stained. Methods using sharp electrodes to inject dyes or enzymatic substrates intracellularly, such as HRP (Cullheim and Kellerth, 1976; Light and Durkovic, 1976) or biocytin (Horikawa and Armstrong, 1988), allow specific neurons to be both labelled and characterized electrophysiologically (Capowski, 1977; Koenderink and Uylings, 1996; Pyapali et al., 1998; Cannon et al., 1998). However, electrophysiological slice preparations typically employ slices of tissue between 200 and 400 μm thick. Histochemical processing of thick tissue slices often generates high non-specific background staining. To avoid this, slices have traditionally been re-sectioned into 40 to 80 μm thick sections after fixation and before processing. Thinner sections allow for ready penetration of antibodies or enzymatic substrates into the tissue and reduce the level of background staining. However, these thinner sections are usually of insufficient thickness to contain the complete dendritic arborization of a neuron within one section. The dendritic arbor of an individual neuron might be distributed across 5 to 10 serial sections, making it necessary to generate a serial reconstruction to appreciate the three dimensional shape of the cell. The sectioning and reconstruction process is time consuming, labor intensive, and fraught with potential artifacts. These include accounting

for shrinkage and distortion induced by fixation and/or dehydration, loosing parts of the tissue during sectioning, and mis-aligning pieces of the cell during reconstruction. These issues have been extensively discussed by other authors (Capowski, 1977; Glaser and Van Der Loos, 1981; Yelnik et al., 1981; Uylings et al., 1984; Wolf et al., 1995; Sojka et al., 1995; Pyapali et al., 1998; Horcholle-Bossavit et al., 2000).

Here we present a method for labelling neurons in slices of brain tissue 400-500 μm thick. Slices of adult rat entorhinal cortex were used to electrophysiologically characterize these cells. Neurons were then labelled and visualized without further sectioning the tissue. Permeabilization of the tissue and extended washing steps allow histochemical reagents to penetrate and be washed from the section, generating limited background staining. The quality of staining and clarity of the slice was sufficient to visualize and reconstruct images of the neurons throughout the entire thickness of the slice.

2.4. Materials and methods

Slice Preparation

Brain slices were derived from male Long Evans rats (150 - 300 g) as described previously (Hamam et al., 2000). The block of brain tissue containing the hippocampus and the parahippocampal region was dissected, glued to a small stage (cyanoacrylate glue) and covered with ice cold (4 - 6°C) oxygenated Ringer's solution containing the following: 124 mM NaCl; 5 mM KCl; 1.25 mM NaH_2PO_4; 2 mM $MgSO_4$; 26 mM $NaHCO_3$; 2 mM $CaCl_2$; and 10 mM glucose; saturated with carbogen (95% O_2/5% CO_2) to maintain pH = 7.4. Horizontal 400 μm thick slices containing the hippocampus and

entorhinal cortex were made with a vibratome (Pelco, Redding, Ca). Slices were collected into oxygenated Ringer solution and allowed to recover for at least 2 hours at room temperature before recording. For sharp electrode recording, individual slices were transferred to an interface chamber maintained at 34 ± 1 °C and superfused with oxygenated Ringer at a rate of 1-2 ml/min. For patch electrode recording slices were submerged in a recording chamber and superfused with oxygenated Ringer solution at room temperature.

Recording, Staining, and Mounting Slices

Sharp electrodes and whole-cell patch electrodes for intracellular recording were made with borosilicate glass (Sutter Instruments Co., Novato, CA) using a P-87 Sutter Instruments puller (Sutter Instruments Co.). Sharp electrodes with a tip resistance of 90 - 120 MΩ were filled with 1 % biocytin in 1.5 M K-acetate. Signals were amplified using an Axoclamp 2A amplifier (Axon Instruments, Foster City, CA), viewed on a digital storage oscilloscope and stored on VHS tape for further analysis. Patch electrodes had a tip resistance of 3-5 MΩ after being filled with a solution containing 0.1 % biocytin in 120 mM K^+ gluconate, 3 mM $CaCl_2$, 5 mM NaCl, 2 mM $MgCl_2$, 10 mM HEPES and 10 mM EGTA. Current- and voltage-clamp recordings were performed using an Axopatch 1D amplifier (Axon Instruments, Foster City, CA, USA). Recorded signals were digitized from tape (Neurocorder, New York, NY) and plotted using Axoscope acquisition software (Axon Instruments).

Using sharp electrodes, target neurons were characterized electrophysiologically and at the end of the experiment, negative 0.3 nA current pulses, 300 ms on/off, were

injected into the neurons to facilitate the diffusion of biocytin into cells. This was not required for whole-cell patch electrodes. Recording electrodes were then carefully removed from the cell to avoid damaging the soma, and the slices left in the chamber for an additional 10 - 15 minutes to allow biocytin diffusion into the distal dendrites and axon. Slices were then fixed by immersion in 4 % paraformaldehyde (PFA) in 0.1 M sodium-phosphate buffer (NaPB, pH = 7.5) for 24 - 48 hours at 4 °C.

To visualize the biocytin filled cells we adapted a method that has been used to process intact embryos for whole-mount imunohistochemistry (Kennedy et al., 1994). Following recording and fixation, slices were washed 3 times for 5 minutes each in 200 µl of 0.1 M NaPB. This and all subsequent incubations were carried out in a single well of a standard 24 well plate (Sarstedt, QC), gently agitated on an orbital shaker at room temperature. Endogenous peroxidase activity present in the brain tissue was suppressed by incubating the slices in 1 ml of 1 % H_2O_2 in 70 % methanol for 30 minutes. To block non-specific protein binding sites and permeabilize the cells, slices were then incubated in PHT (0.1 M NaPB, 1 % heat inactivated normal goat serum, 0.3 % triton X-100, pH = 7.5) for at least two hours and then labelled with an avidin-horseradish peroxidase complex (Vector Laboratories, Burlingham, CA) in NaPB overnight at room temperature. The following day, slices were washed with PHT at room temperature: first, brief washes (5 × 3 minutes), then one wash for 30 minutes, followed by 6 × 1 hour and a final wash step overnight. This extensive washing is essential for reducing non-specific background staining. The final day of processing consisted of first, washing the slices in Tris buffered saline pH = 7.6 (TBS, 3 × 10 minutes) and then incubation in 0.5 mg/ml diaminobenzidine (DAB, Vector Laboratories) with nickel chloride (0.04 %) to enhance

the staining. The development of stain intensity was monitored using a dissecting microscope (SV6, Carl Zeiss) and the reaction stopped by washing the slices in TBS (3 × 10 minutes). Before mounting on slides, the stained slices were equilibrated with increasing concentrations of glycerol (25, 40, 55, 70, 85, and 100 %) for one hour at each concentration. The slices were then mounted in 100 % glycerol on glass slides (Superfrost Plus, Fisher). To accommodate the thickness of the tissue slice, a space was cut into a plastic cover slip (Fisher), creating a spacer up to 500 μm deep containing a square hole (figure 1A). Slices were mounted in glycerol in the well of this spacer and coverslipped using a standard glass coverslip (No. 1) that was then sealed in place with glue (cyanoacrylate). Coverslipped slices were routinely stored at 4 °C. Alternatively, fixed tissue equilibrated in glycerol can be stored long-term at –20 °C without degradation of the staining.

Imaging and Reconstruction of Optical Sections

Photomicrographs were taken using a Carl Zeiss Axioscope 2 microscope equipped with a 20 × objective (Zeiss, Plan Neofluar n.a. = 0.50, figures 1 and 3), a long working distance 63 × oil immersion objective (Zeiss, Neofluar n.a. = 1.25, figure 2) and Nomarski optics. A typical reconstruction was made from a stack of 35 to 40 photomicrographs sampled along the Z axis of the section using a Zeiss MC80 camera (figures 1 and 2) and color slide film (Kodak Ektachrome), or using an Optronics (CA) MagnaFire CCD camera (figure 3). The stack of images along the Z axis could be collected using a motor drive; but in this case, the stack was generated by simply manually stepping the focal plane through the slice using the fine focus and collecting

images of the dendritic arbor at different depths. Photographic slides were scanned using a Nikon (LS - 1000) film scanner and Adobe Photoshop software.

The final image is a composite of all of the images in the Z stack. Adobe Photoshop software was used to generate the composite image containing the regions of the neuron in focus at each focal plane photographed. To do this, the photomicrograph with the soma in focus was chosen as the base image. The rubber stamp tool in Photoshop was then used to copy the portions of the neuron in focus from all of the other images into the base image. The Alt key toggles the rubber stamp tool from a painting mode to a sampling mode. To begin to trace a dendrite, the rubber stamp tool was used in sampling mode to select a region of the dendrite in focus. Then in paint mode the rubber stamp tool was used to paint this in-focus region into the base image. By proceeding sequentially through all of the images along the Z axis, the in-focus portions of a dendrite as it meanders through various images in the Z stack were painted into the base image to generate a single composite image. The size of the regions sampled using the rubber stamp tool can be controlled by selecting the appropriate brush options, so that large portions of the dendritic tree can be painted rapidly using a large brush, while fine details in a crowded region of the image can be painted using a smaller brush.

2.5 Results and Discussion

To illustrate the utility of the method described above, we show images of the dendritic trees of neurons from layer V (figures 1 and 2) and layer II (figure 3) of the adult rat entorhinal cortex. Figure 1C illustrates a polymorphic neuron labelled using a sharp intracellular electrode. These cells typically have dendrites radiating away from the soma in almost all directions, but lack an apical dendrite extending into the superficial layers of the entorhinal cortex (Hamam et al., 2000). Panels i - iv of figure 1C are images of this neuron captured at focal planes approximately 5, 40, 70 and 95 % of the distance through the depth of the slice. The clarity of the tissue and contrast of the staining were not significantly affected by imaging through the 400 μm thickness of the tissue (figure. 1C, panel iv). Panel v shows an image of the complete dendritic tree produced by generating a composite image from each of the focal planes collected through the depth of the tissue. An example of the electrophysiological recordings obtained from this neuron is shown in figure 1B, illustrating the current intensity-voltage (I/V) relationship.

This method of processing provided sufficient resolution to visualize minute details of neuronal structure. As an example, individual dendritic spines are clearly visible in the photomicrographs depicted in figure 2. Panel i shows an example of pedunculate spines projecting from a section of a dendrite in a polymorphic neuron, with the head and neck of the spines clearly distinguishable. Figures 2ii and 2iii show another example of clearly visible dendritic spines of two pyramidal neurons. Finally, panel iv illustrates spines projecting from the dendrites of a typical entorhinal cortex layer V pyramidal cell (Hamam et al., 2000).

We have also used this method to visualize the dendritic arbor of neurons following biocytin injection using a patch electrode. Figure 3 shows a stellate neuron in layer II of the entorhinal cortex labeled using a whole-cell patch electrode. These cells have multiple primary dendrites, typically longer and thicker in the apical portion of the dendritic tree than the basal end (Klink and Alonso, 1997). When inserting a patch electrode into the slice, positive pressure is continuously applied to prevent the tip of the electrode from becoming blocked before it reaches the target cell. As a result, biocytin contained in the electrode diffuses into the tissue around the tip of the electrode. In some cases this caused a halo of cell bodies around the recorded cell to be labeled with biocytin (not shown). This was reduced or eliminated using a lower concentration of biocytin in patch electrodes, 0.1% (figure 3) compared to 1.0% biocytin used in sharp electrodes. A technical difficulty associated with patch electrodes was that in a limited number of cases the relatively large size of the patch electrode tip caused a rupture in the target cell soma, presumably at the end of the experiment when the electrode was retracted. In these slices, the dendritic tree was clearly visible following processing, but the soma had been lost.

By not physically sectioning the slice, we eliminated the possibility of introducing many of the errors that can be caused by re-sectioning. For example, the loss of tissue caused by physical sectioning is avoided, and no-disconnected or miss-aligned pieces of the dendritic arbor can be generated during reconstruction. This technique does not involve dehydrating the tissue, and therefore no dramatic shrinkage or distortion of the neuronal geometry is introduced. In practice, almost every neuron that was recorded from for more than 5 minutes could be stained. However, to completely fill the dendritic arbor of a neuron, a minimum of ~15 minutes of electrode penetration was necessary, likely to

allow a sufficient amount of biocytin to diffuse throughout the cell. We have successfully used this staining method with sections up to 500 μm in thickness without any significant decrease in the clarity of the section following processing.

Potential Further Applications of the Method

Here we demonstrate this method using basic equipment found in most electrophysiological laboratories. We adapted this technique from protocols routinely used to perform whole-mount immunohistochemical analysis of intact embryos. Here we used biocytin to label the cell of interest; however it is likely that this method will be applicable to immunohistochemical characterization of injected neurons in slices of tissue. As such, after characterizing the electrophysiological properties of a neuron, it may be possible to map the arborization of its neurites and determine if the neuron expresses a protein of interest. Of course, the quality of the antibody and the characteristics of the antigen will influence the outcome of immunohistochemical applications of this method. Furthermore, the use of triton X-100 for permeabilization prevents sections processed in this way from subsequently being resectioned and used for electron microscopic ultrastructural analysis.

Here we have limited our application of the method to generating a two dimensional flattened composite image of the dendritic tree; however, software packages are available that reconstruct a three dimensional representation of an object from a stack of images and quantify the characteristics of that object, such as the volume or surface area of axons, cell bodies, dendrites, dendritic spines, and synaptic varicosities. The method described here will likely be compatible with this type of analysis.

In the sections of entorhinal cortex, we often saw the axon traveling away from the cell body and projecting out of the plane of the slice (figures 2 and 3). Adapting this method to recordings made *in vivo,* it may be possible to make serial thick sections and map axonal projections from a single cell over relatively long distances. Cutting and staining thick sections instead of the standard 60 μm sections would substantially reduce the effort required to map the trajectory of an axon over long distances. Furthermore, although we have successfully tested this method with sections up to 500 μm in thickness, whole-mount staining of embryos often uses tissue several millimeters in thickness (Kennedy et al., 1994). It may be possible to extend this method to even thicker sections of brain tissue and visualize the structure of interest. In many cases, the limiting factor may be the focal length of the microscope objective used and its ability to visualize structures deep within a thick slice of tissue.

2.6 Conclusion

We describe a simple method for visualizing the dendrites and axon of single neurons following sharp electrode or whole-cell patch electrode recording. Staining is carried out in the intact section of brain tissue that was used for electrophysiological analysis. The method will be useful to investigators interested in the relationship between the electrophysiological properties of a neuron and its structure.

2.7 References

Cannon RC, Turner DA, Pyapali GK, Wheal HV 1998. An on-line archive of reconstructed hippocampal neurons. J Neurosci Methods 84: 49-54.

Capowski JJ 1977. Computer-aided reconstruction of neuron trees from several serial sections. Comput Biomed Res 10: 617-29.

Cullheim S, Kellerth JO 1976. Combined light and electron microscopic tracing of neurons, including axons and synaptic terminals, after intracellular injection of horseradish peroxidase. Neurosci Lett 2: 307-313.

Glaser EM, Van der Loos H 1981. Analysis of thick brain sections by obverse-reverse computer microscopy: application of a new, high clarity Golgi-Nissl stain. J Neurosci Methods 4: 117-25.

Golgi C (1886). Sulla fina anatomia degli organi centrali del sistema nervoso. U. Hoepli: Milano: 215.

Hamam BN, Kennedy TE, Alonso A, Amaral, DG 2000. Morphological and electrophysiological characteristics of layer V neurons of the rat medial entorhinal cortex. J Comp Neurol 418: 457-72.

Horcholle-Bossavit G, Gogan P, Ivanov Y, Korogod S, Tyc-Dumont S 2000. The problem of the morphological noise in reconstructed dendritic arborizations. J Neurosci Methods 95: 83-93.

Horikawa K, Armstrong WE 1988. A versatile means of intracellular labeling: injection of biocytin and its detection with avidin conjugates. J Neurosci Methods 25: 1-11.

Kennedy TE, Serafini T, de la Torre JR, Tessier-Lavigne M 1994. Netrins are diffusible chemotropic factors for commissural axons in the embryonic spinal cord. Cell 78: 425-435.

Klink R, Alonso A 1997. Morphological characteristics of layer II projection neurons in the rat medial entorhinal cortex. Hippocampus 7: 571-583.

Koenderink MJ, Uylings HB 1996. Morphometric dendritic field analysis of pyramidal neurons in the human prefrontal cortex: relation to section thickness. J Neurosci Methods 64: 115-22.

Light AR, Durkovic RG 1976. Horseradish peroxidase: an improvement in intracellular staining of single, electrophysiologically characterized neurons. Exp Neurol 53: 847-53.

McMullen NT, Glaser EM, Tagamets M 1984. Morphometry of spine-free nonpyramidal neurons in rabbit auditory cortex. J Comp Neurol 222: 383-95.

Pyapali GK, Sik A, Penttonen M, Buzsaki G, Turner DA 1998. Dendritic properties of hippocampal CA1 pyramidal neurons in the rat: intracellular staining in vivo and in vitro. J Comp Neurol 391: 335-52.

Sojka M, Davies HA, Rusakov DA, Stewart MG 1995. 3-dimensional morphometry of intact dendritic spines observed in thick sections using an electron microscope. J Neurosci Methods 62: 73-82.

Uylings HB, Van Eden CG, Verwer RH 1984. Morphometric methods in sexual dimorphism research on the central nervous system. Prog Brain Res 61: 215-22.

Uylings HB, Ruiz-Marcos A, van Pelt J 1986. The metric analysis of three-dimensional dendritic tree patterns: a methodological review. J Neurosci Methods 18: 127-51.

Wolf E, Birinyi A, Pomahazi S 1995. A fast 3-dimensional neuronal tree reconstruction system that uses cubic polynomials to estimate dendritic curvature. J Neurosci Methods 63: 137-45.

Yelnik J, Percheron G, Perbos J, Francois C 1981. A computer-aided method for the quantitative analysis of dendritic arborizations reconstructed from serial sections. J Neurosci Methods 4: 347-64.

2.8 Figures

Figure 1: A; schematic of the slide mount constructed to coverslip 400 μm thick slices. On top, the standard microscope slide, standard glass coverslip, and cut plastic coverslip are aligned as explained in the methods. The final result is shown at the bottom. **B;** intracellular recordings derived from the neuron in figure 1C under current clamp conditions. The current intensity-voltage plot in which the membrane potential deflections in response to variable steps of current injection are superimposed is illustrated. **C;** photomicrographs depicting a polymorphic neuron in layer V of the entorhinal cortex of an adult rat. Panels **i, ii, iii** and **iv** show different focal planes sampled from the same neuron, from the top to the bottom of a 400 μm thick slice at approximately 5, 40, 70 and 95 % of the distance through the tissue, respectively. Note that the dendrites in **iv**, though being viewed through almost the full thickness of the slice, can still be clearly visualized. Panel **v** shows a flattened digital reconstruction of the neuron derived from multiple focal planes of which **i-iv** are examples. Scale bar = 100 μm.

A.

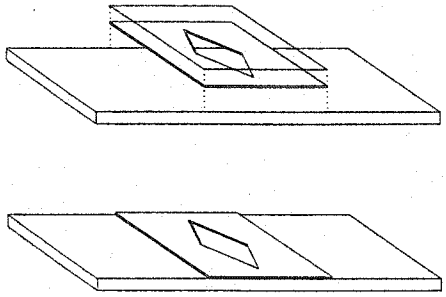

B.

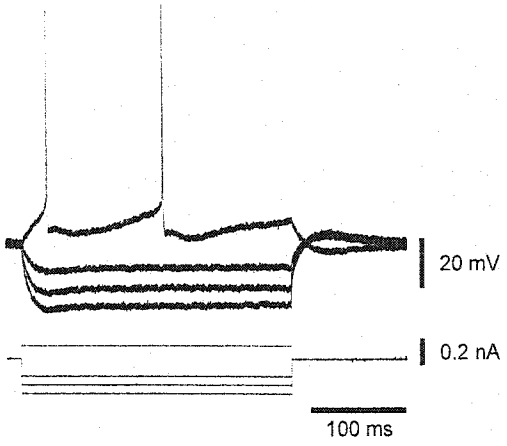

C.

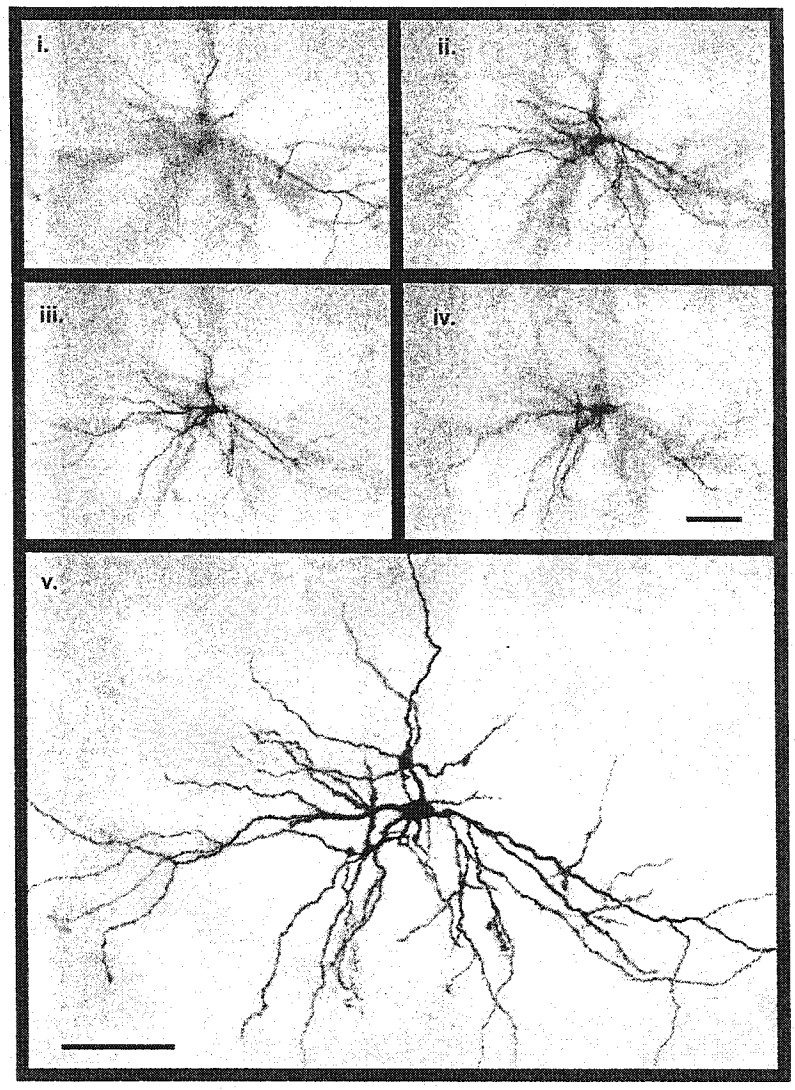

Figure 2: High-magnification photomicrographs of dendrites and dendritic spines from three different neurons in layer V of the entorhinal cortex. Panel **i** shows an example from a polymorphic cell. Panel **ii** is a pyramidal cell dendrite and panels **iii** and **iv** are a second pyramidal neuron. In panel **iv**, the dendritic spines (black arrowheads), the axon (white arrowhead), and the soma are all visible. Scale bar: in **i - iii** = 4 μm; in **iv** = 20 μm.

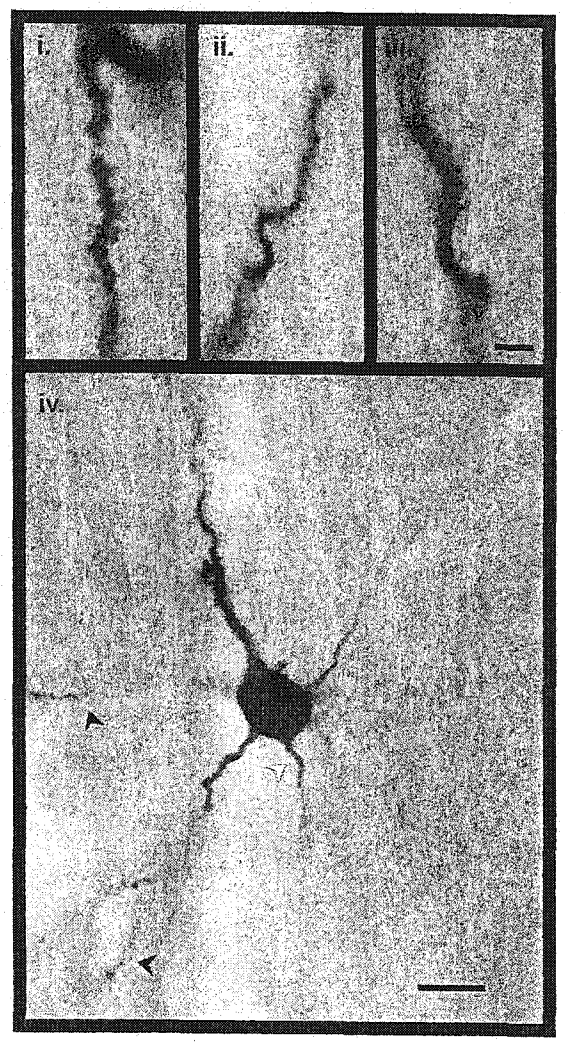
i.
ii.
iii.
iv.

Figure 3: Composite image showing the dendritic tree of a stellate neuron in layer II of the entorhinal cortex labelled using a whole-cell patch electrode. The white arrowhead points to a bead of black staining typical of the cut end of the axon as it exits the tissue slice. Scale bar = 100 μm.

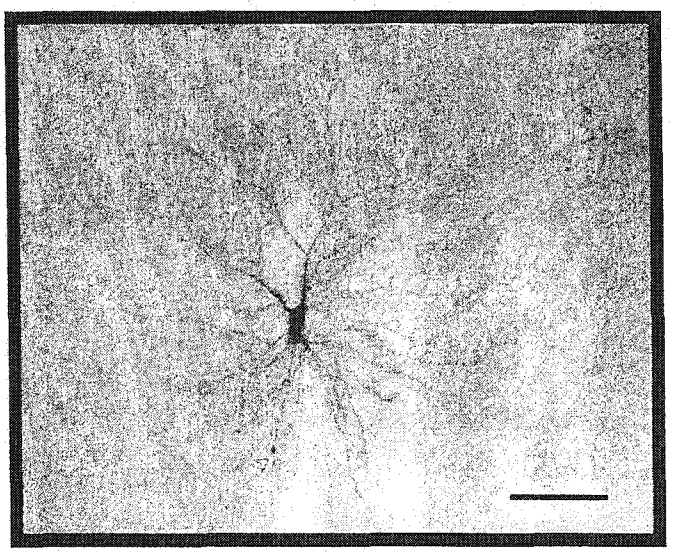

Chapter Three

3. Morphological and Electrophysiological Characteristics of Layer V Neurons of the Rat Medial Entorhinal Cortex

3.1 Preface

After optimizing the previously described histochemical processing technique to our purpose, we applied it in conjunction with current clamp recording to label and record from neurons in layer V of the rat MEA. We chose to investigate cells in MEA because much of the previously described work in the entorhinal cortex has been done in the medial area. More relevant, there were few studies detailing the intrinsic electrophysiological, and in others, morphological properties of layer V neurons in this area. The general idea was that layer V cells of the entorhinal cortex behave in a similar way to neurons in the relevant layer of the neocortex. Thus, the aim of the following study was to characterize the intrinsic electrophysiological and morphological properties of layer V neurons of the entorhinal cortex. The details of our results are presented in this chapter and are discussed in relation to previously published and relevant data.

3.2 Abstract

This study aimed to characterize the morphological and electrophysiological properties of neurons in layer V of the entorhinal cortex in the rat brain. Using the in vitro hippocampal slice preparation and sharp electrode techniques, we recorded from layer V neurons located in the medial entorhinal cortex. Recorded cells were also labelled with biocytin. Based on morphological criteria, layer V of the entorhinal cortex is comprised of three categories of neurons: pyramidal cells, horizontal cells and polymorphic cells. Horizontal cells could be easily distinguished from the pyramidal cells since the bulk of their dendritic plexus extended horizontally within layer V. Polymorphic cells vary in size and shape. Interestingly, they typically do not have apical dendrites and at least some of these had dendrites that extend into the subiculum. Based on electrophysiological criteria alone, it is not possible to unequivocally distinguish the morphological cell types since they were rather heterogeneous with respect to several parameters including inward rectification, spike-frequency adaptation and intrinsic oscillations. Nevertheless, while most horizontal cells displayed time-dependent inward rectification, most pyramidal cells displayed fast inward rectification exclusively. None of the entorhinal cortex layer V cells displayed oscillatory activity like that of neocortical layer V "bursting" cells, though neurons from all groups displayed rhythmic subthreshold membrane potential oscillations. In summary, we have found that layer V of the rat entorhinal cortex consists of three morphologically distinct neuronal subtypes that cannot be clearly distinguished from each other by traditional electrophysiological measures.

3.3 Introduction

It is now well established that the entorhinal cortex occupies a key position as the main input/output interface for neocortical communication with the hippocampus. Via a cascade of cortico-cortical projections, polysensory information from much of the entire cortical mantle converges upon the superficial layers (II and III) of the entorhinal cortex (Jones and Powell, 1970; Room and Groenewegen, 1986; Insausti et al., 1997; Burwell and Amaral, 1998a and b). This information is then relayed to the dentate gyrus, hippocampus and subiculum via the perforant path (Ramon y Cajal, 1902; Steward and Scoville, 1976; Witter and Amaral, 1991; Dolorfo and Amaral, 1998b). The hippocampus and subiculum provide feedback pathways that end primarily upon the deep layers (V-VI) of the entorhinal cortex (Swanson and Cowan, 1977; Sorensen and Shipley, 1979) which, in turn, give rise to long-range projections that project back to the neocortex (Swanson and Kohler, 1986; Insausti et al., 1997). In addition to projecting out of the entorhinal cortex, axons of the deep entorhinal neurons also give off collaterals that innervate the superficial cell layers thereby closing an entorhinal-hippocampal loop (Lorente de No, 1933; Kohler, 1986; Dolorfo and Amaral, 1998a). Layers V and VI of the entorhinal cortex are thus a crucial interface in the neocortical-hippocampal-neocortical circuitry.

Numerous lines of evidence indicate that the hippocampal formation, including the entorhinal cortex, constitutes an essential component of the machinery used to encode so called "declarative" (or episodic) memory in the human brain (Scoville and Milner, 1957; Squire, 1998). A recent theory derived from animal studies suggests that high frequency bursts of activity (the so called "sharp waves") generated by the deep entorhinal cortex layers during sleep may actually constitute part of the mechanism by

which encoded information is consolidated in the neocortex as long term memory (Buzsáki, 1996). If this is the case, the neurons of the deep layers of the entorhinal cortex could significantly contribute to the formation of normal memories and might be a particularly vulnerable point for disruption of the storage of long term memories.

Considerable evidence has accumulated that the entorhinal cortex is also critical in the pathophysiology of temporal lobe epilepsy (Walther et al., 1986; Rutecki et al., 1989; Jones et al., 1992; Stringer and Lothman, 1992; Goldring et al., 1993; Spencer and Spencer, 1994; Bragin et al., 1997; Scharfman et al., 1998). Recent *in vitro* analysis of epileptogenic mechanisms in the entorhinal cortex point out that networks of neurons within layer V can easily be biased to generate hypersynchronous epileptogenic activity (Jones and Heinemann, 1988; Dickson and Alonso, 1997). Discharges of layer V neurons generate prolonged excitatory responses in layer III pyramidal cells (Scharfman, 1996; Gloveli et al., 1997), that degenerate in epilepsy (Du et al., 1993; Du et al., 1995).

The electrophysiological and morphological characteristics of layer V principal neurons in the neocortex have been the subject of numerous investigations. Two main categories of neurons have been established electrophysiologically, "regular" spiking and "intrinsically" bursting neurons which also display distinct morphologies (Connors et al., 1982; Mason and Larkman, 1990; McCormick, 1992; Yang et al., 1996). Intrinsically bursting cells have been proposed to act as "pacemaker" neurons for the generation of epileptogenic events. In the entorhinal cortex, the electrophysiological and morphological characteristics of neurons in layers II and III have been extensively investigated (Alonso and Klink, 1993; Jones, 1994; Gloveli et al., 1997; van der Linden and Lopes da Silva, 1998). However, no comprehensive analysis of the intrinsic electroresponsiveness and

morphological attributes of layer V neurons in the entorhinal cortex has been carried out. In fact, it has often been assumed that layer V neurons in the entorhinal cortex resemble neocortical layer V cells (Jones and Heinemann, 1988; Schmitz et al., 1998).

A detailed understanding of the intrinsic electrophysiological and morphological characteristics of principal neurons in layer V of the entorhinal cortex would be an important step in elucidating the processes by which this cortical layer contributes to normal memory function and to pathophysiological conditions such as epilepsy. The goal of the present study was to carry out such an investigation by means of intracellular recording and biocytin labeling of layer V neurons of the rat entorhinal cortex. We found three morphologically distinct cell types that share a diversity of electrophysiological attributes. None of the recorded cells, however, displayed a profile equivalent to that described for intrinsically bursting cells in the neocortex. Some of the material presented in this study had been previously published in abstract form (Hamam et al., 1997).

3.4 Materials and Methods

General

Brain slices were obtained from male Long Evans rats (150-300 g) using standard procedures (Alonso and Klink, 1993). The animals were decapitated, the brain was quickly removed, and a block of tissue containing the parahippocampal region was placed in cold (4-6°C) oxygenated Ringer's solution containing (in mM): 124 NaCl; 5 KCl; 1.25 NaH_2PO_4; 2 $MgSO_4$; 26 $NaHCO_3$; 2 $CaCl_2$; and 10 mM glucose; pH was maintained at 7.4 by saturation with carbogen (95% O_2/5% CO_2). Horizontal slices containing the entorhinal cortex as well as the rest of the hippocampal formation were cut at 400 μm

thickness using a vibratome (Pelco, Redding, CA). Slices were then incubated in Ringer's solution at room temperature, and after at least 2 hours of recovery, individual slices were transferred into an interface chamber maintained at 34°C ± 1°C and superfused at a rate of 1-2 ml/minute. The layers of the entorhinal cortex were identified with a dissecting microscope by transillumination.

Recording procedures

Intracellular recording electrodes were made from borosilicate glass (Sutter Instruments co., Novato, CA) with a Sutter Instruments puller, P-87 (Sutter Instruments co., Novato, CA). Electrodes were filled with 1% biocytin in 1.5 M K-acetate (tip resistance of 90-120 Megaohms). Signals were amplified using an Axoclamp 2A amplifier (Axon Instruments, Foster City, CA), viewed on-line using a digital storage oscilloscope, and stored on VHS tape (Neurocorder, New York, NY) for further analysis using a 386-based computer. Recorded traces were digitized from tape and plotted using a software acquisition package (Acqui, SICMU, Geneva, Switzerland).

During the recording session we identified layer V and attempted to fill cells confined to the layer. Within this layer, cell bodies visible with transillumination tend to be larger than in layer III. Layer V was often separated from layer III by the cell sparse, fiber rich narrow layer that constitutes the lamina dissecans. The deep border with layer VI is indicated by a change to smaller more densely packed cells. Some layer VI cells were inevitably labeled and these were eliminated from further analysis by examining the stained section with DIC optics which provided a clearer appearance of the border

between layers V and VI. All neurons were recorded from the dorsal 2/3rds of the medial entorhinal cortex (Blackstad, 1956).

Impaled neurons were first characterized electrophysiologically under current clamp conditions, then injected with biocytin using 0.3 nA, (0.3 second) negative current pulses delivered every 0.6 second. At the end of the experiment, electrodes were carefully removed from the recorded cell and slices were kept in the chamber for an additional 15-20 minutes to allow biocytin transport into distal processes. Following this, slices were transferred into 4% paraformaldehyde (PFA) in 0.1 M sodium-phosphate buffer (NaPB, pH=7.5) and fixed for 24 to 48 hours at 4°C.

Histochemical Processing

Adapting a protocol used for embryo whole-mount immunohistochemistry (Kennedy et al., 1994) fixed slices were removed from PFA, washed with 0.1 M NaPB (3 X 5 minutes), and processed without further sectioning. To suppress endogenous peroxidase activity, slices were incubated in 1 % H_2O_2 in 70 % methanol for 30 minutes at room temperature and then washed with 0.1 M NaPB (3 X 5 minutes). Non-specific binding sites were blocked by incubation in PHT (1% normal goat serum, 0.3 % triton X-100, 0.1 M NaPB; pH=7.5) for at least two hours at room temperature and then labeled with an avidin-biotin-horseradish-peroxidase complex (Vector Laboratories, Burlingame, CA) in NaPB overnight at room temperature.

The following day, slices were extensively washed in PHT: first, brief washes (5 X 3 minutes), followed by 1 X 30 minutes, and then long washes (6 X 1 hour), and finally a wash overnight. Slices were then washed with 0.1 M tris buffered saline pH=7.6 (TBS)

(3 X 10 minutes) and incubated in 0.5 mg/ml diaminobenzidine (DAB, Vector Laboratories, Burlingame, CA). Nickel (0.04%) was added to the DAB to intensify the reaction product. The DAB reaction was halted by washing the slices in TBS (3 X 10 minutes). Finally, the slices were equilibrated in increasing concentrations of glycerol (25, 40, 55, 70, 85,100 %) and stored in 100 % glycerol at room temperature.

In order to obtain high magnification photomicrographs of dendritic spines, the 400 μm slices were embedded in paraffin and resectioned. Slices stored in glycerol were washed briefly in PBS pH=7.5 at room temperature, and then post-fixed overnight in 4% PFA in PBS at 4 °C. Slices were then equilibrated in an ethanol series (70%, 95%, 100%, 100% 20 minutes each) at room temperature, then equilibrated in xylene overnight at room temperature, followed by equilibration in paraffin overnight at 60 °C. The slice was then embedded in paraffin (Formula R, Surgipath), 7 μm sections cut on a microtome, mounted onto Superfrost + slides (Fisher), dewaxed by immersion in xylene, and coverslipped with Permount (Fisher). Photomicrographs were taken using an Zeiss Axiophot microscope equipped with Nomarski optics.

Data analysis

The current and voltage (I-V) relationship plots were made with Origin software for data analysis (Origin, Microcal Software, Northampton, MA); power spectrums for the membrane potential oscillatory activity were made with the Matlab data analysis program (Matlab, The Math Works, Natick, MA). Neurons were reconstructed in 3-D using the neuron tracing system (Neurolucida, Microbrightfield Inc., Colchester, VT) from which the quantitative data related to neuronal cell bodies and dendrites were

obtained. Photomicrographs were taken at various depths through the slice using a Leitz DMR microscope. Negatives were scanned using a Polaroid Sprintscan Plus slide scanner and Adobe Photoshop software. Neuronal segments that were in focus in each negative were digitally reconstructed to produce the half tone montages that are depicted in Figs. 2A, 7A, and 9A.

The input resistance was measured from the voltage deflection in response to a 0.1 nA negative current pulse injection, and the time constant was calculated as the time it took the voltage deflection to reach 63% of its maximal response. The spike amplitude was measured from threshold to peak and the duration was calculated at the threshold level. In addition, the afterhyperpolarization (AHP) amplitude was calculated from the threshold of the action potential to the peak of the AHP. Finally, the time dependent rectification was presented as "sag" percentage (Sag% or rectification index), which was calculated as the percentage difference between the voltage response at peak and steady state to a current pulse that induced about -25 mV voltage deflection. Only neurons in which sag percentages greater than 5 % could be measured were considered to present time-dependent inward rectification.

3.5 Results

The results are based on observations of 62 labelled neurons from layer V of the medial entorhinal cortex. We have defined layer V in accordance with Ramon y Cajal (1902). His layer V, located just subjacent to layer IV (lamina dissecans) consisted mainly of horizontally oriented or spindle shaped cells but we also include the band of pyramidal cells that forms what Lorente de No has called the layer of deep pyramidal

cells (Lorente de No, 1933). Data were taken from neurons that were stable for at least 15 minutes during intracellular recording. After the neurons were electrophysiologically characterized, they were injected with biocytin for subsequent morphological analysis. All recorded neurons had resting membrane potentials of at least -55 mV, and apparent input resistance larger than 30 MΩ, and an overshooting spike.

As summarized in Figure 1, layer V neurons constitute a heterogeneous population in which we could distinguish three distinct morphological cell types. The first category of neuron (n=38) has a pyramidal cell appearance (Fig. 1A). The second category consists of cells (n=15) that, like the pyramidal cells, have a distinct apical dendrite but, unlike the pyramidal cells, have a basal dendritic plexus that extends predominantly and for long distances in the horizontal plane. These dendrites remain, for the most part, within the limits of layer V. We refer to this second category as horizontal cells (Fig. 1B). The rest of the labelled layer V cells (n=9) were distinct from pyramidal and horizontal cell types in that they typically had a multipolar dendritic arborization and polymorphic somatic cell shape. We named this category polymorphic cells (Fig. 1C).

With respect to the intrinsic electroresponsiveness of these neurons, most of the layer V entorhinal cells fall within the broad category of "regular" spiking cells. However, we found that they were nevertheless very heterogeneous with respect to several electrophysiological parameters such as spike-frequency adaptation, inward rectification and expression of intrinsic oscillations. None of the activity recorded from layer V cells was typical of neocortical layer V "bursting" neurons. Thus, while the recorded cells could be easily categorized morphologically, we did not find an

unequivocal correlation between the three morphological cell types and profiles of electrophysiological attributes.

Several electrophysiological parameters, including voltage-current relationships, apparent input resistance, spike amplitude and waveform and subthreshold oscillations were analyzed for all neurons. Tables 1 and 2 provide a summary of some of the basic morphological and electrophysiological parameters, respectively, that correspond to the three morphological cell types. Our detailed description of layer V neurons begins with the most prominent cell type, the pyramidal cell, continues with the horizontal cell and concludes with a description of some of the polymorphic neurons that were observed. Morphological and electrophysiological attributes are integrated for each category of neuron.

Pyramidal Cells

Pyramidal cells were the most common cell type that we encountered in layer V. The 38 pyramidal cells that we labelled accounted for 61% of the total labelled cells. This population was composed of neurons with a rather wide range of somal sizes. Differences in somal size were reflected in the range of cross sectional areas that were measured in the 10 pyramidal cells that were subjected to quantitative analysis. The cross sectional areas ranged from a low of 151 μm^2 to a high of 337 μm^2. Examples of pyramidal cells with relatively large somas are illustrated in Figures 1A, 3A and 4C, and an example of a pyramidal cell with small soma is illustrated in Figure 2A.

In all pyramidal cells, a prominent apical dendrite was directed towards the pial surface. The apical dendrite occasionally gives off a few branches close to the soma that

mainly stay within layer V. But most of the branching takes place at the distal extreme of the apical dendrite within the superficial aspect of layer II and within layer I. In fact, the apical dendrites typically do not branch at all within layer III or within the deep half of layer II. In this respect, the neuron illustrated in Figure 1A is very characteristic. The basal dendrites extend rather profusely in all directions within layers V and VI. The pyramidal cells with small soma tended to have a greater number of basal dendritic branches and at least some of these basal dendrites extended farther than those of the large pyramidal cells.

We also noticed that pyramidal cells with small somas appeared to have larger and more densely distributed spines than those with larger somas (Fig. 2A, lower inset). Since these neurons were analyzed in the unsectioned 400 μm slice, it was difficult to quantitatively evaluate the size and density of the spines. Yet the longer spine lengths appeared to be a typical feature of the small pyramidal cells. Further detailed analysis will need to be carried out in order to determine whether the longer dendritic spines distinguish a specific population of pyramidal cells with small cell bodies. The axon of these pyramidal cells could usually be followed through the deep layers of the entorhinal cortex and towards the angular bundle. Typically, several branches were made but could not be followed very far from the cell body.

Pyramidal cells were electrophysiologically heterogeneous and shared a number of properties with the other cell types located in layer V. As is the case for the cell illustrated in figure 2, we found a large proportion of pyramidal cells that displayed fast, but not time-dependent, inward rectification (Fig. 2B and C) as well as a monophasic single spike AHP (Fig. 2B, inset). Similar to what was observed in horizontal cells and

polymorphic cells (see below) many pyramidal cells (Fig. 3A) did, however, display time-dependent inward rectification as evidenced by the depolarizing "sag" evoked by membrane hyperpolarization (Fig. 3B) and the upward bending of the steady-state voltage-current relation (Fig. 3D). We obtained an index for this rectification by estimating the percent change in membrane potential from the early peak to steady state during ~ 25mV hyperpolarizing current steps. In 18 pyramidal cells where significant rectification was detected, this index (sag percentage) was 13.9 ± 5.8 (mean ± s.d.; range, 5.2 – 25.5). Interestingly, pyramidal cells that displayed time-dependent inward rectification also tended to discharge with spike-doublets as the early response to a step depolarization and to display a biphasic single spike AHP (Fig. 3B, inset).

Different from the entorhinal cortex, a subpopulation of layer V neocortical pyramidal cells display a robust intrinsic bursting discharge (Connors et al., 1982) which is largely dependent on the activation of Ca^{2+} conductances (Gutnick, 1982). Firing with a spike-doublet was not only observed in some pyramidal cells (Fig. 3B), but also in some horizontal cells (Fig.6B) and polymorphic cells. This feature represents firing behavior that is reminiscent of that displayed by neocortical bursting cells. We have never observed, however, repetitive discharge in spike-doublets, and the spike-doublet firing we typically saw in these cells is primarily dependent on the activation of Na^{+} conductances and not Ca^{2+} conductances (not shown).

With respect to spike-frequency adaptation, pyramidal cells that displayed time-dependent inward rectification also tended to display little adaptation (Fig. 3C), while those which manifested only fast inward rectification displayed from moderate (Fig. 4A) to very robust (Fig. 4C) levels of adaptation. Interestingly, pyramidal cells that display

clear adaptation, also manifested the presence of rhythmic subthreshold membrane potential oscillations when the cells were depolarized from their resting level close to firing threshold (Fig. 4B). The frequency of these oscillations at about -54 mV ranged from 4.0 to 14.8 Hz and had an amplitude of 2 to 7 mV (n=25).

Horizontal cells

Computer-aided reconstructions of typical horizontal cells are shown in Figures 1B and 6A. A horizontal cell is documented photomicrographically in Figure 7A1 and 2. Fifteen cells of this type were labeled and thus constituted approximately 24% of the population of cells that were observed. Horizontal cells are similar to pyramidal cells in that both cell types have a prominent apical dendrite as well as a basal dendritic tree. However, the basal dendritic tree of the horizontal cells extends mainly in the horizontal plane. The horizontally oriented dendritic plexus of these cells was essentially confined to the borders, even following the curvature, of layer V. Some of these dendrites extended for long distances (up to 1 mm from the cell body). In order to quantitatively assess the differences, in terms of dendritic arborization, between horizontal cells and pyramidal cells we performed a Sholl analysis that involved counting the number of basal dendritic intersections with the surface of spheres increasing in radius (20 μm steps) centered on the cell body. The results of this analysis are shown in Figure 5. Panel A depicts the Sholl analysis procedure utilized with a horizontal cell at the center of concentric spheres of increasing diameter. In panel B, the average number of dendritic intersections for both pyramidal cells (filled triangles) and horizontal cells (empty circles) is plotted as a function of the distance from the cell body. Both cell types branch mostly within a radius

of about 400 μm from the cell body, but the number of dendritic branches is larger for the horizontal cells than for the pyramidal cells. While panel B shows that horizontal cells have a more prominent basal dendritic plexus than the pyramidal cells, it does not show the differences in basal dendritic orientation. To address this issue, we estimated the percentage of dendritic intersections below an imaginary plane 100 μm deep to the horizontal plane through the cell body (panel A). While, as shown by the histogram in panel C, the pyramidal cells have 20 ± 14% of their intersections located in the sampled region, the horizontal cells only display 4 ± 6.6% 100 μm below the cell body ($P < 0.05$; independent *t*-test). This indicates that far fewer of the basal dendrites are oriented deep to the cell body in the horizontal cells than in the pyramidal cells.

Horizontal cells also differ from the pyramidal cells in that their soma is not pyramidally shaped (Fig. 7A). Moreover, while the apical dendrites of horizontal cells do extend to the pial surface, they tend to be only slightly thicker than the remaining dendrites. The pyramidal cell apical dendrites are typically much thicker than the basal dendrites. And, in contrast to the pyramidal cells, the apical dendrite often branches within layer III or within the deeper portion of layer II and then gives rise to additional, higher order branches in layer I. All of the dendrites of the horizontal cells are sparsely covered with spines; these are more abundant along the apical dendrite than along the rest of the primary dendrites. The axon of the horizontal cells was always found to travel towards the angular bundle (Fig. 1C and 6A) and give off branches extending into layers V-VI.

As with the other layer V cell groups, the horizontal cells are electrophysiologically heterogeneous. Nevertheless, as for the cell illustrated in Figure 6

(and a salient feature with respect to the other cell groups), the vast majority of horizontal cells (n=13) displayed time-dependent inward rectification (Fig. 6B and D). The rectification index ranged from 6 to 29 with an average value of 15.5 ± 6.14. With respect to the spike afterpotentials, most of the horizontal cells (n=10) displayed a biphasic AHP with usually a minor depolarizing afterpotential (Fig. 6B; inset).

The analysis of the discharge behavior of the horizontal cells in response to long step depolarizations revealed a wide range in the degree of spike frequency adaptation. While some horizontal cells displayed minimal spike frequency adaptation (Fig. 6C), others responded to step depolarizations with a rapidly adapting spike train that could be followed by a pronounced slow AHP (Fig. 7B1 and 2).

Interestingly, as observed with the pyramidal cells (see above), those horizontal cells that displayed robust spike-frequency adaptation also tended to express robust subthreshold membrane potential oscillations upon d.c. membrane depolarization (n=4). The frequency of the subthreshold oscillations at about –54 mV ranged from 3.4 to 11.2 Hz and was thus very similar to that of the pyramidal cells. A typical case of subthreshold oscillations in a horizontal cell is illustrated in Figure 8 (same cell as Fig. 7B). Panel A illustrates the changes in membrane potential of the horizontal cell as the membrane potential (upper trace) is progressively depolarized by d.c. current injection (lower trace). Note the progressive increase in apparent membrane noise (reflecting the emergence of subthreshold oscillations) as the membrane potential approaches firing level. With strong depolarization, the firing does not become tonic but the spikes tend to cluster and intermingle with subthreshold oscillations (inset to the left). The progressive increase in oscillatory activity and the emergence of its rhythmic character with membrane

depolarization is shown in panel B. Traces "a" to "e" correspond to the periods marked in Panel A. Note that clear rhythmic oscillatory activity (as assessed by the autocorrelation function of the membrane potential) emerged at level "c" at an initial frequency of about 10Hz. The oscillatory frequency increases with membrane depolarization to about 15 Hz (level "e").

Polymorphic cells

Neurons that made up this group (n=9) were morphologically very different from pyramidal and horizontal cells. They have numerous primary dendrites that are oriented in all directions, branch repeatedly and travel for long distances (Figs. 9A and D). In contrast to the other cell groups, polymorphic cells generally do not have a prominent apical dendrite. In some polymorphic cells, some of the primary dendrites are longer than the others, but these longer dendrites travel in any direction either within the deep layers (Fig. 9A) or obliquely towards layer III. In one polymorphic neuron (Fig. 10A), a prominent dendrite extended through the angular bundle and into the pyramidal cell layer of the subiculum. At least one other neuron had dendrites with similar trajectories (Fig. 10B). Typical pedunculate, short spines are distributed along the dendrites of this cell type. The axons of these neurons usually projected into, or in the direction of, the angular bundle.

As in the other cell types, the electrophysiological profile of the polymorphic cells is rather heterogeneous. While most of these cells display instantaneous inward rectification (Fig. 9B), only a few (n=4) display time-dependent inward rectification (Fig. 9E). In some cells the spike AHP was monophasic, while in others it was biphasic (not shown). While in some cells spike-frequency adaptation was robust (Fig. 9C), in others it

was very weak (Fig. 9F). Finally, robust, low-frequency subthreshold oscillations (4 to 12 Hz at about –54 mV) were also observed in most cases (n= 6) (Fig. 9C), though they lacked apparent spike clustering.

3.6 Discussion

The entorhinal cortex occupies a pivotal position as the neocortical-hippocampal interface and is likely to play a central role in normal memory function (Scoville and Milner, 1957; Zola-Morgan and Squire, 1993; Klingberg et al., 1994; Alvarez et al., 1995; Fernandez et al., 1999) as well as in the pathophysiology of temporal lobe epilepsy (Wilson et al., 1988; Spencer and Spencer, 1994; Dickson and Alonso, 1997; Engel et al., 1997). Paraphrasing Ramon y Cajal (1902), if one understands the function of the entorhinal cortex then one will gain substantial insight into the function of the entire hippocampal formation. Morphological and electrophysiological analysis of the entorhinal cortex has lagged behind studies of the other hippocampal fields but is clearly essential for understanding its information processing capacity. This study continues previous work on the morphological and electrophysiological attributes of entorhinal neurons (Alonso and Klink, 1993; Dickson et al., 1997; Klink and Alonso, 1997) that focused on layers II and III of the rat entorhinal cortex.

In the present study, we focused on neurons in layer V. We found that the neuronal population in this cortical layer is both morphologically and electrophysiologically more complex than previously demonstrated (Jones and Heinemann, 1988; Lingenhöhl and Finch, 1991; Gloveli et al., 1997). Indeed, we found three clearly distinct morphological cell types and a wide spectrum of

electrophysiological profiles. Our data suggest that layer V of the entorhinal cortex may play a much more significant role in the processing of hippocampal inputs and outputs than previously appreciated.

With regard to previous morphological analysis of layer V neurons, Ramon y Cajal (1902) described three Golgi-stained layer V cell types in his preparations. These he described as having "a globular body with one or two thick lateral dendrites of horizontal course". Lorente de No (1933), made a more extensive Golgi analysis of this layer and reported that "pyramidal cells" were the most numerous cell type in this layer. His description of the layer V pyramidal cells stated that "the ascending shaft is thin and neither does it give off any branch in the third and second layers nor ramifies itself in the first layer". Here, we found that the apical dendrites of both the pyramidal cells and the horizontal cells invariably branched within layers II and I. The apical dendrites of the horizontal cells but not the pyramidal cells sometimes branched in the deep part of layer II and in layer III. Lorente de No also described a group of "polygonal cells" and another group of "star cells" which resemble some of the neurons that we have included in our pyramidal cell category. However, Lorente de No indicated that his star and polygonal cells have an ascending axon. We could not follow the axons of labeled pyramidal cells for long distances but most were directed towards the angular bundle.

The most extensive and detailed morphological analysis of neurons in the rat entorhinal cortex is the in vivo intracellular labeling study by Lingenhold and Finch (1991). These authors studied 24 neurons injected with horseradish peroxidase that were distributed throughout all layers of the rat entorhinal cortex. Their observations of neurons located in or adjacent to layer V (their layers IV and V) were generally consistent

with our current results. They indicated, for example, that the basal dendritic trees of at least some of their "large pyramidal cells" were maintained largely within layer V and oriented parallel to the cell layers (see their figure 6). These appear to resemble our horizontal cells. They also described a single nonpyramidal cell that had dendrites extending into the angular bundle; this is reminiscent of some of the polymorphic cells that we observed. They also reported a "spindle shaped cell" that had both a small cell body with an apical dendrite extending to the pial surface and a basal dendritic plexus that extended through the angular bundle and into the subiculum. The polymorphic cells that we describe having dendrites that extend into the subiculum did not have apical dendrites. Close examination of these cells at high magnification convinced us that there was no truncation of an apical dendrite during preparation of the slice. In fact, most of the neurons that we labeled had cell bodies that were located near the middle of the slice. Their "spindle shaped cell" also resembles our small pyramidal cells and raises the possibility that some of the distal basal dendrites of the small pyramidal cells (that appeared to extend farther from their cell body than those of the large pyramidal cells) may have been transected. It would be useful to have a larger sample of in vivo labeled neurons to resolve this issue.

Previous electrophysiological studies (Jones and Heinemann, 1988) have classified entorhinal cortex layer V neurons into three categories based on studies carried out in the neocortex, i.e., non-bursting cells that fire tonically in response to a depolarizing current pulses; bursting cells that have a depolarizing envelop carrying a train of decrementing action potentials in response to a strong depolarizing current pulse injection; and fast spiking cells in which the frequency of action potentials in response to

a depolarizing current pulse is high and in some cases incrementing at the end of a prolonged depolarizing injection. While many of the neurons we recorded could be loosely considered as regularly spiking neurons, clearly, none of them had the typical attributes of cortical bursting cells such as those present in layer V of the neocortex or the hippocampal CA3 subfield (Kandel and Spencer, 1961; Connors et al., 1982; Agmon and Connors, 1989; Connors and Gutnick, 1990). The closest resemblance was from a few cells that discharged with a low-threshold doublet and these may correspond to those classified as layer V bursting neurons by Jones and Heinemann (1988). However, while Ca^{2+} conductances appear to be implicated in the intrinsic bursting activity of neocortical and hippocampal CA3 pyramidal cells (Wong and Prince, 1978), the low-threshold doublets of entorhinal cortex layer V neurons may be strictly Na^{+}-dependent (unpublished observations).

We did not find a clear cut electrophysiological distinction between different morphological cell types in layer V as has been observed in layer II of the entorhinal cortex (Alonso and Klink, 1993; van der Linden and Lopes da Silva, 1998). Distinct electrophysiological profiles of neocortical layer V neurons have also been correlated with different morphological attributes (Chagnac-Amitai et al., 1990; Connors and Gutnick, 1990; Yang et al., 1996). However, the final electrophysiological profile of a particular neuron is a complex result emerging from the details of its dendritic structure, as well as the array of ion channels it possess and the somato-dendritic distribution of these channels (Mainen and Sejnowski, 1996). It is not surprising, therefore, that neurons with equivalent morphological attributes have distinct electrophysiological profiles, or vice versa.

Perhaps, one of the most interesting electrophysiological characteristics of many of the recorded neurons was the presence of rhythmic subthreshold membrane potential oscillations. A similar observation was recently made by Schmitz et al. (1998) who reported the presence of subthreshold oscillations in entorhinal cortex layer V pyramidal cells. We found, however, that subthreshold oscillations were not unique to pyramidal cells but were also present in the horizontal cells and polymorphic neurons. The averaged frequency of these oscillations was very similar in the three cell types and ranged from 3.4 to 14.8 Hz at about -54 mV. Within the entorhinal cortex, this type of pacemaker activity was originally described in the stellate cells of layer II (Alonso and Llinas, 1989; Alonso and Klink, 1993; Klink and Alonso, 1993). In the stellate cells, subthreshold oscillations depend largely on the interplay of a persistent Na^+ current (I_{NaP}) and an inward rectifying non-specific cationic current (I_h) (Alonso and Llinas, 1989). Similar to layer II cells, entorhinal cortex layer V neurons also posses a prominent I_{NaP} (unpublished observations). However, I_h is unlikely to have any significant role in the generation of subthreshold oscillations by layer V neurons since many neurons displayed robust subthreshold oscillations and no I_h, and the degree of time-dependent inward rectification of layer V cells is minimal when compared to that of layer II stellate cells (~ 15% vs. 50%, respectively) (Alonso and Klink, 1993).

What might the role of the subthreshold oscillations be? Considerable evidence indicates that the subthreshold oscillatory activity displayed by the entorhinal cortex layer II stellate cells is a determining mechanism for the genesis of theta rhythmicity by the layer II network (Alonso and García-Austt, 1987; Alonso and Llinas, 1989; Chrobak and Buzsaki, 1994). Though it is generally assumed that theta field activity in the entorhinal

cortex is exclusively generated by the superficial cell layers, rhythmic theta cells have also been observed in the deep layers (Alonso and García-Austt, 1987). In this respect, it is well known that during periods of cortical activation and theta rhythm, the basal forebrain cholinergic system is activated (Celesia and Jasper, 1966) and layer V of the entorhinal cortex does receive a very robust cholinergic innervation from the basal forebrain (Milner et al., 1983; Alonso and Köhler, 1984; Lysakowski et al., 1989). Significantly, we have observed that muscarinic activation depolarizes layer V neurons and brings them into the range of subthreshold oscillatory activity (Hamam et al., 1997). In vitro, muscarinic depolarization of layer V cells does, in fact, lead to synchronous population activity of the entorhinal cortex network paced by layer V cells (Dickson and Alonso, 1997).

It has been argued that intrinsically bursting cells from layer V in the neocortex are critical for the genesis of epileptiform discharges (Connors et al., 1982; Gutnick, 1982). However, even though layer V of the entorhinal cortex is highly epileptogenic (Jones and Heinemann, 1988; Jones and Lambert, 1990; Dickson and Alonso, 1997), it seems to lack overtly bursting cells. Moreover, intrinsic bursting activity in entorhinal layer V neurons does not develop during processes such as cholinergic activation (Hamam et al., 1997), that do lead to the production of epileptiform activity (Dickson and Alonso, 1997). It seems, therefore, that epileptogenic mechanisms in entorhinal cortex layer V do not depend on intrinsic cellular bursting mechanisms. We propose that they may arise from specialized synaptic interactions between layer V cells, and that subthreshold oscillations may play a role in the synchronization process (Silva et al., 1991).

In summary, neurons from layer V of the entorhinal cortex constitute a more complex neuronal population than previously described. Additional information is needed to determine the chemical neuroanatomy of the described neurons, the distribution of their axonal connections and their pharmacological attributes. It will be of interest to determine which of these neurons contribute to the associational connections between layer V and layers II and III as well as to determine with which neurons the layer V neurons are monosynaptically connected. All of these pieces of information will provide an essential framework for determining the role of layer V neurons in hippocampal information processing and their contribution to normal memory function. This may be particularly important in understanding the pathophysiology of dementing disorders such as Alzheimer's disease where layer V neurons suffer early and near total devastation.

3.7 References

Agmon A, Connors BW. 1989. Repetitive burst-firing neurons in the deep layers of mouse somatosensory cortex. Neurosci Lett 99: 137-141.

Alonso A, García-Austt E. 1987. Neuronal sources of theta rhythm in the entorhinal cortex of the rat. II. Phase relations between unit discharges and theta field potentials. Exp. Brain Res. 67: 502-509.

Alonso A, Klink R. 1993. Differential electroresponsiveness of stellate and pyramidal-like cells of medial entorhinal cortex layer II. J. Neurophysiol. 70: 128-143.

Alonso A, Köhler C. 1984. A study of the reciprocal connections between the septum and the entorhinal area using anterograde and retrograde axonal transport methods in the rat brain. J. Comp. Neurol. 225: 327-343.

Alonso A, Llinas RR. 1989. Subthreshold Na^+-dependent theta-like rhythmicity in stellate cells of entorhinal cortex layer II. Nature 342: 175-177.

Alvarez P, Zola-Morgan S, Squire LR. 1995. Damage limited to the hippocampal region produces long-lasting memory impairment in Monkeys. J. Neurosci. 15: 3796-3807.

Blackstad TW. 1956. Commissural connections of the hippocampal region in the rat, with special reference to their mode of termination. J Comp Neurol 105: 417-537.

Bragin A, Csicsvari J, Penttonen M, Buzsaki G. 1997. Epileptic afterdischarge in the hippocampal-entorhinal system: Current source density and unit studies. Neurosci 76: 1187-1203.

Brown DA, Adams PR. 1980. Muscarinic suppression of a novel voltage-sensitive K current in a vertebrate neuron. Nature 183: 673-676.

Burwell RD, Amaral DG. 1998a. Cortical afferents of the perirhinal, postrhinal, and entorhinal cortices of the rat. J Comp Neurol 398: 179-205.

Burwell RD, Amaral DG. 1998b. Perirhinal and postrhinal cortices of the rat: interconnectivity and connections with the entorhinal cortex. J Comp Neurol 391: 293-321.

Buzsáki G. 1996. The hippocampo-neocortical dialogue. Cerebral Cortex 6: 81-92.

Celesia GG, Jasper HH. 1966. Acetylcholine released from cerebral cortex in relation to state of activation. Neurology (Minneap) 16: 1053-1070.

Chagnac-Amitai Y, Luhmann HJ, Prince DA. 1990. Burst generating and regular spiking layer 5 pyramidal neurons of rat neocortex have different morphological features. J Comp Neurol 296: 598-613.

Chrobak JJ, Buzsaki G. 1994. Selective activation of deep layer (V-VI) retrohippocampal cortical neurons during hippocampal sharp waves in the behaving rat. J. Neurosci. 14: 6160-6170.

Connors BW, Gutnick MJ. 1990. Intrinsic firing patterns of diverse neocortical neurons. Trends Neurosci. 13: 99-104.

Connors BW, Gutnick MJ, Prince D. 1982. Electrophysiological properties of neocortical neurons in vitro. J. Neurophysiol. 48: 1302-1320.

Dickson CT, Alonso A. 1997. Muscarinic induction of synchronous population activity in the entorhinal cortex. J. Neurosci. 17: 6729-6744.

Dickson CT, Mena AR, Alonso A. 1997. Electroresponsiveness of medial entorhinal cortex layer III neurons *in vitro*. Neuroscience 81: 937-950.

Dolorfo CL, Amaral DG. 1998a. Entorhinal cortex of the rat: organization of intrinsic connections. J Comp Neurol 398: 49-82.

Dolorfo CL, Amaral DG. 1998b. Entorhinal cortex of the rat: topographic organization of the cells of origin of the perforant path projection to the dentate gyrus. J Comp Neurol 398: 25-48.

Du F, Tore E, Kohler C, Lothman EW, Schwarcz R. 1995. Preferential neuronal loss in layer III of the medial entorhinal cortex in rat models of temporal lobe epilepsy. J. Neurosci. 15: 8301-8313.

Du F, Whetsell WO, Abou-Khalil B, Blumenkopf B, Lothman EW, Schwarcz R. 1993. Preferential neuronal loss in layer III of the entorhinal cortex in patients with temporal lobe epilepsy. Epilepsy Res. 16: 223-233.

Engel JJ, Williamson PD, Wieser H-G. 1997. Mesial temporal lobe epilepsy. In: Engel JJ, Pedley TA, eds. Epilepsy: A Comprehensive Textbook. Philadelphia: Lippincott-Raven. p 2417-2426.

Fernandez G, Brewer JB, Zhao Z, Glover GH, Gabrieli JD. 1999. Level of sustained entorhinal activity at study correlates with subsequent cued-recall performance: a functional magnetic resonance imaging study with high acquisition rate [In Process Citation]. Hippocampus 9: 35-44.

Gloveli T, Schmitz D, Empson RM, Dugladze T, Heinemann U. 1997. Morphological and electrophysiological characterization of layer III cells of the medial entorhinal cortex of the rat. Neurosci 77: 629-648.

Goldring S, Edwards I, Harding.G.W., Bernardo KL. 1993. Temporal lobectomy that spares the amygdala for temporal lobe epilepsy. Epilepsy Surg 4: 263-272.

Gutfreund Y, Yarom Y, Segev I. 1995. Subthreshold oscillations and resonant frequency in guinea-pig cortical neurons: physiology and modelling. J. Physiol. (Lond.) 483: 621-640.

Gutnick MJ, Connors, B.W. and Price, D. 1982. Mechanisms of neocortical epileptogenesis in vitro. J. Neurophysiol. 48: 1321-1335.

Hamam BN, Dickson CT, Alonso A. 1997. Electrophysiological characterization and cholinergic modulation of entorhinal cortex (EC) layer V neurons in rat brain slices. Soc. Neurosci. Abstr. 23: 488.

Insausti R, Herrero MT, Witter MP. 1997. Entorhinal cortex of the rat: cytoarchitectonic subdivisions and the origin and distribution of cortical efferents. Hippocampus 7: 146-183.

Jones EG, Powell TPS. 1970. An anatomical study of converging sensory pathways within the cerebral cortex of the monkey. Brain 93: 793-820.

Jones R, S.G. 1994. Synaptic and intrinsic properties of neurons of origin of the perforant path in layer II of the rat entorhinal cortex in vitro. Hippocampus 4: 335-353.

Jones RSG, Heinemann UFH, Lambert JDC. 1992. The entorhinal cortex and generation of seizure activity: Studies of normal synaptic transmission and epileptogenesis. In: Avanzini G, Engel JJ, Fariello R, Heinemann U, eds. Neurotransmitters in Epilepsy (Epilepsy Res. Suppl. 8). Amsterdam: Elsevier. p 173-180.

Jones RSG, Heinemann V. 1988. Synaptic and intrinsic responses of medial entorhinal cortical cells in normal and magnesium-free medium "in vitro". J. Neurophysiol. 59: 1476-1496.

Jones RSG, Lambert JDC. 1990. Synchronous discharges in the rat entorhinal cortex *in vitro*: site of initiation and the role of excitatory amino acid receptors. Neuroscience 34: 657-670.

Kandel ER, Spencer WA. 1961. Electrophysiology of hippocampal neurons. II. After-potentials and repetitive firing. J. Neurophysiol. 24: 243-259.

Kennedy TE, Serafini T, de la Torre JR, Tessier-Lavigne M. 1994. Netrins are diffusible chemotropic factors for commissural axons in the embryonic spinal cord. Cell 78: 425-435.

Klingberg T, Roland PE, Kawashima R. 1994. The human entorhinal cortex participates in associative memory. NeuroReport 6: 57-60.

Klink R, Alonso A. 1993. Ionic mechanisms for the subthreshold oscillations and differential electroresponsiveness of medial entorhinal cortex layer II neurons. J. Neurophysiol. 70: 144-157.

Klink R, Alonso A. 1997. Morphological characteristics of layer II projection neurons in the rat medial entorhinal cortex. Hippocampus 7: 571-583.

Kohler C. 1986. Intrinsic connections of the retrohippocampal region in the rat brain. II. The medial entorhinal area. J. Comp. Neurol. 246: 149-169.

Lingenhöhl K, Finch DM. 1991. Morphological characterization of rat entorhinal neurons in vivo: soma-dendritic structure and axonal domains. Exp. Brain Res. 84: 57-74.

Lorente de No R. 1933. Studies on the structure of the cerebral cortex. I. The area entorhinalis. J. Psychol. Neurol. 45: 381-438.

Lysakowski A, Wainer BH, Bruce G, Hersh LB. 1989. An atlas of the regional and laminar distribution of choline acetyltransferase immunoreactivity in rat cerebral cortex. Neurosci 28: 291-336.

Mainen ZF, Sejnowski TJ. 1996. Influence of dendritic structure on firing pattern in model neocortical neurons. Nature 382: 363-366.

Mason A, Larkman A. 1990. Correlations between morphology and electrophysiology of pyramidal neurons in slices of rat visual cortex. II. Electrophysiology. J. Neurosci. 10: 1415-1428.

McCormick DA. 1992. Neurotransmitter actions in the thalamus and cerebral cortex and their role in neuromodulation of thalamocortical activity. Prog. Neurobiol. 39: 337-388.

Milner TA, Loy R, Amaral DG. 1983. An anatomical study of the development of the septo-hippocampal projection in the rat. Devl Brain Res 8: 343-371.

Ramon y Cajal S. 1902. Sobre un ganglio especial de la corteza esfeno-occipital. Trab. del Lab. de invest. Biol. Univ. Madrid 1: 189-201.

Room P, Groenewegen HJ. 1986. The connections of the parahippocampal cortex in the cat. I Cortical afferents. J. Comp. Neurol. 251: 415-450.

Rutecki PA, Grossman RG, Armstrong D, Irish-Loewen S. 1989. Electrophysiological connections between the hippocampus and entorhinal cortex in patients with complex partial seizures. J. Neurosurg. 70: 667-675.

Scharfman HE. 1996. Hyperexcitability of entorhinal cortex and hippocampus after application of aminooxyacetic acid (AOAA) to layer III of the rat entorhinal cortex in vitro. J. Neurophysiol. 76: 2986-3001.

Scharfman HE, Goodman JH, Du F, Schwarcz R. 1998. Chronic changes in synaptic responses of entorhinal and hippocampal neurons after amino-oxyacetic acid (AOAA)-induced entorhinal cortical neuron loss. J Neurophysiol 80: 3031-3046.

Schmitz D, Gloveli T, Behr J, Dugladze T, Heinemann U. 1998. Subthreshold membrane potential oscillations in neurons of deep layers of the entorhinal cortex. Neuroscience 85: 999-1004.

Scoville WB, Milner B. 1957. Loss of recent memory after bilateral hippocampal lesions. J. Neurol. Neurosurg. Psychiat. 20: 11-21.

Silva LR, Amital Y, Connors BW. 1991. Intrinsic oscillations of neocortex generated by layer 5 pyramidal neurons. Science 251: 432-434.

Sorensen KE, Shipley MT. 1979. Projections from the subiculum to the deep layers of the ipsilateral presubicular and entorhinal cortices in the guinea pig. J. Comp. Neurol. 188: 313-334.

Spencer SS, Spencer DD. 1994. Entorhinal-hippocampal interactions in medial temporal lobe epilepsy. Epilepsia 35: 721-727.

Squire LR. 1998. Memory systems. C R Acad Sci III 321: 153-156.

Steward O, Scoville SA. 1976. The cells of origin of entorhinal afferents to the hippocampus and fascia dentata of the rat. J. Comp. Neurol. 169: 347-370.

Stringer JL, Lothman EW. 1992. Reverberatory seizure discharges in hippocampal-parahippocampal circuits. Exp. Neurol. 116: 198-203.

Swanson LW, Cowan WM. 1977. An autoradiographic study of the organization of the efferent connections of the hippocampal formation in the rat. J. Comp. Neurol. 172: 49-84.

Swanson LW, Kohler C. 1986. Anatomical evidence for direct projections from the entorhinal area to the entire cortical mantle in the rat. J. Neurosci. 6: 3010-3023.

van der Linden S, Lopes da Silva FH. 1998. Comparison of the electrophysiology and morphology of layers III and II neurons of the rat medial entorhinal cortex in vitro. Eur J Neurosci 10: 1479-1489.

Walther H, Lambert JDC, Jones RSG, Heinemann U, Hamon B. 1986. Epileptiform activity in combined slices of the hippocampus, subiculum and entorhinal cortex during perfusion with low magnesium medium. Neurosci.Lett. 69: 165-161.

Wilson WA, Swartzwelder HS, Anderson.W.W., Lewis.D.V. 1988. Seizure activity in vitro: A dual focus model. Epilepsy Res. 2: 289-293.

Witter MP, Amaral DG. 1991. Entorhinal cortex of the monkey: V. Projections to the dentate gyrus, hippocampus, and subicular complex. J. Comp. Neurol. 307: 437-459.

Wong RK, Prince DA. 1978. Participation of calcium spikes during intrinsic burst firing in hippocampal neurons. Brain Res 159: 385-390.

Yang CR, Seamans JK, Gorelova N. 1996. Electrophysiological and morphological properties of layers V-VI principal pyramidal cells in rat prefrontal cortex in vitro. J Neurosci 16: 1904-1921.

Zola-Morgan S, Squire LR. 1993. Neuroanatomy of memory. Annu. Rev. Neurosci. 16: 547-563.

3.8 Tables

Table 1. Summary of morphological parameters[1]

Cell Type	Soma Perimeter(μm) (range)	Soma Area(μm²) (range)	Dendrite Length(μm) (range)
HC	84.21±21.6 (64-126)	320.1±46.17 (250-383)	7786±2740 (4321-11803)
PY	67.74±14.23 (45-98)	251.34±67.94 (151-337)	5186±2218 (2485-9824)
PC	69.7±13.02 (58-92)	270.6±103.3 (144-428)	8255±3339 (4680-13424)

[1]Values are means ± s.d. and range for 6 horizontal cells (HC), 10 pyramidal cells (PY) and 5 polymorphic cells (PC).

Table 2. Summary of electrophysiological parameters[1]

Cell Type	Rin (MΩ)	Time constant(ms)	RMP(mV)	Spike Thre.(mV)	Amp.(mV)	Dur.(ms)	AHP Amp.(mV)	SAG% (n/nT)
HC	73.3±17.84	14.75±2.72	-62.48±3.45	-44.89±4.81	65.9±6.47	1.56±0.22	16.14±2.76	15.5 ± 6.14 (13/15)
PY	75.67±28.72	12.83±3.65	-65.02±3.8	-42.88±5.9	64.96±6.53	1.53±0.28	17.44±2.64	13.89±5.78 (18/38)
PC	78.89±25.34	11.51±3.41	-63.32±4.07	-40.99±2.09	68.32±3.55	1.42±0.25	18.05±2.06	17.0 ± 5.7 (4/9)

[1]Values are means ± s.d. for 15 horizontal cells (HC), 38 pyramidal cells (PY) and 9 polymorphic cells (PC). **Rin**, input resistance; **RMP**, resting membrane potential; Spike threshold, amplitude and duration; **AHP**, after hyperpolarization amplitude; **SAG%**, sag percentage (rectification index). See Methods section for details on measurements.

3.9 Figures

Fig. 1: Morphological subtypes of entorhinal cortex layer V cells. **A-C:** computer-aided reconstruction of a pyramidal, a horizontal and a polymorphic cell, respectively. Dashed lines represent the borders of the indicated layers. Scale bar = 200 μm.

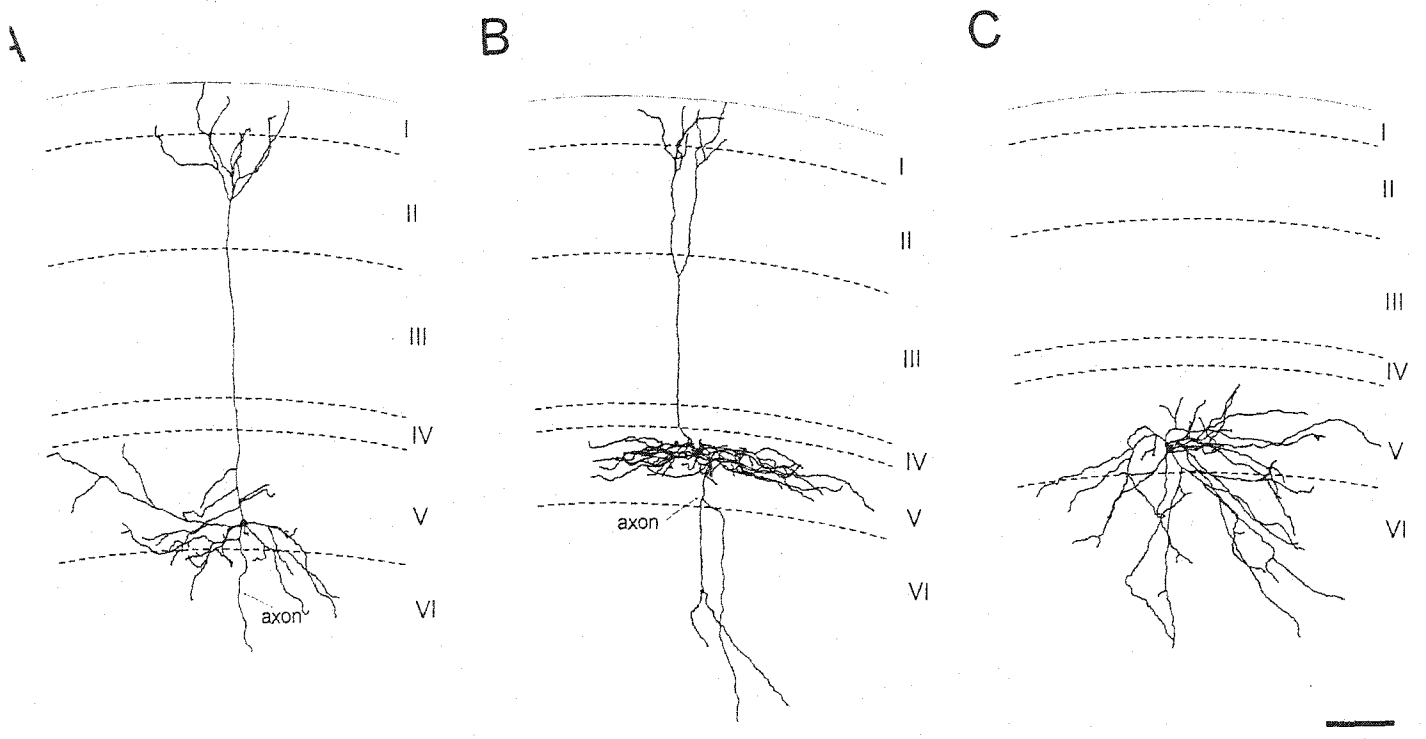
A
B
C
I
II
III
IV
V
VI
axon
axon

Fig. 2: Most pyramidal cells display fast, but not time-dependent, inward rectification. **A:** low power photomicrograph of a small pyramidal cell. Scale bar = 100 μm. The location of the recorded cell in the slice is indicated in the upper inset. The bottom inset depicts a high magnification photomicrograph showing two spines from the same neuron. Scale bar = 1 μm. **B:** voltage responses to depolarizing and hyperpolarizing current pulses in the same neuron as in A. Scale bars = 0.1 second, 0.5 nA and 20 mV. The inset shows, with an expanded time scale, the shape of the single spike AHP. Scale bar = 0.01 second, 20 mV. **C:** current/voltage relation (I/V) plot from B. Note the upward bending towards the negative end of the curve.

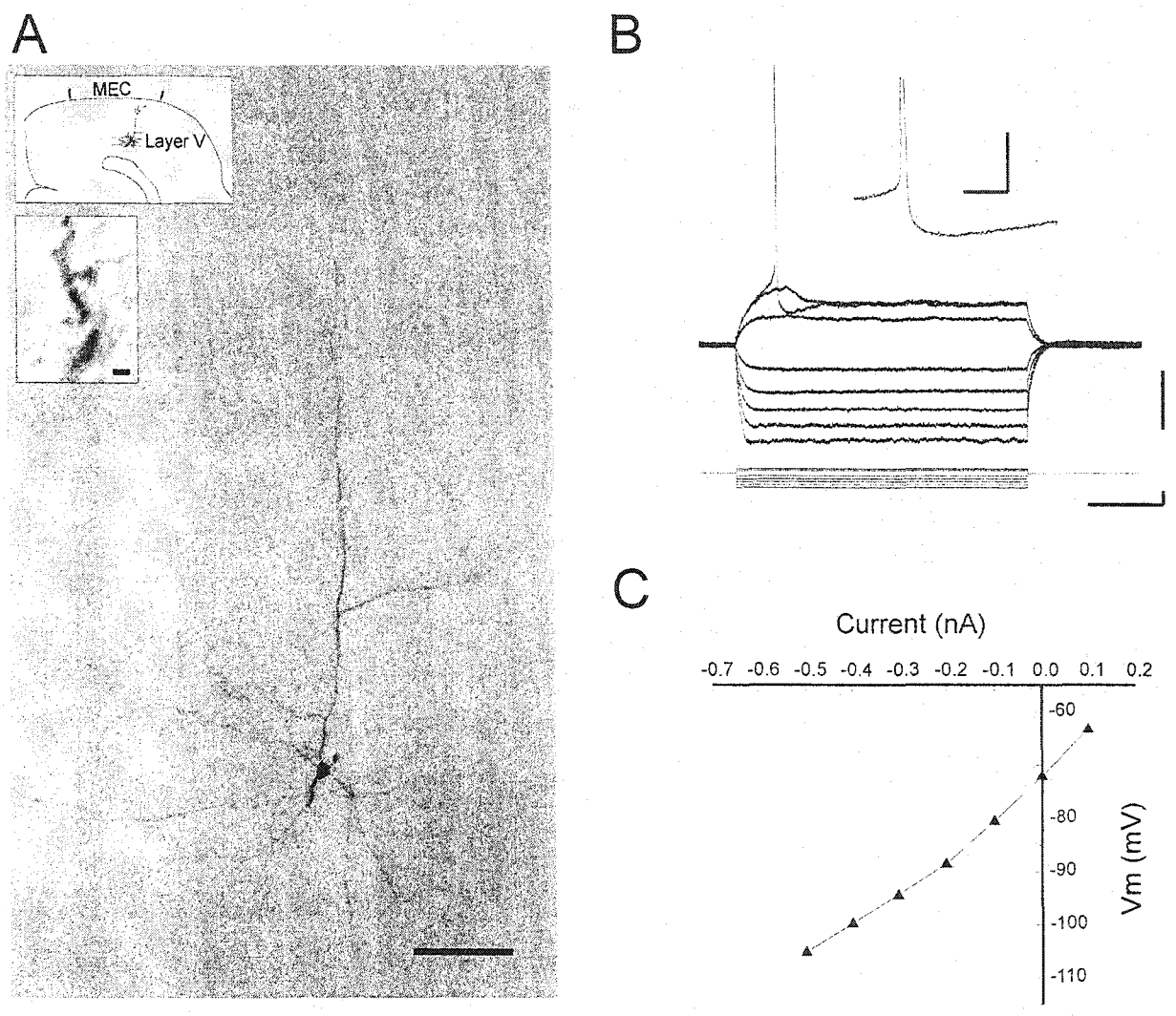
A
MEC
Layer V
B
C
Current (nA)
-0.7 -0.6 -0.5 -0.4 -0.3 -0.2 -0.1 0.0 0.1 0.2
-60
-80
-90
-100
-110
Vm (mV)

Fig. 3: Some pyramidal cells also display time-dependent inward rectification. **A:** computer-aided reconstruction of a large pyramidal cell. Scale bar = 100 μm. **B:** voltage responses to a depolarizing and a hyperpolarizing current pulse in the same neuron as in A. Note that the voltage response to the hyperpolarizing current pulse shows an early peak followed by a depolarizing "sag". Scale bars = 0.1 second, 0.4 nA, 20 mV. The inset shows a representative spike from this neuron with the first arrow, asterix and the second arrow indicating a fast AHP, depolarizing after potential and slow AHP respectively. Scale bars = 0.05 second, 10 mV. **C:** the same neuron responds to a depolarizing current pulse application with very little spike-frequency adaptation. Scale bars = 1 second, 0.4 nA, 20 mV. **D:** plot of the peak (filled squares) and steady state (s.s.; filled circles) I-V relations in this neuron. The difference between the peak and the s.s. response demonstrate the time-dependent inward rectification.

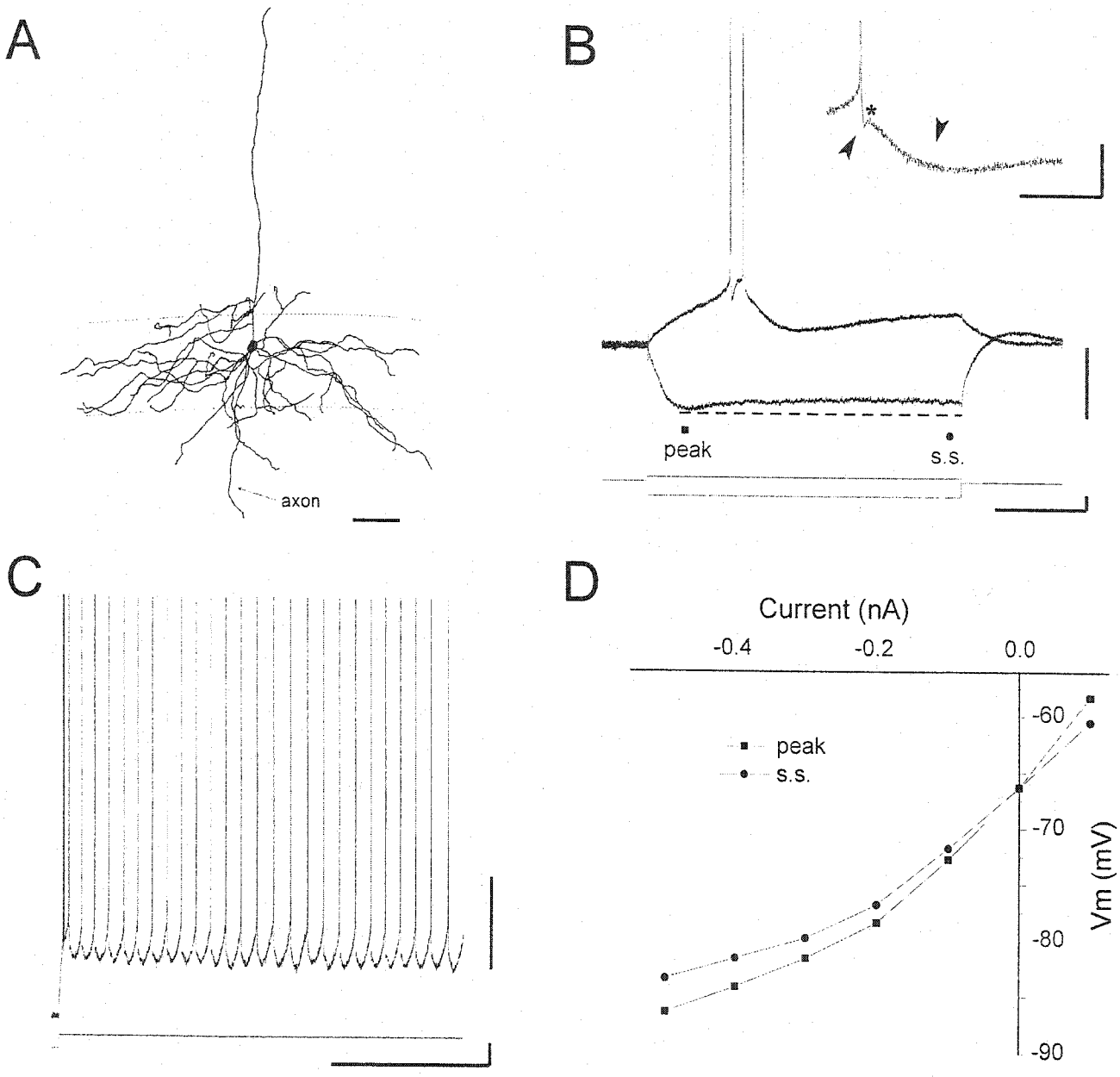
A
axon
B
peak
s.s.
C
D
Current (nA)
-0.4
-0.2
0.0
peak
s.s.
-60
-70
-80
-90
Vm (mV)

Fig. 4: Spike-frequency adaptation and subthreshold oscillations in pyramidal cells. A and B, same cell as figure 2. **A:** a 0.2 nA **(1)** and a 0.4 nA **(2)** current pulse trigger an initial action potential followed by subthreshold oscillations and a rapidly adapting spike-train followed by intermittent discharge in spike-clusters, respectively. Resting potential is about –73 mV. Scale bars = 1 second, 0.8 nA, 20 mV **B:** rhythmic subthreshold membrane potential oscillations during direct current depolarization to about –54 mV **(1)**. The power spectrum of the membrane potential **(2)** demonstrates a clear peak at about 14 Hz. Scale bars = 0.5 second, 10 mV. **C:** in a different pyramidal cell (1) (scale bar = 200 μm) a 0.1 nA **(2)** and a 0.5 nA **(3)** current pulse trigger an initial action potential followed by subthreshold oscillations and a rapidly adapting spike-train followed by a slow afterhyperpolarization, respectively. Resting potential is about –65 mV. Scale bars = 1 second, 0.4 nA, 20 mV.

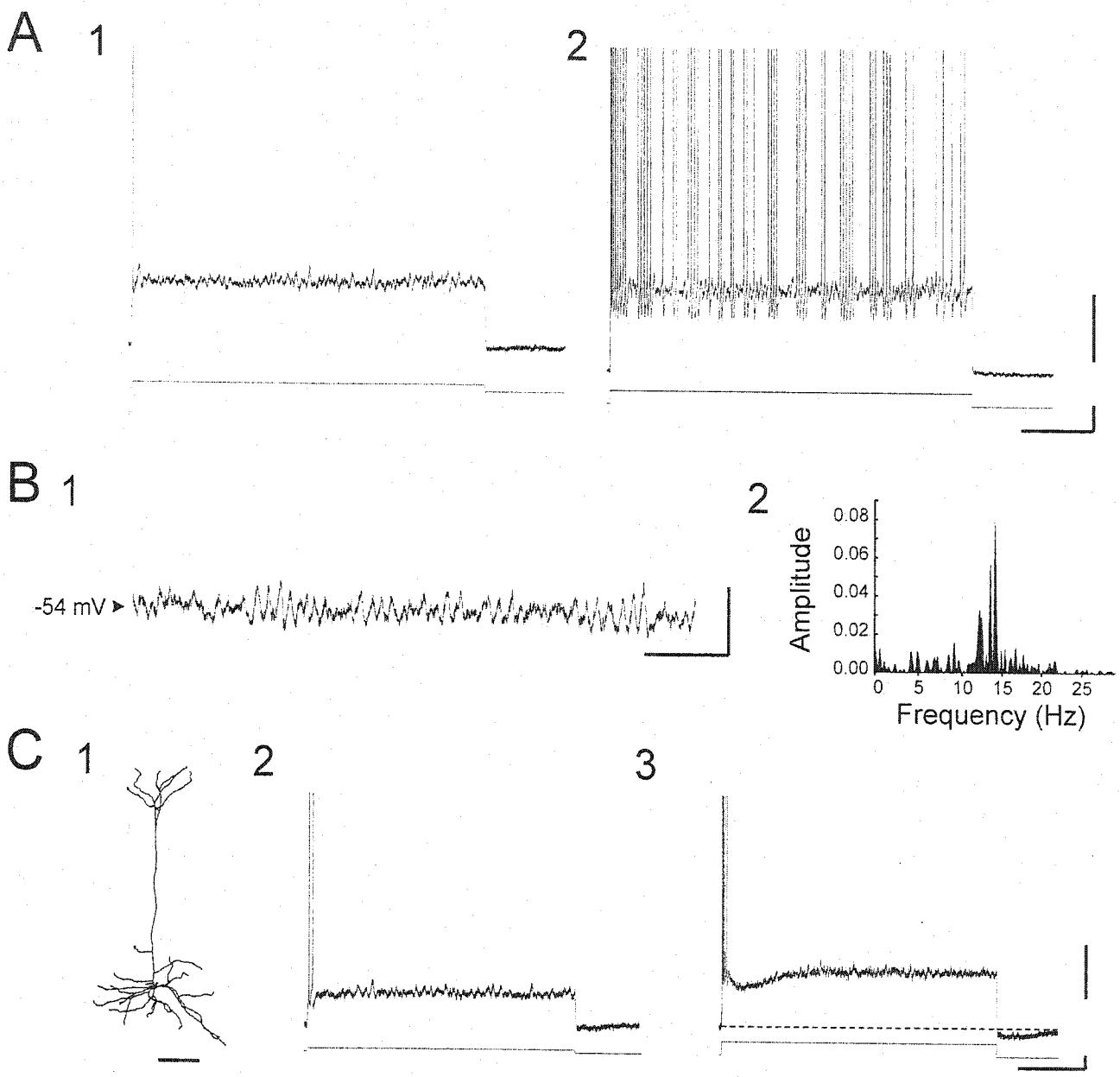
A
1
2
B
1
-54 mV
2
Amplitude
0.08
0.06
0.04
0.02
0.00
0
5
10
15
20
25
Frequency (Hz)
C
1
2
3

Fig. 5: Differences in the basal dendritic arborization between pyramidal cells and horizontal cells demonstrated by Sholl analysis. **A:** representation of the Sholl analysis procedure. This involved counting the number of basal dendritic intersections that intersect the surface of concentric spheres of increasing radius (20 μm steps) centered on the cell body. Scale bar = 200 μm. **B:** plot of the basal dendritic intersections through spheres of increasing radius demonstrated that the dendrites of the horizontal cells (open circles) branch more profusely and extend further away from the soma **C:** histogram of the percentage of basal dendritic intersections that pyramidal and horizontal cells make below an imaginary horizontal plane 100 μm deeper than the cell body (as represented in panel A).

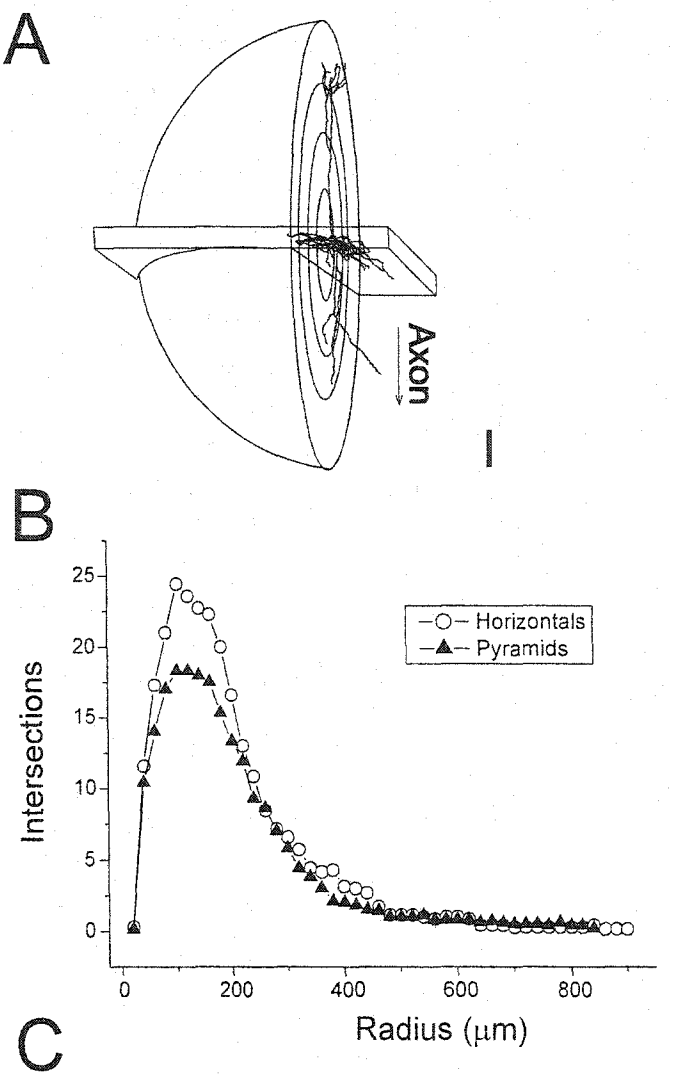
A
Axon
B
Intersections
25
20
15
10
5
0
0
200
400
600
800
Radius (μm)
Horizontals
Pyramids
C
% Deep (-100μm) Intersections
25
20
15
10
5
0
Pyramids
Horizontals

Fig. 6: Typical electrophysiological profile of most horizontal cells. **A:** Computer-aided reconstruction of a horizontal cell. Scale bar = 200 μm. **B:** in the same neuron, voltage responses to depolarizing and hyperpolarizing current pulses from the resting level. Scale bars = 0.1 second, 0.4 nA, 20 mV. The inset shows a typical bi-phasic AHP with a small depolarizing afterpotential. Scale bars = 0.05 second, 10 mV. **C:** very little spike adaptation is seen in response to a relatively large depolarizing current pulse. Scale bars = 1 second, 0.2 nA, 20 mV. **D:** plot of the I/V relation in B; note the instantaneous and time-dependent inward rectification as demonstrated by the upwards bending of both the peak and s.s. I/V curves, and the difference between them.

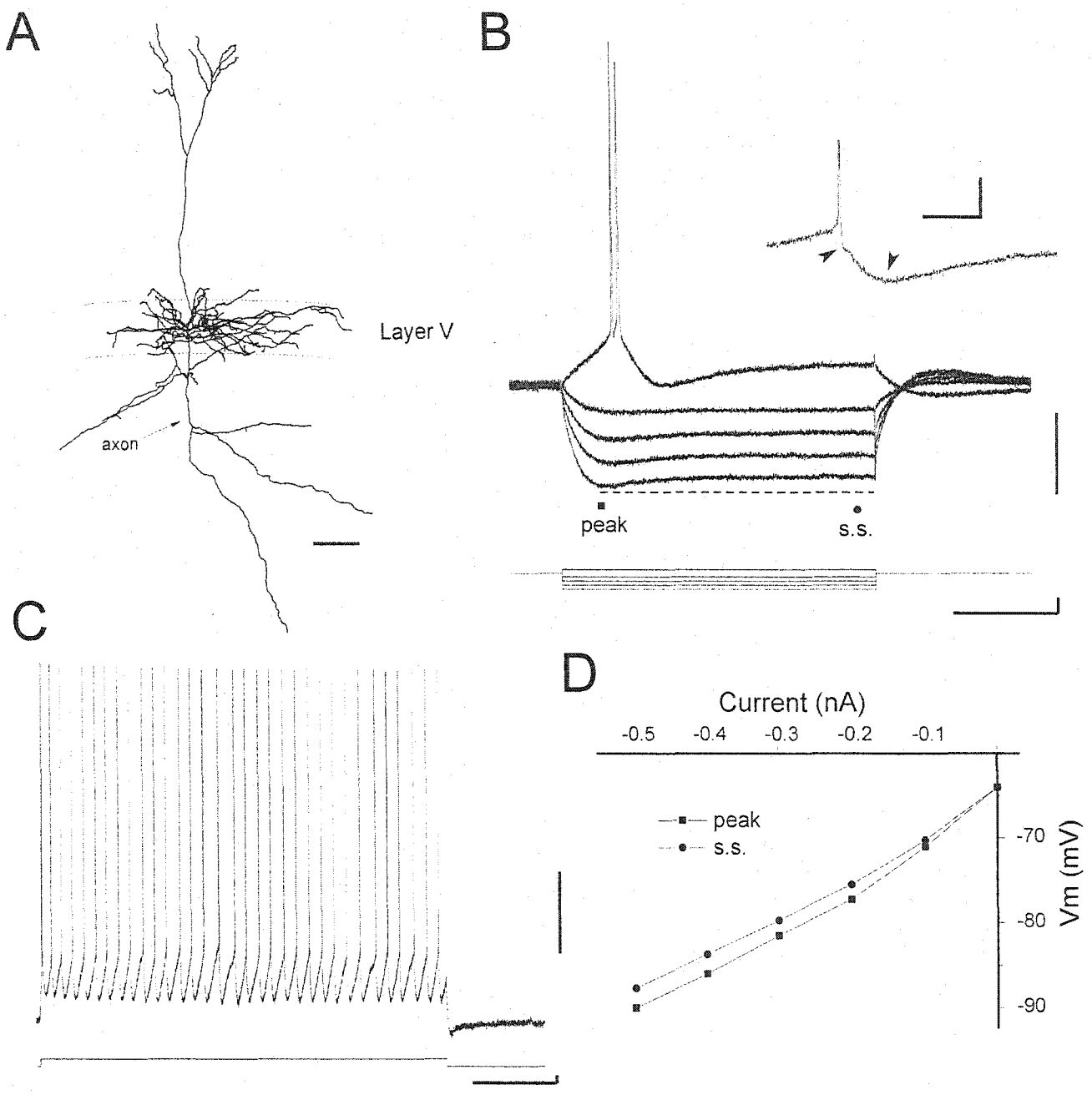
A
Layer V
axon
B
peak
s.s.
C
D
Current (nA)
-0.5
-0.4
-0.3
-0.2
-0.1
peak
s.s.
-70
-80
-90
Vm (mV)

Fig. 7: Some horizontal cells also displayed robust spike-frequency adaptation. **A:** low-power photomicrograph of a typical horizontal neuron is presented in **(1)**. The limit of the different cortical layers is indicated to the right The angular bundle (ab) is also labeled. Scale bar = 100 μm. The expansion of the rectangular area in 1 is shown in **(2)**. Scale bar = 100 μm. **B:** in a different horizontal cell (inset), **(1)** voltage response from the resting level (about –56 mV) to a relatively strong depolarizing current step. Note the initial train of action potentials followed by a large amplitude AHP and intermittent spiking. Scale bars = 1 second, 0.8 nA, 20 mV. In **(2)**, the slow AHP is particularly revealed by applying a shorter depolarizing current pulse. Scale bars = 0.5 second, 0.8 nA, 20 mV.

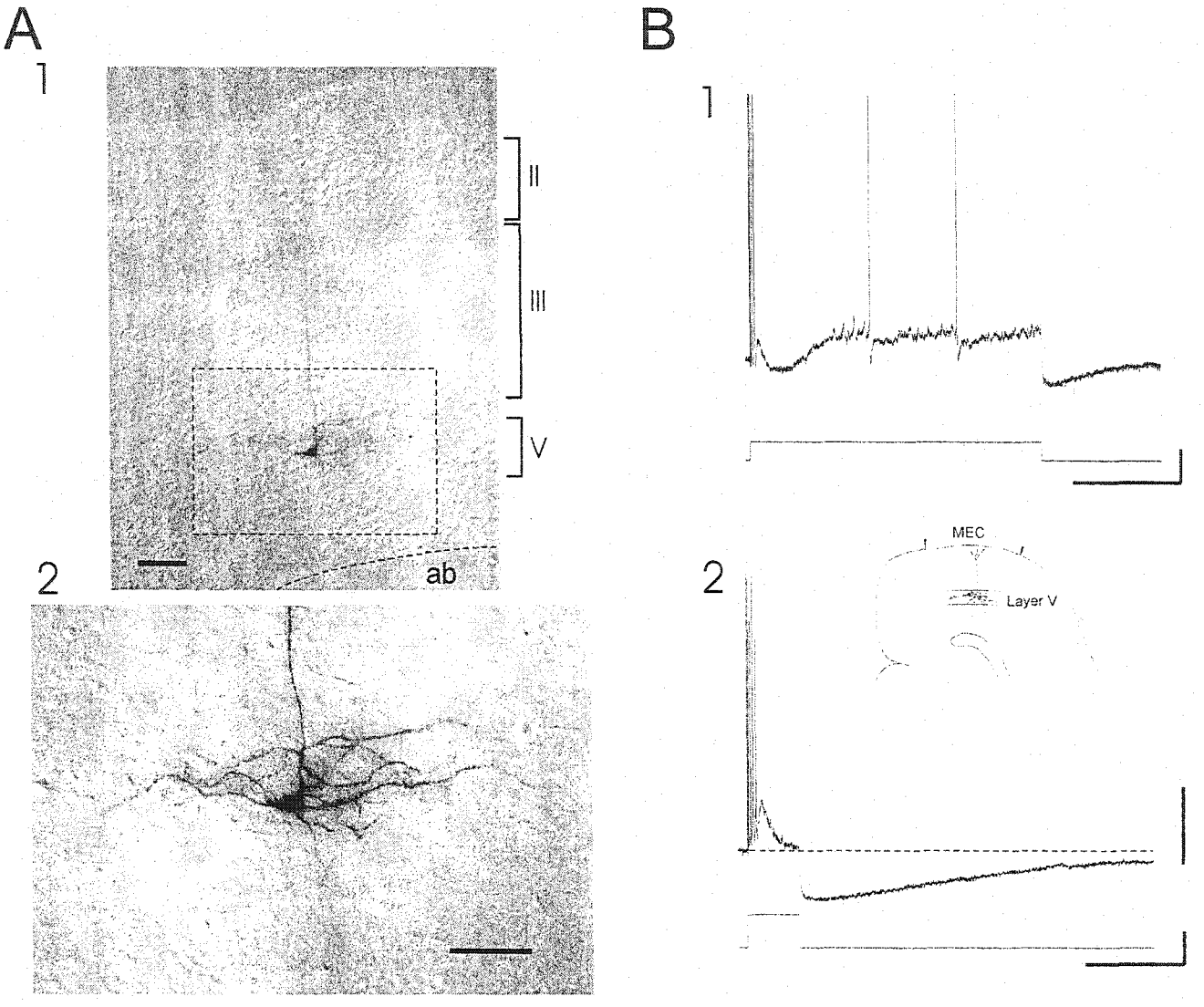
A
1
II
III
V
ab
2
B
1
2
MEC
Layer V

Fig. 8: Horizontal cells can also display robust subthreshold oscillatory activity. Same neuron as figure 7B. **A:** long lasting trace demonstrating the changes in membrane potential as the cell is progressively depolarized by d.c. current injection from its resting level (about –64 mV). Scale bars = 20 second, 0.5 nA, 20 mV. The increase in the voltage trace noise is a reflection of the emergence of subthreshold oscillations (as detailed in panel B). Note that at the most depolarized level the cell does not display tonic repetitive discharge, but rather intermittent spiking consisting of spike clusters interspersed by subthreshold oscillations (inset to the left, asterisk). Scale bars = 0.5 second, 20 mV. **B:** expanded traces from A taken at the times indicated (a to e) demonstrating the appearance of robust subthreshold oscillations with membrane depolarization. Scale bars = 0.5 second, 5 mV. The lower graphs are the power spectrum of the membrane potential and the corresponding autocorrelation function (inset; scale bar = 0.2 second) for each period. Note that the membrane potential is most rhythmic when the membrane potential is just below firing threshold (c and d).

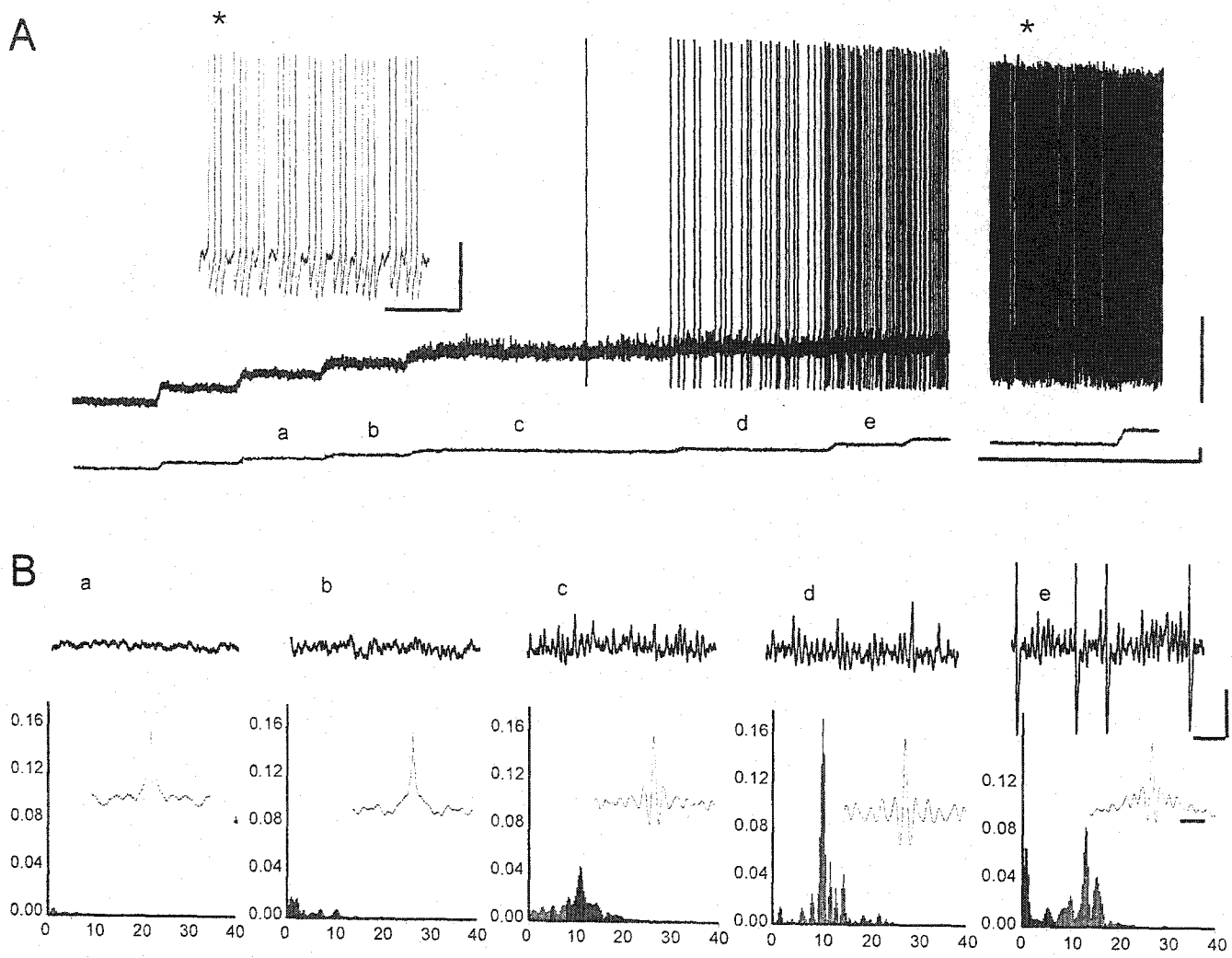
A
*
*
a
b
c
d
e
B
a
b
c
d
e
0.16
0.12
0.08
0.04
0.00
0
10
20
30
40

Fig. 9: Basic morphological and electrophysiological profile of polymorphic cells. **A**: low-power photomicrograph of a polymorphic neuron. Scale bar = 100 μm. The inset illustrates the position of the neuron within the entorhinal cortex. **B:** I-V relation for the same neuron showing only instantaneous inward rectification. Scale bars = 0.1 second, 0.8 nA, 20 mV. **C:** depolarizing current step application to the same neuron reveal moderate-type spike frequency adaptation. Scale bars = 1 second, 0.4 nA, 20 mV. **D:** computer-aided reconstruction of another polymorphic neuron. Scale bar = 200 μm. **E:** I-V relation for the same neuron demonstrating time-dependent inward rectification. Scale bars = 0.1 second, 0.6 nA, 20 mV. **F:** in the same neuron, the voltage response to a long-lasting depolarizing current pulse demonstrates that this cell display a very low level of spike-frequency adaptation. Scale bars = 1 second, 0.4 nA, 20 mV.

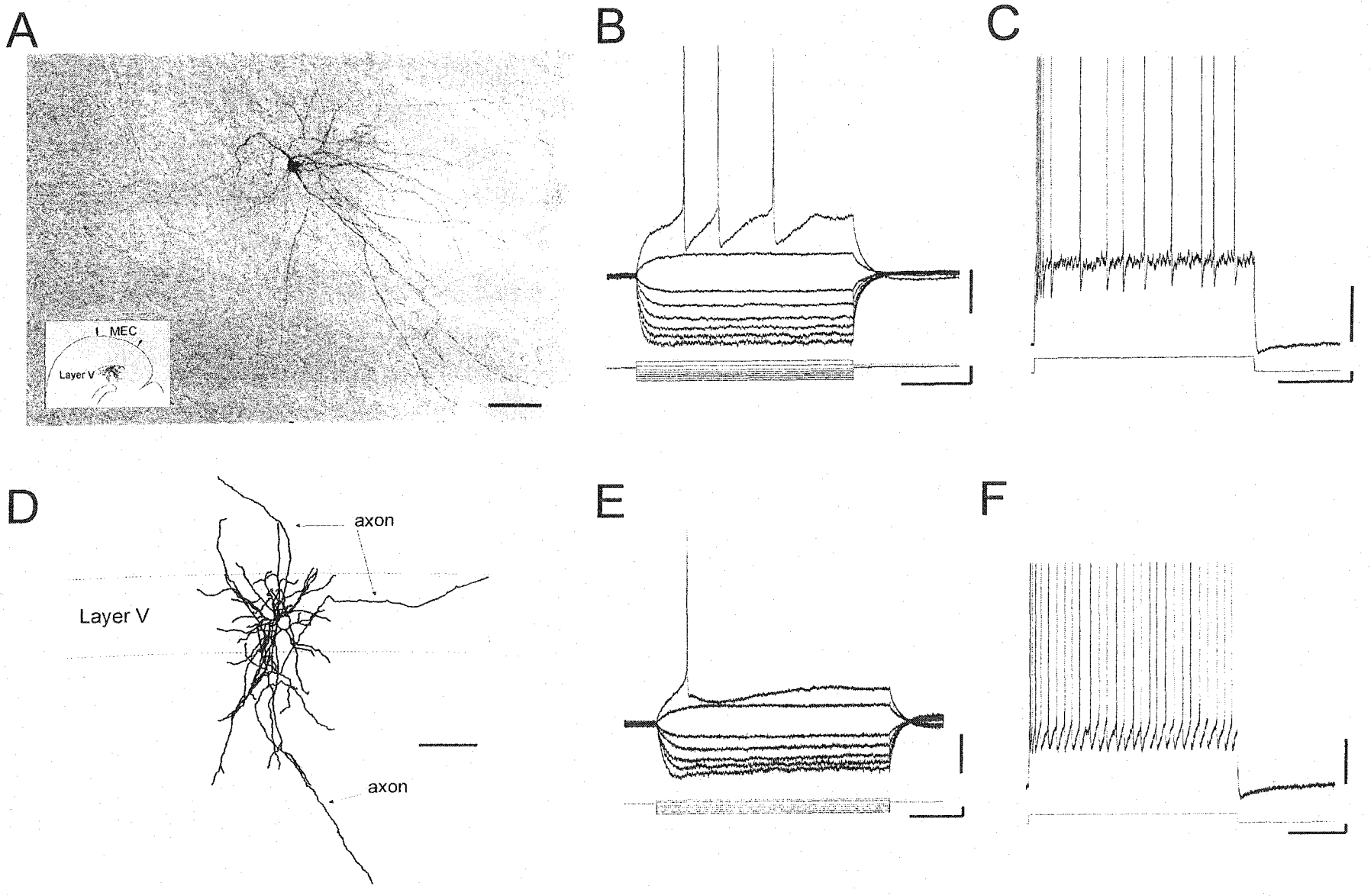
A
L. MEC
Layer V
B
C
D
Layer V
axon
axon
E
F

Fig. 10: Some polymorphic cells have dendrites that reach into the subiculum. **A, B:** two different examples. The upper diagrams indicate the position of the labeled cells in the slice. The lower traces are the enlarged computer-aided reconstruction of these neurons showing in greater detail their dendritic distribution. The angular bundle (ab) and the subiculum (Sub) are also indicated. Scale bar = 200 μm.

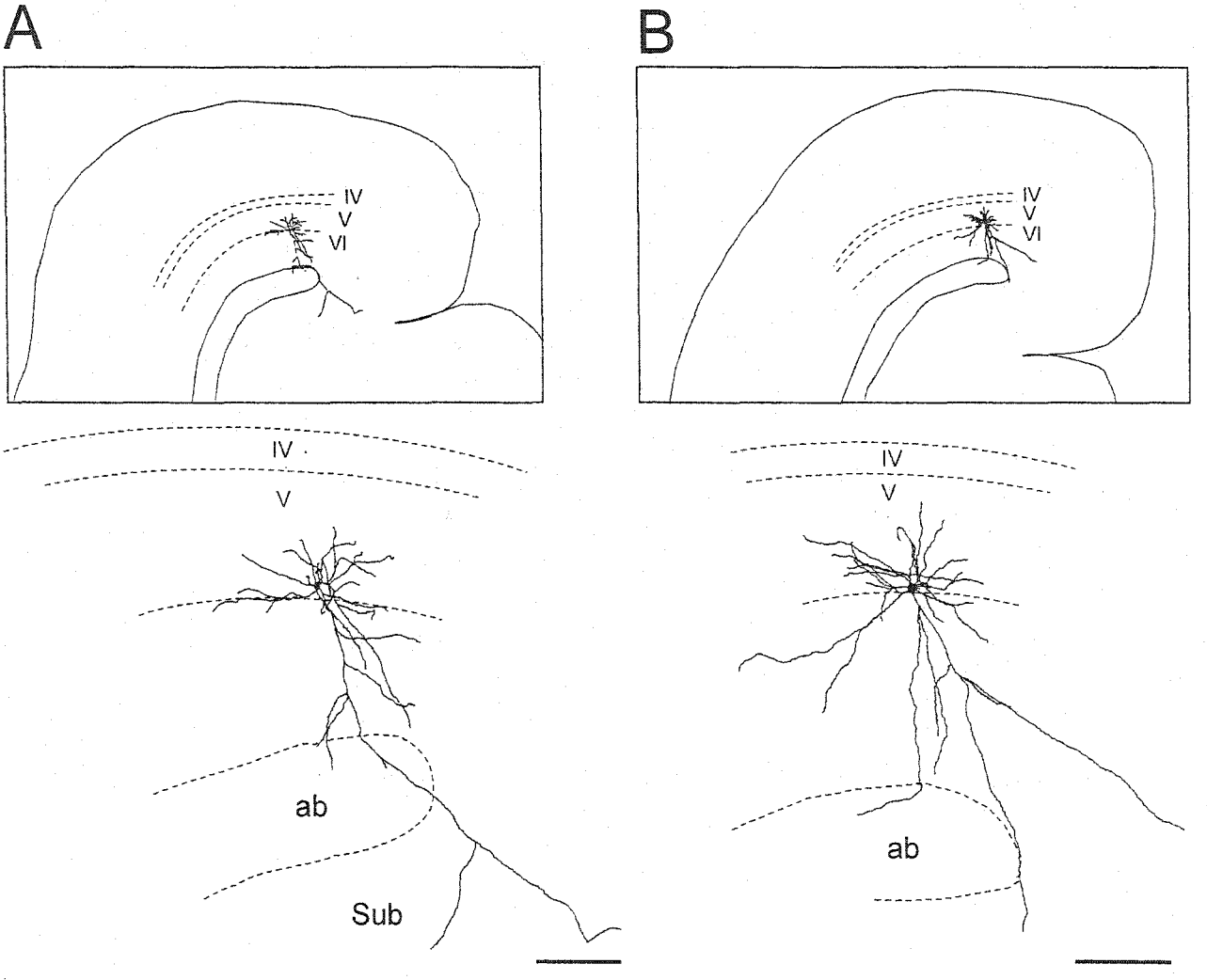
A
IV
V
VI
IV
V
ab
Sub
B
IV
V
VI
IV
V
ab

Chapter Four

4. Morphological and Electrophysiological Characteristics of Layer V Neurons of the Rat Lateral Entorhinal Cortex

4.1 Preface

The conclusions from of the previous study indicate that layer V neurons of the MEA are made up of three distinct morphological cell types with surprisingly similar electrophysiological profiles. Given the differences between the MEA and the LEA as summarised in the first chapter of this thesis, on anatomical (cytoarchitectural and connectional), physiological and functional levels, we decided to investigate properties of layer V neurons in the LEA. As far as we could tell, this is the first extensive attempt in this direction. Hence, the aim of this study is to characterize the intrinsic electrophysiological and morphological properties of neurons in the LEA, similar to what we have done in the MEA, and to compare the properties of layer V neurons in both areas. Because of the differences between cells in the superficial layers of the MEA and LEA, we expected large differences to differentiate layer V cells in the MEA and LEA.

4.2 Abstract

The intrinsic electrophysiological and morphological properties of lateral entorhinal area (LEA) layer V neurons were investigated by sharp electrode intracellular recording and biocytin labelling in vitro. The morphological analysis revealed that layer V of the LEA contains three distinct subtypes of principal neurons that were classified as pyramidal, horizontal and polymorphic neurons. Pyramidal cells were the most abundant subtype (57 %) and could be further subdivided into neurons with large, small and star-like somas. Similar to pyramidal cells, horizontal neurons (11 %) had a prominent apical dendrite. However, their distinctive basal dendritic plexus extended primarily in the horizontal plane. Polymorphic neurons (32 %) were characterized by a multipolar dendritic organization. Electrophysiological analysis of neurons in the three categories demonstrated a diversity of electrophysiological profiles within each category and no significant differences between groups. Neurons in the three subgroups could display instantaneous and/or time-dependent inward rectification, and different degrees of spike frequency adaptation. None of the recorded cells displayed an intrinsic oscillatory bursting discharge. Many neurons in the three subgroups displayed, however, slow (3.5 to 14 Hz) sustained subthreshold membrane potential oscillations.

The morphological and electrophysiological diversity of principal neurons in the LEA parallels that previously reported for the medial entorhinal area and suggests that, with respect to the deep layers, similar information processing is performed across the medio-laterat extent of the entorhinal cortex. Layer V of the entorhinal cortex may undertake very complex operations beyond acting as a relay station of hippocampal processed information to the neocortex.

4.3 Introduction

It is now well established that the entorhinal cortex (EC) occupies a key anatomical position in the temporal lobe since it acts as the main conduit for the bi-directional flow of information between the hippocampus and the rest of the cortical mantle (Lavenex and Amaral, 2000; Witter et al., 2000). The EC is also considered to play a critical role in memory function although its particular contributions have only recently begun to be investigated (Leonard et al., 1995; Suzuki et al., 1997; Suzuki and Eichenbaum, 2000; Baxter and Murray, 2001).

Numerous anatomical studies in both rodents and primates have demonstrated that information from all sensory modalities ultimately converges on the superficial cell layers (II and III) of the EC and this information is then conveyed to the hippocampus (i.e., dentate gyrus, hippocampus proper and subiculum) via the perforant path (Van Hoesen and Pandya, 1975; Insausti et al., 1987; Witter and Amaral, 1991; Insausti et al., 1997; Burwell and Amaral, 1998a; Burwell and Amaral, 1998b; Dolorfo and Amaral, 1998b). The subiculum, in turn, projects back to the EC and this hippocampal feedback predominantly terminates on the deep cell layers of EC (V and VI) (van Groen and Lopes da Silva, 1986; van Groen et al., 1986; Naber et al., 2001). The neocortical-EC-hippocampal loop is then closed by projections from layer V neurons of the EC that largely reciprocate the cortical input (Insausti et al., 1997; Lavenex and Amaral, 2000). Neurons in layer V of the EC also give rise to intra-entorhinal ascending projections to layers III and II thus closing a nested hippocampal-entorhinal loop (Deadwyler et al 1975; Kohler, 1986; Dickson and Alonso, 1997; Dolorfo and Amaral, 1998a).

Thus, layer V neurons of the EC are ideally positioned to deeply influence the operations of the neocortical-hippocampal circuits. Indeed, it is known that in Alzheimer's disease EC neurons from layers V and II are severely affected and their degeneration is though to be responsible, in part, for the memory impairments associated with this disease (Hyman et al., 1984; Braak and Braak, 1991; Gomez-Isla et al., 1996). It is also known, that the EC is highly epileptogenic (Spencer and Spencer, 1994; Bernasconi et al., 1999) and that EC layer V, similarly to neocortical layer V, includes the necessary neuronal and synaptic elements to act as a pacemaker for epileptiform activity (Jones and Heinemann, 1988; Jones and Lambert, 1990; Jones et al., 1992; Bragin et al., 1997; Dickson and Alonso, 1997; Gloveli et al., 1997).

The EC can be subdivided into a medial entorhinal area (MEA) and a lateral entorhinal area (LEA). Cytoarchitectonic of layers II and III provide the basis for this distinction in the rat (Blackstad, 1956). The MEA and LEA also differ with respect to their connections. For example, while the MEA receives its densest cortical innervation from the pyriform and postrhinal cortices, the LEA receives its densest innervation from the perirhinal cortex (Burwell and Amaral, 1998b). Also, the medial and lateral components of the perforant path have distinct termination fields in the dentate gyrus, hippocampus and subiculum (Hjorth-Simonsen and Jeune, 1972; Dolorfo and Amaral, 1998b; Naber et al., 2001). The distinction between the MEA and the LEA is also apparent at the physiological level. Beta activity is dominant in the LEA while theta is most dominant in the MEA (Boeijinga and Lopes da Silva, 1988). Finally, in temporal lobe epilepsy there is a rather selective degeneration of neurons in layer III of the MEA

but not in the LEA (Du et al., 1995). All the above data indicates important differences in the functional organization of the medial and lateral areas of the EC.

While substantial progress has been made over the last decade in our understanding of the intrinsic electrophysiological properties and morphological characteristics of neurons in the superficial and deep cell layers of the MEA (Alonso and Klink, 1993; Scharfman, 1996; Dickson et al., 1997; Gloveli et al., 1997; Klink and Alonso, 1997; Schmitz et al., 1998; van der Linden and Lopes da Silva, 1998) much less is known about the LEA. In a recent study (Hamam et al., 2000) we demonstrated that principal neurons in MEA layer V could be subdivided into three morphological categories: pyramidal cells, horizontal cells and polymorphic neurons. Significantly, neurons in the three subgroups displayed a diverse range of electrophysiological profiles but the different morphological subgroups could not be distinguished from each other according to traditional electrophysiological criteria. The present study is a continuation and extension of our previous work in layer V. Our main goal was to investigate potential differences in the intrinsic electroresponsiveness and/or morphological characteristics of principal neurons in layer V of the LEA as compared to those of the MEA. We have found that neurons with essentially the same morphological and electrophysiological profiles are present in the LEA and in the MEA layer V. The proportion of morphological subtypes, however, appear to be different in the two areas. These data also imply that functional differences between the MEA and LEA might be more dependent on superficial rather than on deep cell layer characteristics.

4.4 Materials and Methods

Brain slice preparation

Entorhinal cortex slices were obtained using standard procedures as previously described (Hamam et al., 2000). Briefly, male Long Evans rats (150-300 g) were decapitated according to a procedure approved by the Animal Care Committee of the Montreal Neurological Institute and compliant with the Canadian laws and NIH guidelines on animal research, the brain was quickly removed, and a block of tissue containing the parahippocampal region was placed in cold (4-6°C) oxygenated Ringer's solution containing (in mM): 124 NaCl; 5 KCl; 1.25 NaH_2PO_4; 2 $MgSO_4$; 26 $NaHCO_3$; 2 $CaCl_2$; and 10 mM glucose; pH was maintained at 7.4 by saturation with carbogen (95% O_2/5% CO_2). Horizontal slices containing the hippocampal and parahippocampal areas were made with a vibratome (Pelco, Redding, CA) at 400 μm thickness and then incubated in oxygenated Ringer's solution at room temperature. Following a two hours recovery period, slices were individually transferred into an interface recording chamber maintained at 34°C ± 1°C and superfused at a rate of 1-2 ml/minute with oxygenated Ringer's solution. The different areas of the hippocampal formation and the layers of the entorhinal cortex were identified with a dissecting microscope through transillumination.

Recording procedures and extracellular stimulation

Intracellular recording electrodes (borosilicate glass; Sutter Instruments co., Novato, CA) were made with a Sutter Instruments puller, P-87 (Sutter Instruments co., Novato, CA) and filled with 1% biocytin in 1.5 M K-acetate to make a tip resistance of 90-120 MΩ. Extracellular concentric bi-polar electrodes (FHC, Inc. Bowdoinham, ME)

were used to induce synaptic responses by white matter stimulation. Signals from impaled neurons were amplified with an Axoclamp 2A amplifier (Axon Instruments, Foster City, CA), viewed on-line using a digital storage oscilloscope, and stored on VHS tape (Neurocorder, New York, NY) for further analysis. Stored traces were digitized from tape and plotted using Axoscope acquisition software (Axon Instruments).

Impaled neurons included in this study were restricted to layer V of the lateral entorhinal area. Layer V somas, visible with trans-illumination, tend to be larger than those in layer III. The deep border of layer V with layer VI was more difficult to differentiate; however, layer VI was marked by a change to more densely packed smaller neurons. Despite attempts at impaling only layer V cells, some neurons in layers III and VI were labeled. These cells were eliminated from further analysis by examining the fixed slice under Nomarski optics, which provided a clearer appearance of the borders between layers (Hamam et al., 2000). The medial border of the LEA was where layer II breaks up from a clear single layer in the medial entorhinal area into two sub-layers of cellular islands. The lateral border of layer V is at the rhinal fissure. All neurons were recorded from the ventral two thirds of the ventro-dorsal aspect of the lateral entorhinal area (Blackstad, 1956).

Neurons were recorded under current clamp conditions. First their intrinsic membrane properties and synaptic responses to white matter stimulation (0.1 ms, 0 – 500 μA) were characterized. Second, the cells were injected with biocytin applying negative current pulses of 0.3 nA and 0.3 seconds (50% duty cycle) for at least five minutes. At the end of the experiment, electrodes were carefully pulled out from the recorded cell and slices were kept in the chamber for an additional 15-20 minutes to allow biocytin

transport into remote processes. Finally, slices were transferred into 4 % paraformaldehyde (PFA) in 0.1 M sodium-phosphate buffer (NaPB, pH = 7.5) and fixed for 24-48 hours at 4°C.

Histochemical processing

Fixed tissue slices were removed from PFA solution and washed in 0.1 M NaPB (3 × 5 minutes). Then, endogenous peroxidase activity was removed by incubating slices in 1 % H_2O_2 in 70 % methanol for 30 minutes at room temperature, the slices were then washed with 0.1 M NaPB (3 × 5 minutes). To block non-specific binding sites, the tissue was incubated in PHT (0.1 M NaPB; 1 % heat inactivated normal goat serum, 0.3 % Triton X-100; pH = 7.5) for at least two hours, then the slices were washed in avidin-biotin-horseradish-peroxidase complex (Vector Laboratories, Burlingame, CA) in NaPB overnight at room temperature. The following day the slices were washed extensively in PHT: first, brief washes (5 × 3 minutes), followed by 1 × 30 minutes, and then a series of long washes (6 × 1 hour), and finally a wash overnight. Slices were then washed with 0.1 M tris buffered saline (TBS; pH= 7.6) (3 × 10 minutes) and then transferred into 0.5 mg/ml diaminobenzidine (DAB, Vector Laboratories, Burlingame, CA) with Nickel (0.04 %). The latter was added to the DAB to intensify the reaction product. The DAB reaction was stopped when the desired staining was reached by washing the slices in TBS (3 × 10 minutes). As a final step in processing, the slices were equilibrated in increasing concentrations of glycerol (25, 40, 55, 70, 85, 100 %), mounted on glass slides in 100 % glycerol, coverslipped and stored at 4°C for further analysis.

Data analysis

Neurons were three-dimensionally reconstructed using the neuron tracing system Neurolucida (Microbrightfield Inc., Colchester, VT) from which all the quantitative data related to neuronal cell bodies, dendritic measurements and distribution were obtained. The dendritic stick histograms (Glaser et al., 1979; McMullen et al., 1984) and the fan-in plots (Glaser and McMullen, 1984) were derived from the three-dimensionally reconstructed neurons using the NeuroExplorer software (Microbrightfield Inc.). In addition, by averaging the angle and magnitude of all individual dendritic "sticks" in each histogram we derived the "average" dendritic orientation of individual neurons and the compound population. Photomicrographs were taken at various depths through the slice using a Zeiss Axioscope 2 microscope equipped with Nomarski optics with an MC80 camera (Carl Zeiss) and color slide film (Kodak Ektachrome). The slides were then scanned using a Nikon (LS-1000) film scanner and Adobe Photoshop software. Neuronal segments that were in focus in each of the slides were digitally reconstructed using Adobe Photoshop to produce two-dimensional composites of neurons.

The data for the current-voltage relationships were taken from the Axoscope program and plotted using Origin software (Origin, Microcal Software, Northampton, MA). The rhythmic character of the subthreshold oscillatory activity and its dominant frequency were estimated by computing, using the Matlab data analysis package (Matlab, The Math Works, Natick, MA), the autocorrelation function and power spectra of 3- to 5-s segments of membrane potential at a just below firing threshold voltage level. A coefficient of rhythmicity was derived by calculating the ratio of the second to first peak in the autocorrelation function for each cell. The apparent input resistance was estimated

from the membrane potential deflection in response to a 0.1 nA hyperpolarizing current pulse, and the time constant was calculated as the time it took the corresponding voltage deflection to reach 63% of its maximal value. The degree of time-dependent inward rectification was estimated by calculating the "sag" percentage (Sag% or rectification index) which consisted of the percent change in membrane potential from peak to steady state during a hyperpolarizing current pulse that caused a peak voltage deflection of ~ 25 mV. Neurons which had a Sag% < 5 % were not considered to display time-dependent inward rectification. Action potential amplitude was measured from threshold to peak. Action potential duration was measured at threshold level. Finally, the afterhyperpolarization (AHP) amplitude, was calculated from the spike threshold level to maximal peak of the AHP.

4.5 Results

The data presented in this study are based on observations from 37 intracellularly recorded and labelled neurons from layer V of the lateral entorhinal area. After obtaining a stable recording, the neurons were electrophysiologically characterized and subsequently injected with biocytin for later histochemical processing and morphological analysis. All neurons described in this study were recorded for at least 20 minutes, had a minimum resting membrane potential of - 57 mV, an input resistance larger than 35 MΩ, an overshooting action potential and a clearly identifiable morphology.

As in our analysis of the medial aspect of the entorhinal cortex (Hamam et al., 2000), we distinguished three different subtypes of principal cells in the lateral subdivision of the entorhinal area (Fig. 1). Briefly, the most abundant cell type (n=21)

were pyramidal cells which had a typical apical dendrite that extended to layer I and a profuse basal dendritic tree that extended mainly into layers V and VI (Fig. 1 A and B). We also found a second, far less numerous (n=4), group of cells that also had an ascending dendrite that extended to layer I. However, the basal dendritic tree had a horizontal axis of orientation parallel to layer V. We named this the "horizontal" cell. We also observed a third rather abundant group of cells (n= 12), which had a multipolar soma and a stellate arrangement; this cell type lacked a prominent apical dendrite. We named this cell type the "polymorphic" cell. While we could distinguish three morphological principal cell subtypes in layer V of the LEA, our electrophysiological analysis revealed that the intrinsic electroresponsive properties of neurons within each morphological category was rather heterogeneous and we could not detect any electrophysiological feature that clearly distinguished any of the morphological cells groups. As in the MEA, in the LEA we found neurons in all categories with different degrees of time-dependent inward rectification, cells that could display a low-threshold discharge in spike-doublets (Agrawal et al., 2001) and neurons that could generate intrinsic rhythmic subthreshold membrane potential oscillations at low-frequency. A series of basic electrophysiological parameters (presented in Table 2) were also measured and none showed significant differences among morphological cell groups. A detailed description of the morphological attributes of the different cell types follows with examples of their electrophysiological diversity. A description of the synaptic responses to white matter stimulation is also presented at the end.

Pyramidal Cells

Pyramidal neurons were the most abundant cell type in our sample, and accounted for about 57% of encountered neurons. All pyramidal cells typically had a prominent apical dendrite which was much thicker at the base (4.23 ± 1.61 μm, n= 5) than throughout the rest of the primary dendrites (1.68 ± 0.92 μm; n= 37 in five neurons). The apical dendrite ascended towards the superficial layers and gave off some branches proximally within layers V and III. Most of the branching occurred, however, within layers II and I (Figs. 1A, 2A). The distribution of the basal dendritic plexus was the most distinctive feature of these neurons. Most of the basal dendrites branched within layers V and VI, and had an overall ventral orientation. The "stick" polar histogram and the fan-in-diagram of the basal dendrites of the pyramidal cell population is illustrated in figure 1B and C, respectively. The compound orientation angle (see Methods) for the basal dendrites of these neurons was 254° (range 238° - 276°; n= 6) demonstrating their predominant ventral orientation.

While most of these cells had a typical pyramidal shaped soma, a small percentage (10%; n= 2) displayed a star shaped cell body with basal primary dendrites coming from all directions but still maintaining an overall basal orientation. An example of a pyramidal cell with a star-like soma is illustrated in figures 5A and B. Similar to what we found in the MEA (Hamam et al., 2000), pyramidal cells in the LEA displayed a wide range of soma's sizes. Table 1 gives the average and range of the cross sectional areas for six digitally traced pyramidal cells. Note how the largest soma (467 μm^2) is more than twice the size of the smallest soma (200 μm^2). Examples of pyramidal cells with large and small soma are given in figures 1A and 2, and figure 4, respectively.

All dendrites of pyramidal cells were covered with typical pedunculate spines and there was no apparent difference between their distributions on different areas of the same neuron. However, we noted that pyramidal cells with a small soma were more densely covered with spines. Moreover, many of these spines appeared to have a longer neck than those typical of pyramidal cells. Since labelled neurons were processed in relatively thick slices (400 μm), which limits microscopic resolution, it was not possible to quantitatively assess this difference. In most cases, axons from pyramidal cells gave off some branches locally and within layer VI before the main branch traveled in the direction of the lateral aspect of the angular bundle (Fig. 2, 4A and B, 5A and B).

All pyramidal cells we recorded could be classified within the broad category of cortical "regularly" spiking neurons. Detailed analysis of their input/output relations revealed that they were rather heterogeneous and electrophysiologically indistinguishable from the other morphological cell types in layer V. As in the case illustrated in figure 3, all pyramidal cells displayed inward rectification (IR) in both the hyperpolarizing and depolarizing direction as reflected by the upward bending (convexity) of the I/V relation at both its positive and negative ends (Fig. 3B). In some cases (19 %), hyperpolarizing IR was "instantaneous" (Fig. 3A; note the absence of time-dependent "sag" but most frequently it displayed a clear time-dependent component) as evidenced by the depolarizing "sag" evoked by membrane hyperpolarization (Fig. 4C and D, and Fig. 5C and D). Time-dependent IR is indicative of the hyperpolarization activated cation current I_h (Dickson et al., 2000b). We obtained a value for the rectification index (see Methods) in these "sagging" neurons of 14.2 ± 4.8 (Table 2) which is about the same as that displayed by other cell types in layer V, but much lower than that previously reported for

layer II cells (Alonso and Klink, 1993). We noted that a substantial number of pyramidal cells (43%) displayed an early response to a just-threshold current step that consisted of a spike-doublet riding on a slow depolarizing envelope (Fig. 4C and E). None of these neurons displayed the bursting discharge typical of some neocortical layer V pyramidal cells (Connors and Gutnick, 1990). The doublet-firing cells did not tend to manifest robust spike-frequency adaptation (Fig. 4F).

Notably, as in the case illustrated in figure 3, many pyramidal cells (66 %) displayed slow rhythmic subthreshold membrane potential oscillations when their membrane potential was depolarized from its resting level close to firing threshold. The subthreshold oscillations were most stable at a membrane potential of about -46 mV and, at this level, had a rather fixed frequency for any given cell though this frequency could vary from cell to cell (range: 3.5 -12 Hz; average: 6.41 ± 2.67 Hz, n= 21). The amplitude of the oscillation varied from cycle to cycle and we observed a range across cells from ~ 2 to 8 mV. On average, the coefficient of rhythmicity (see methods) of subthreshold oscillations in pyramidal cells was 0.51 ± 0.15 (range 0. 3 - 0.85; table 3). We noted that neurons that displayed subthreshold oscillations also manifested pronounced spike frequency adaptation in response to depolarizing current steps (Fig. 3C). In addition, during prolonged suprathreshold depolarizations, the oscillating neurons did not fire tonically. Instead, they displayed a repetitive bursting activity consisting of spike "clusters" interspersed by silent periods with subthreshold oscillations (Fig. 3C and D). Finally, subthreshold oscillations could be expressed by neurons that either did or did not display time-dependent IR (Fig. 3).

Horizontal cells

We found a group of cells in the LEA that had a prominent apical dendrite, the basal dendritic tree, however, extended primarily in the horizontal plane (i.e., parallel to layer V). Horizontal cells appeared to be in the LEA less numerous than in the MEA representing only 11% of the total population of recorded neurons. A computer aided reconstruction of a horizontal cell is illustrated in figure 1 and the neuron is documented photomicrographically in figure 6. The apical dendrite of the horizontal cells had a similar thickness (5.21 ± 0.66 μm, n= 3) to that of the pyramidal cells and typically gave off a few branches towards its proximal portion within layers V-III and then branched repeatedly towards the superficial end of layer III and within layers II and I (Fig. 1 and 6). The basal primary dendrites of the horizontal cells were significantly thicker (3.31 ± 1.30 μm; n= 19 in 3 cells) than those of the pyramidal cells ($p< 0.001$, t-student). All dendrites of the horizontal cells were sparsely covered with pedunculate spines to a similar degree. Detailed examples are provided in figure 6a to d. Horizontal cells had polygonal shaped somas that tended to be the largest of the three groups of cells, though the difference was not statistically significant (Table 1). With respect to their axon, this was always seen to travel in the direction of the angular bundle and, as in the other cell types, give off some branches locally and within layer VI (Fig. 6A). A high-power photomicrograph depicting an axon branch is given in figure 6A panel e.

The most characteristic feature of horizontal neurons is that their basal dendritic plexus extends primarily in the horizontal plane, parallel to layer V. This characteristic becomes particularly evident in the stick polar histograms (Fig. 1B) from which we derived the compound dendritic orientation angle that for these neurons was of 40°

degrees (range: 35° -56°, n=3) To further establish the morphological difference between pyramidal and horizontal cells we also used the data derived from the stick polar histogram to estimate the dendritic area within and outside a region of ± 30° from the horizontal plane (hereafter referred to as "horizontal region", Fig. 1B). We found that while in the cells classified as horizontal 80% of the compound basal dendritic area was within the horizontal band region only 29% of the compound basal dendritic area of the pyramidal cells occupied the same region.

Horizontal cells were heterogeneous with respect to their intrinsic electroresponsiveness and displayed electrophysiological profiles essentially indistinguishable from those of pyramidal or polymorphic cells. Some of the cells, as is the one illustrated in figure 7, displayed time-dependent IR while others did not. The degree of spike frequency adaptation was also variable and some cells displayed biphasic single spike AHPs (Fig. 7C) while others did not. As we observed in the pyramidal and polymorphic neurons, some (3 out of 4) horizontal cells also displayed rhythmic subthreshold oscillations (Table 3).

Polymorphic cells

Polymorphic neurons were quite numerous accounting for 32 % of the sampled population. In contrast to the other subtypes, these neurons lacked a prominent apical dendrite. Rather, they were characterized by multiple equally prominent primary dendrites (6.5±1.73 number of primary dendrites, range 5-9; n= 4) that were oriented in all directions giving their soma a multipolar appearance (Fig. 1A and 8). Some of the main dendritic trees were longer than the others but when they traveled superficially they

generally took an oblique orientation. When the dendritic orientation of the total population was examined in a stick polar histogram it was apparent that the larger proportion of the dendritic tree extended deep to the cell bodies, within layers V and VI (Fig. 1C). The total dendritic length of the polymorphic neurons tended to be larger than that of the pyramidal and horizontal cells though this difference was not statistically significant (Table 1). All dendrites of the polymorphic cells were sparsely covered with pedunculate spines. The photomicrographs of two typical polymorphic neurons are presented in figure 8. Axons, in most cases, were found to travel towards the angular bundle and in the example given in figure 9A, the axon crossed into the far lateral aspect of the angular bundle. In most cases, the axon gave off some branches locally and, in 2 cases, at least one of the branches was followed into the superficial portion of layer III (data not shown).

Polymorphic cells were electrophysiologically heterogeneous and shared similar features with the other layer V cell types. As illustrated in figure 9, some polymorphic cells displayed time-dependent IR ($A_{1,2}$) and minimal spike-frequency adaptation (A_3). Subthreshold oscillations were not typical of these "sagging" neurons. Other polymorphic cells displayed no "sagging" response but instantaneous IR exclusively ($B_{1,2}$). These neurons also tended to display pronounced spike frequency adaptation and manifested subthreshold oscillatory activity (B_3). The characteristics of the subthreshold oscillations were very similar to those of the other cell types (Table3).

Extracellular stimulation

The synaptic response to white matter stimulation (Fig. 10A) applied at low frequency (≤ 0.1 Hz) was examined in cells belonging to all the morphological categories. The most common response observed in all morphological cell groups (n = 6 pyramidal, n = 3 horizontal and n = 4 polymorphic neurons) consisted of a monosynaptic excitatory post-synaptic potential (e.p.s.p.) in isolation (Fig. 10C). In two cases (one pyramidal and one polymorphic) the response was biphasic initiated by an early e.p.s.p followed by an inhibitory postsynaptic potential that reversed at about -67 mV (Fig. 10B).

4.6 Discussion

We have carried out a detailed investigation of the intrinsic electrophysiological properties in relation to the somatodendritic organization of principal neurons in layer V of the LEA. Our main observation is that in layer V of the LEA there are three distinct morphological types of projection neurons: pyramidal cells, horizontal cells and polymorphic neurons. Each morphological subtype is electrophysiologically heterogeneous and no clear distinction among subtypes could be made according to electrophysiological criteria.

Our results indicate that cells in the LEA have similar properties to those in the MEA with the main difference being a smaller proportion of horizontal cells in the LEA However, we can not rule out the possibility that this finding represents an artifact of the relatively small sample size. Pyramidal cells are the most abundant subtype in the LEA and some of these neurons have a star-like soma which we did not observe in MEA pyramidal cells (Hamam et al., 2000). Overall, our data indicates that EC layer V is rather

homogeneous throughout the cortex. This suggests that in spite of the cytoarchitectonic differences of the superficial cell layers in MEA and LEA (Blackstad, 1956), and in spite of the different cortical inputs to the two subdivisions of EC (Burwell and Amaral, 1998b), layer V neurons may carry out a common type of operation across the entire EC It is intriguing that EC layer V gives rise to the most robust intrinsic associational connections of all EC layers (Kohler, 1988; Dolorfo and Amaral, 1998a). These associational fibers terminate primarily in the superficial cell layers but they also extend within layer V. Importantly, while intralaminar associational connections appear to be present in all EC layers, only layer V appears to gives rise to fibers that communicate bidirectionally the MEA and LEA (Kohler, 1988). Again, this seems consistent with layer V being a conduit for communication and common processing across the entire EC. Indeed, when oscillatory population activity is generated in layer V by pharmacological treatment in slices, this typically initiates in a small restricted region from where it uniformly travels in both the medial and lateral direction to invade the entire EC (Iijima et al., 1996; Dickson and Alonso, 1997; Kajiwara et al., 1997).

Our morphological results are generally consistent with previous descriptions of layer V neurons. Ramon y Cajal (Ramon y Cajal, 1902) reported a refractoriness of EC layer V towards the Golgi stain and described only three Golgi stained cells. Lorente de No (1933) provided a more extensive account of neurons within layer V. He indicated that pyramidal cells were the most prominent cell group, which is consistent with our own findings. However, Lorente de No described pyramidal cells as having a thin apical dendrite which ascends to layer I without ramifying and without giving off any branches in layers II and III. We found, however, that both pyramidal cells and horizontal cells

have apical dendrites that typically give off some branches in layer III and ramify with a characteristic apical tuft within layers II and I. Lorente de No also described a horizontal cell which had dendrites that ramified chiefly within the fourth layer. He did not describe, however, the presence of an apical dendrite in this group of cells and it is thus unclear whether they represent the same subtype as the one we have referred to as horizontal cells. In most layer V neurons, Lorente de No reported that the axon gives off a branch that ascends towards the superficial layers and branches repeatedly in layers III, II and I. We were usually unable to follow axonal branches very far from the soma. In most cases, we found the main axon to be directed towards the angular bundle giving off few branches in layers V and VI. In some cases, axonal branches traveled towards the upper layers but we were not able to follow these branches any more superficial than layer III.

We found that neurons in the LEA were electrophysiologically heterogeneous and that no clear electrophysiological distinctions could be made between the three morphological cell groups. Pyramidal, horizontal and polymorphic neurons displayed different degrees of spike-frequency adaptation, inward rectification in both the hyperpolarizing and depolarizing direction and single spikes with monophasic or biphasic AHPs. Significantly, we did not find any neuron that displayed an intrinsic rhythmic bursting behavior similar to that characteristic of a subpopulation of neocortical layer V cells (Connors and Gutnick, 1990). We did find, however, neurons that displayed an early response to a depolarizing step consisting of a spike doublet riding on a low-threshold slow depolarizing envelope. It is possible that this type of discharge is largely dependent on the activation of low-threshold persistent Na^+ current (Agrawal et al., 2001). A similar

mechanism also appears to operate in CA1 pyramidal cells (Azouz et al., 1996; Su et al. 2001).

The intrinsic firing pattern of a particular neuron results from the complex interactions of its morphological structure and the types and somatodendritic distribution of the voltage-gated channels it is endowed with (Llinas, 1988; Mainen and Sejnowski, 1996; Johnston et al., 2000a). The fact that we found within each of the three morphological subgroups neurons with distinct electrophysiological phenotypes suggests that a particular cell type can demonstrate substantial differences in their voltage-gated ion channel composition. It is possible that more detailed biophysical and/or histochemical characterization of layer V neurons will lead to further subclassifications. The inability to discriminate electrophysiologically between the different morphological subgroups has also been reported in other cortical regions such in the perirhinal cortex (Faulkner and Brown, 1999; McGann et al., 2001). An interesting question is why layer V neurons with equivalent somatodendritic structure express distinct intrinsic firing patterns. Perhaps the reason is that while they may receive similar inputs (as suggested by their similar dendritic arrangements) they process these inputs in very different ways. Further investigations will be needed to address these issues.

White matter stimulation typically induced in layer V cells a short latency, monosynaptic, e.p.s.p that could be followed by an i.p.s.p. This is consistent with previous reports that hippocampal feed-back is mainly excitatory on deep EC layer neurons (Finch et al., 1986; van Groen and Lopes da Silva, 1986; Jones, 1987; Jones and Heinemann, 1988; van Haeften et al., 1995).

A salient electrophysiological feature of many neurons from all morphological subtypes in the LEA was their ability to generate slow (3.5 - 14 Hz) rhythmic subthreshold membrane potential oscillations (Schmitz et al., 1998; Hamam et al., 2000; Gloveli et al., 2001). We have noted that subthreshold oscillations in LEC layer V neurons are abolished by tetrodotoxin but persist during pharmacological block of synaptic transmission (unpublished observations) thus suggesting that they are dependent on a low-threshold Na+ conductance (I_{NaP}). While the subthreshold oscillations expressed by EC layer II neurons are dependent on the interaction of I_{NaP} and the time-dependent inward rectifier I_h (Dickson et al., 2000b), we found that subthreshold oscillations in LEA layer V cells are present in neurons that lack I_h. It thus appears that in EC layer V neurons the outward current driving the repolarizing phase of the oscillation is likely to be a low-threshold slow delayed rectifier current such as the M-current (Gutfreund et al., 1995).

In addition to expressing subthreshold oscillations, many oscillating neurons also displayed a repetitive spike cluster discharge. It is not clear what the function of these patterns of activity might be. Subthreshold oscillations in some layer V cells are very robust in terms of their amplitude (up to 8 mV) and rhythmic character (coefficient of rhythmicity of up to 0.85). In EC layer II neurons similar oscillatory activity appears to serve as a basic mechanism for the generation of the theta rhythm (Alonso and Llinas. 1989; Dickson et al., 2000a). Oscillatory activity in layer V neurons may have a similar role though it is unclear how prominent theta activity is in layer V neurons "in vivo" and, particularly, in behaving animals (Chrobak and Buzsaki, 1998; Frank et al., 2001). We have previously proposed that subthreshold oscillation in EC layer II neurons may implement the basic network synchronizing mechanism necessary for creating the proper

temporal relations among converging sensory signals that contribute to a memory event (Alonso and Klink, 1993). A major input to EC layer V neurons is the hippocampal feedback and, while most cortical inputs to the EC terminate primarily on its superficial cell layers II and III (Suzuki and Amaral, 1994; Lavenex and Amaral, 2000). EC layer V also receives substantial projections from limbic and paralimbic cortical areas (Room and Groenewegen, 1986; Rempel-Clower and Barbas, 2000). In addition, the apical dendrites of EC layer V cells are also likely targets of cortical afferents to the superficial cell layers. We suggest that oscillatory activity in EC layer V neurons may also play a role in creating the appropriate temporal dynamics for the coordination of converging hippocampal and cortical information, thereby perhaps allowing layer V cells to act as hippocampal input-output comparators and/or coincidence detectors.

Layer V of the entorhinal cortex demonstrates a very robust epileptic tendency (Jones and Heinemann, 1988; Dickson and Alonso, 1997). However, we have not found intrinsic bursting neurons in the EC. It is possible that the epileptogenic tendency of EC may be more related to highly plastic properties of the synaptic interactions among layer V neurons than to their intrinsic excitability. Basically nothing is known, however, with regard to the dendritic excitability of these neurons which might be very relevant to generate an oscillatory bursting discharge (Turner et al., 1994; Magee and Carruth, 1999; Johnston et al., 2000b) during network interactions (Silva et al., 1991).

In conclusion, layer V of the entorhinal cortex is composed of a heterogeneous population of principal neurons both in terms of morphological (Lingenhahl and Finch, 1991; Hamam et al., 2000; Gloveli et al., 2001) as well as electrophysiological attributes (Jones and Heinemann, 1988; Hamam et al., 2000; Gloveli et al., 2001). This, and the

substantial level of convergence of neocortical and hippocampal inputs onto these neurons suggests that they may play a more significant role in the memory operations of the medial temporal lobe than simply as relay cells for hippocampal feed-back to the neocortex.

4.7 References

Agrawal N, Hamam BN, Magistretti J, Alonso A, Ragsdale DS. 2001. Persistent sodium channel activity mediates subthreshold membrane potential oscillations and low-threshold spikes in rat entorhinal cortex layer V neurons. Neuroscience 102:53-64.

Alonso A, Klink R. 1993. Differential electroresponsiveness of stellate and pyramidal-like cells of medial entorhinal cortex layer II. J. Neurophysiol. 70:128-143.

Alonso A, Llinas RR. 1989. Subthreshold Na^+-dependent theta-like rhythmicity in stellate cells of entorhinal cortex layer II. Nature 342:175-177.

Azouz R, Jensen MS, Yaari Y. 1996. Ionic basis of spike after-depolarization and burst generation in adult rat hippocampal CA1 pyramidal cells. J Physiol 492:211-223.

Baxter MG, Murray EA. 2001. Impairments in visual discrimination learning and recognition memory produced by neurotoxic lesions of rhinal cortex in rhesus monkeys. Eur J Neurosci 13:1228-1238.

Bernasconi N, Bernasconi A, Andermann F, Dubeau F, Feindel W, Reutens DC. 1999. Entorhinal cortex in temporal lobe epilepsy: a quantitative MRI study. Neurology 52:1870-1876.

Blackstad TW. 1956. Commissural connections of the hippocampal region in the rat, with special reference to their mode of termination. J. Comp. Neurol. 105:417-537.

Boeijinga PH, Lopes da Silva FH. 1988. Differential distribution of b and O EEG activity in the entorhinal cortex of the cat. Brain Res. 448:272-286.

Braak H, Braak E. 1991. Neuropathological stageing of Alzheimer-related changes. Acta Neuropathol 82:239-259.

Bragin A, Csicsvari J, Penttonen M, Buzsaki G. 1997. Epileptic afterdischarge in the hippocampal-entorhinal system: Current source density and unit studies. Neurosci 76:1187-1203.

Burwell RD, Amaral DG. 1998a. Cortical afferents of the perirhinal, postrhinal, and entorhinal cortices of the rat. J. Comp. Neurol. 398:179-205.

Burwell RD, Amaral DG. 1998b. Perirhinal and postrhinal cortices of the rat: interconnectivity and connections with the entorhinal cortex. J Comp Neurol 391:293-321.

Chrobak JJ, Buzsaki G. 1998. Gamma oscillations in the entorhinal cortex of the freely behaving rat. J. Neurosci. 18:388-398.

Connors BW, Gutnick MJ. 1990. Intrinsic firing patterns of diverse neocortical neurons. Trends Neurosci. 13:99-104.

Deadwyler SA, West JR, Cotman CW, Lynch G. 1975. Physiological studies of the reciprocal connections between the hippocampus and entorhinal cortex. Exp. Neurol. 49:35-57.

Dickson CT, Alonso A. 1997. Muscarinic induction of synchronous population activity in the entorhinal cortex. J. Neurosci. 17:6729-6744.

Dickson CT, Magistretti J, Shalinsky M, Hamam B, Alonso A. 2000a. Oscillatory activity in entorhinal neurons and circuits. Mechanisms and function. Ann N Y Acad Sci 911:127-150.

Dickson CT, Magistretti J, Shalinsky MH, Fransen E, Hasselmo ME, Alonso A. 2000b. Properties and role of I(h) in the pacing of subthreshold oscillations in entorhinal cortex layer II neurons. J Neurophysiol 83:2562-2579.

Dickson CT, Mena AR, Alonso A. 1997. Electroresponsiviness of medial entorhinal cortex layer III neurons *in vitro*. Neuroscience 81:937-950.

Dolorfo CL, Amaral DG. 1998a. Entorhinal cortex of the rat: organization of intrinsic connections. J. Comp. Neurol. 398:49-82.

Dolorfo CL, Amaral DG. 1998b. Entorhinal cortex of the rat: topographic organization of the cells of origin of the perforant path projection to the dentate gyrus. J Comp Neurol 398:25-48.

Du F, Tore E, Kohler C, Lothman EW, Schwarcz R. 1995. Preferential neuronal loss in layer III of the medial entorhinal cortex in rat models of temporal lobe epilepsy. J. Neurosci. 15:8301-8313.

Faulkner B, Brown TH. 1999. Morphology and physiology of neurons in the rat perirhinal-lateral amygdala area. J Comp Neurol 411:613-642.

Finch DM, Wong EE, Devian EL, Babb TL. 1986. Neurophysiology of limbic system pathways in the rat: projections from the subicular complex and hippocampus to the entorhinal cortex. Brain Res. 397:205-213.

Frank LM, Brown EN, Wilson MA. 2001. A comparison of the firing properties of putative excitatory and inhibitory neurons from ca1 and the entorhinal cortex. J Neurophysiol 86:2029-2040.

Glaser EM, McMullen NT. 1984. The fan-in projection method for analyzing dendrite and axon systems. J Neurosci Methods 12:37-42.

Glaser EM, Van der Loos H, Gissler M. 1979. Tangential orientation and spatial order in dendrites of cat auditory cortex: a computer microscope study of Golgi-impregnated material. Exp Brain Res 36:411-431.

Gloveli T, Dugladze T, Schmitz D, Heinemann U. 2001. Properties of entorhinal cortex deep layer neurons projecting to the rat dentate gyrus. Eur J Neurosci 13:413-420.

Gloveli T, Schmitz D, Empson RM, Dugladze T, Heinemann U. 1997. Morphological and electrophysiological characterization of layer III cells of the medial entorhinal cortex of the rat. Neurosci 77:629-648.

Gomez-Isla T, Price JL, McKeel DW, Morris JC, Growdon JH, Hyman BT. 1996. Profound loss of layer II entorhinal cortex neurons occurs in very mild Alzheimer's disease. J. Neurosci. 16:4491-4500.

Gutfreund Y, Yarom Y, Segev I. 1995. Subthreshold oscillations and resonant frequency in guinea-pig cortical neurons: physiology and modelling. J. Physiol. (Lond.) 483:621-640.

Hamam BN, Kennedy TE, Alonso A, Amaral DG. 2000. Morphological and electrophysiological characteristics of layer V neurons of the rat medial entorhinal cortex. J. Comp. Neurol. 418:457-472.

Hjorth-Simonsen A, Jeune B. 1972. Origin and termination of the hippocampal perforant path in the rat studied by silver impregnation. J. Comp. Neurol. 174:591-606.

Hyman BT, Van Hoesen GW, Damasio AR, Barnes LL. 1984. Alzheimer's disease: cell-specific pathology isolates the hippocampal formation. Science 225:1168-1170.

Iijima T, Witter MP, Ichikawa M, Tominaga T, Kajiwara R, Matsumoto G. 1996. Entorhinal-hippocampal interactions revealed by real-time imaging. Science 172:1176-1179.

Insausti R, Amaral DG, Cowan WM. 1987. The entorhinal cortex of the monkey: II. Cortical afferents. J. Comp. Neurol. 264:356-395.

Insausti R, Herrero MT, Witter MP. 1997. Entorhinal cortex of the rat: cytoarchitectonic subdivisions and the origin and distribution of cortical efferents. Hippocampus 7:146-183.

Johnston D, Hoffman DA, Magee JC, Poolos NP, Watanabe S, Colbert CM, Migliore M. 2000a. Dendritic potassium channels in hippocampal pyramidal neurons. J Physiol 525 Pt 1:75-81.

Johnston D, Hoffman DA, Poolos NP. 2000b. Potassium channels and dendritic function in hippocampal pyramidal neurons. Epilepsia 41:1072-1073.

Jones RS. 1987. Complex synaptic responses of entorhinal cortical cells in the rat to subicular stimulation in vitro: demonstration of an NMDA receptor- mediated component. Neurosci Lett 81:209-214.

Jones RSG, Heinemann UFH, Lambert JDC. 1992. The entorhinal cortex and generation of seizure activity: Studies of normal synaptic transmission and epileptogenesis. In: Avanzini G, Engel JJ, Fariello R, Heinemann U, Avanzini G, Engel JJ, Fariello R, Heinemann UAvanzini G, Engel JJ, Fariello R, Heinemann Us. Neurotransmitters in Epilepsy (Epilepsy Res. Suppl. 8). Amsterdam: Elsevier. p 173-180. .

Jones RSG, Heinemann V. 1988. Synaptic and intrinsic responses of medial entorhinal cortical cells in normal and magnesium-free medium "in vitro". J. Neurophysiol. 59:1476-1496.

Jones RSG, Lambert JDC. 1990. Synchronous discharges in the rat entorhinal cortex *in vitro*: site of initiation and the role of excitatory amino acid receptors. Neuroscience 34:657-670.

Kajiwara R, Matsukawa M, Alonso A, Iijima T. 1997. High speed optical imaging of muscarinic induced epileptiform activity in the entorhinal cortex (EC) network. Soc Neurosci Abs Submitted.

Klink R, Alonso A. 1997. Morphological characteristics of layer II projection neurons in the rat medial entorhinal cortex. Hippocampus 7:571-583.

Kohler C. 1986. Intrinsic connections of the retrohippocampal region in the rat brain. II. The medial entorhinal area. J. Comp. Neurol. 246:149-169.

Kohler C. 1988. Intrinsic connections of the retrohippocampal region in the rat brain. III. The lateral entorhinal area. J. Comp. Neurol. 271:208-228.

Lavenex P, Amaral DG. 2000. Hippocampal-neocortical interaction: a hierarchy of associativity. Hippocampus 10:420-430.

Leonard BW, Amaral DG, Squire LR, Zola-Morgan S. 1995. Transient memory impairment in monkeys with bilateral lesions of the entorhinal cortex. J. Neurosci. 15:5637-5659.

Lingenhöhl K, Finch DM. 1991. Morphological characterization of rat entorhinal neurons in vivo: soma-dendritic structure and axonal domains. Exp. Brain Res. 84:57-74.

Llinas RR. 1988. The intrinsic electrophysiological properties of mammalian neurons: Insights into central nervous system function. Science 242:1654-1664.

Magee JC, Carruth M. 1999. Dendritic voltage-gated ion channels regulate the action potential firing mode of hippocampal CA1 pyramidal neurons. J Neurophysiol 82:1895-1901.

Mainen ZF, Sejnowski TJ. 1996. Influence of dendritic structure on firing pattern in model neocortical neurons. Nature 282:363-366.

McGann JP, Moyer JR, Jr., Brown TH. 2001. Predominance of late-spiking neurons in layer VI of rat perirhinal cortex. J Neurosci 21:4969-4976.

McMullen NT, Glaser EM, Tagamets M. 1984. Morphometry of spine-free nonpyramidal neurons in rabbit auditory cortex. J Comp Neurol 222:383-395.

Naber PA, Lopes da Silva FH, Witter MP. 2001. Reciprocal connections between the entorhinal cortex and hippocampal fields CA1 and the subiculum are in register with the projections from CA1 to the subiculum. Hippocampus 11:99-104.

Ramon y Cajal S. 1902. Sobre un ganglio especial de la corteza esfeno-occipital. Trab. del Lab. de invest. Biol. Univ. Madrid 1:189-201.

Rempel-Clower NL, Barbas H. 2000. The laminar pattern of connections between prefrontal and anterior temporal cortices in the Rhesus monkey is related to cortical structure and function. Cereb Cortex 10:851-865.

Room P, Groenewegen HJ. 1986. Connections of the parahippocampal cortex. I. Cortical afferents. J. Comp. Neurol. 251:415-450.

Scharfman HE. 1996. Hyperexcitability of entorhinal cortex and hippocampus after application of aminooxyacetic acid (AOAA) to layer III of the rat entorhinal cortex in vitro. J. Neurophysiol. 76:2986-3001.

Schmitz D, Gloveli T, Behr J, Dugladze T, Heinemann U. 1998. Subthreshold membrane potential oscillations in neurons of deep layers of the entorhinal cortex. Neuroscience 85:999-1004.

Silva LR, Amital Y, Connors BW. 1991. Intrinsic oscillations of neocortex generated by layer 5 pyramidal neurons. Science 251:432-434.

Spencer SS, Spencer DD. 1994. Entorhinal-hippocampal interactions in medial temporal lobe epilepsy. Epilepsia 35:721-727.

Su H, Alroy G, Kirson ED, Yaari Y. 2001. Extracellular calcium modulates persistent sodium current-dependent burst-firing in hippocampal pyramidal neurons. J Neurosci 21:4173-4182.

Suzuki W, Amaral DG. 1994. Topographic organization of the reciprocal connections between the monkey entorhinal cortex and the perirhinal and parahippocampal cortices. J Neurosci 14:1856-1857.

Suzuki WA, Eichenbaum H. 2000. The neurophysiology of memory. Ann N Y Acad Sci 911:175-191.

Suzuki WA, Miller EK, Desimone R. 1997. Object and place memory in the macaque entorhinal cortex. J. Neurophysiol. 78:1062-1081.

Turner RW, Maler L, Deerinck T, Levinson SR, Ellisman MH. 1994. TTX-sensitive dendritic sodium channels underlie oscillatory discharge in a vertebrate sensory neuron. J Neurosci 14:6453-6471.

van der Linden S, Lopes da Silva FH. 1998. Comparison of the electrophysiology and morphology of layers III and II neurons of the rat medial entorhinal cortex in vitro. Eur. J. Neurosci. 10:1479-1489.

van Groen T, Lopes da Silva FH. 1986. The organization of the reciprocal connections between the subiculum and the entorhinal cortex in the cat. II. An electrophysiological study. J. Comp. Neurol. 251:111-120.

van Groen T, van Haren FJ, Witter MP, Groenewegen HJ. 1986. The organization of the reciprocal connections between the subiculum and the entorhinal cortex in the cat: I. A neuroanatomical tracing study. J Comp Neurol 250:485-497.

van Haeften T, Jorritsma-Byham B, Witter MP. 1995. Quantitative morphological analysis of subicular terminals in the rat entorhinal cortex. Hippocampus 5:452-459.

Van Hoesen G, Pandya DN. 1975. Some connections of the entorhinal (area 28) and perirhinal (area 35) cortices of the rhesus monkey. I. Temporal lobe afferents. Brain Res 95:1-24.

Witter MP, Amaral DG. 1991. Entorhinal cortex of the monkey: V. Projections to the dentate gyrus, hippocampus, and subicular complex. J. Comp. Neurol. 307:437-459.

Witter MP, Naber PA, van Haeften T, Machielsen WC, Rombouts SA, Barkhof F, Scheltens P, Lopes da Silva FH. 2000. Cortico-hippocampal communication by way of parallel parahippocampal- subicular pathways. Hippocampus 10:398-410.

4.8 Tables

Table 1. Summary of morphological parameters[1]

Cell Type	Soma Area (μ²) (range)	Dendrite Length (μ) (range)	Number of Primary Dendrites (range)	Basal Dendrites Diameter* (μ) (range)	Apical Dendrites Diameter* (μ) (range)
PY	373.55±123.01 (200-467)	7826±2919 (2805-1173)	6.33±2.16 (4-9)	1.69±0.93 (0.59-4.48) (n= 5)	4.24±1.6 (2.53-6.05)
HC	425.9±59.49 (360-475)	8197±3731 (4721-12138)	7.33±2.08 (5-9)	3.32±1.3 (1.31-4.99) (n= 3)	5.22±0.67 (4.65-5.95)
PC	392.65±37.54 (343-425)	10893±1301 (9488-12567)	6.5±1.73 (5-9)	3.4±1.44 (1.35-6.02) (n= 3)	-

[1]Values are means ± s.d. and range for 6 pyramidal cells (PY), 3 horizontal cells (HC) and 4 polymorphic cells (PC). *Measurements were made at the base of the primary branches.

Table 2. Summary of electrophysiological parameters[1]

Cell Type	Rin (MΩ)	Time Constant (ms)	RMP (mV)	Spike Thre. (mV)	Amp. (mV)	Dur. (ms)	AHP Amp. (mV)	SAG% (n/nT)
PY	55.14±13.42	12.91±2.1	63.19±3.58	42.68±2.56	66.65±5.23	1.59±0.22	17.58±2.64	14.25±4.88 (17/21)
HC	59.52±18.39	10.53±2.17	62.66±4.35	42.77±2.79	63.36±7.35	1.65±0.18	15.69±2.61	16.61±12.46 (2/4)
PC	53.96±12.32	12.30±2.51	62.4±2.68	40.08±4.93	62.43±9.31	1.59±0.38	17.63±3.32	14.15±3.18 (7/12)

[1]Values are means ± s.d. for 21 pyramidal cells (PY), 4 horizontal cells (HC) and 12 polymorphic cells (PC). **Rin**, input resistance; **RMP**, resting membrane potential; Spike threshold, amplitude and duration; **AHP**, after hyperpolarization amplitude; **SAG%**, sag percentage (rectification index). See Methods section for details on measurements.

Table 3. Summary of the parameters for the subthreshold oscillatory activity[1]

Cell Type	Frequency (Hz) (n/nT)	Frequency range (Hz)	Amp. Range (mV)	Rhythmicity Coefficient (n/nT)
PY	6.41±2.67 (14/21)	(3.5-12)	2-7.8	0.51±0.15 (14/21)
HC	10.76±3.5 (3/4)	(7.05-14)	1.6-5	0.41±0.17 (3/4)
PC	8.86±2.43 (7/12)	(6.2-12.9)	1.9-8.3	0.47±0.09 (7/12)

[1]Values are means ± s.d. for 21 pyramidal cells (PY), 4 horizontal cells (HC) and 12 polymorphic cells (PC). All measurements were taken at a membrane potential just below spike threshold (~ –46 mV).

4.9 Figures

Fig. 1: Morphological subtypes in lateral entorhinal area (LEA) layer V. **A**: digitally reconstructed examples of a pyramidal, horizontal and a polymorphic neuron. The different layers of the entorhinal cortex are also indicated for each example. Scale bar = 100 μm. **B**: compound stick polar histogram plot is indicated for the basal dendrites of each of the three distinct morphological subtypes. In the case of the pyramidal and horizontal polar plots, the shaded area represents 29 and 80 % of the total dendritic distribution, respectively. Note the significant preference for the latter group towards horizontal basal dendritic distribution. White arrows represent the compound dendritic orientation angle for pyramidal and horizontal neurons (see methods). **C**: the corresponding fan-in-diagram plots for the compound stick histograms in B.

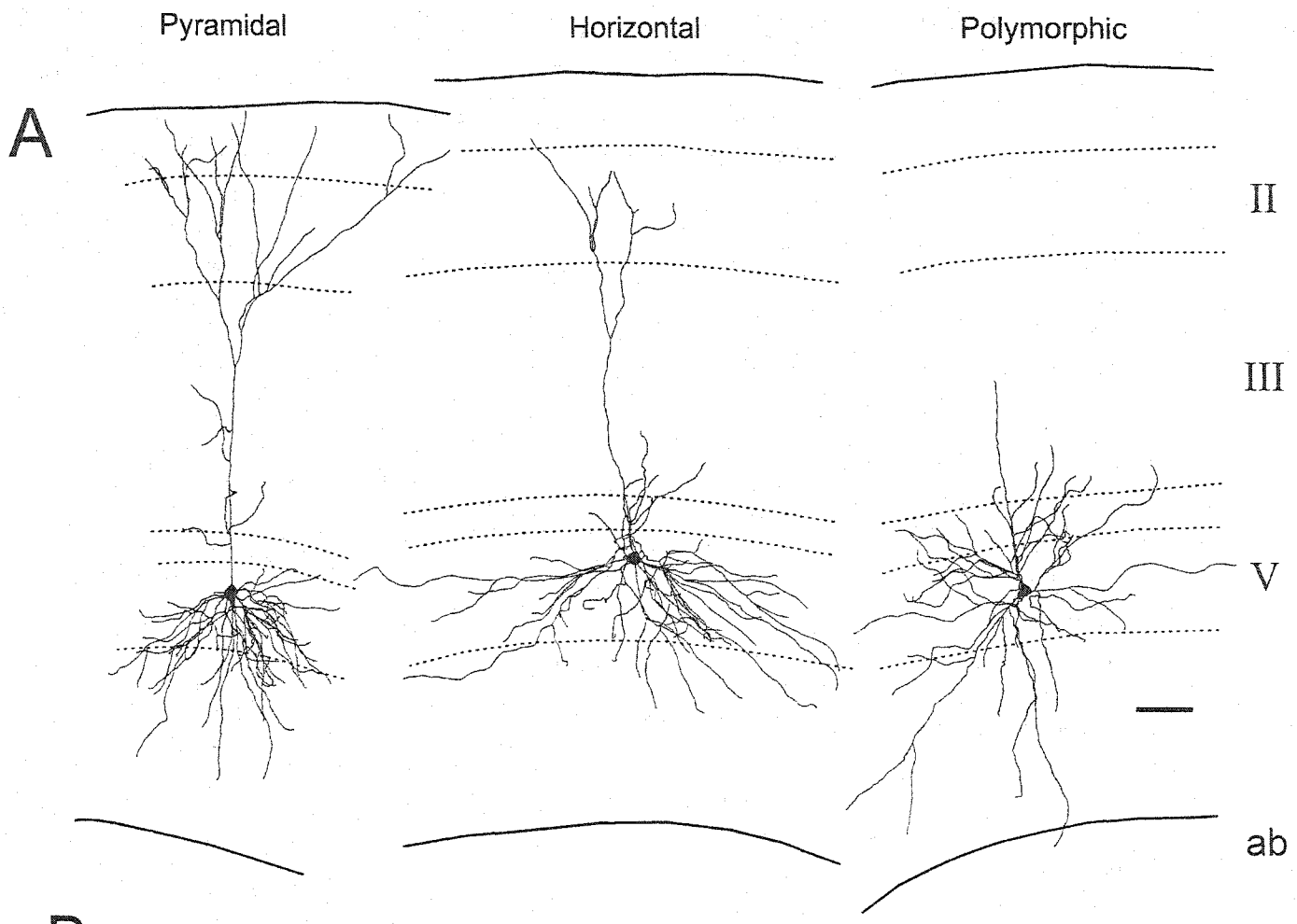
Pyramidal
Horizontal
Polymorphic
A
II
III
V
ab

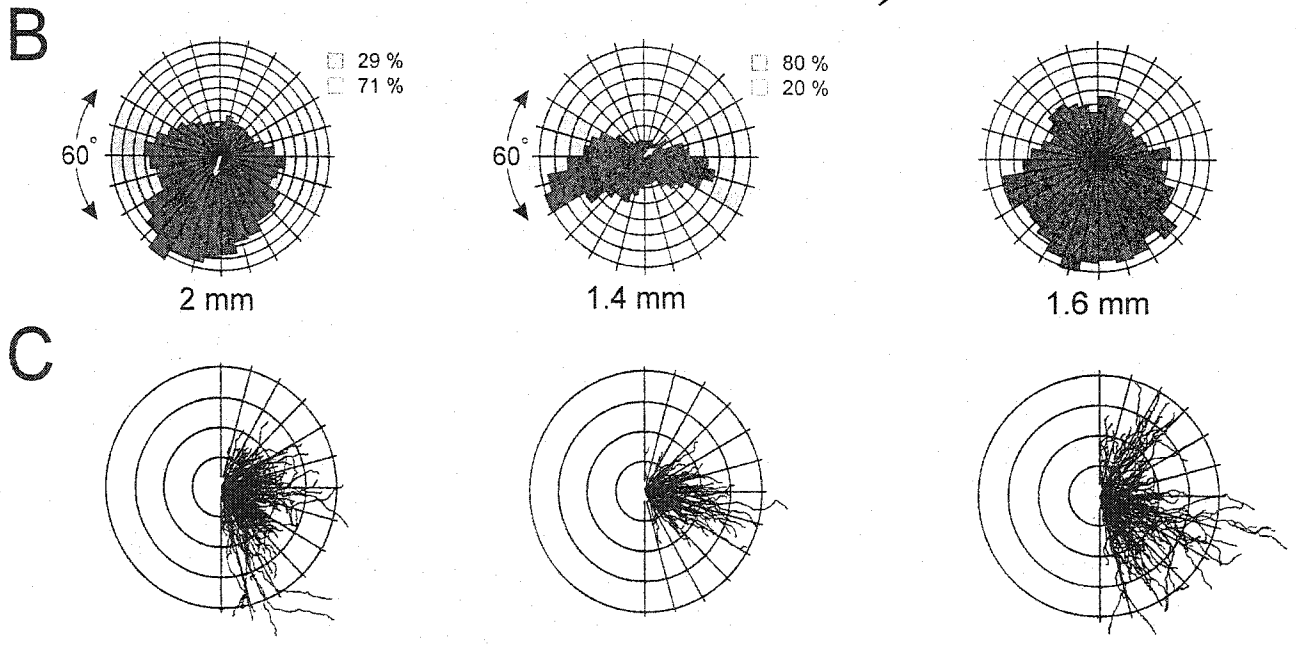
B
29 %
71 %
60°
2 mm
80 %
20 %
60°
1.4 mm
1.6 mm
C

Fig 2: A typical pyramidal neuron with a large soma in layer V of the LEA. **A**: Low power photomicrograph of this neuron. Note the main axonal branch as indicated by the arrow. Scale bar = 100 μm. **B**: soma and basal dendritic plexus of the neuron in A at an expanded scale. Scale bar = 100 μm. The inset in B indicates the position of the neuron in the horizontal brain slice. Scale bar = 1 mm.

A

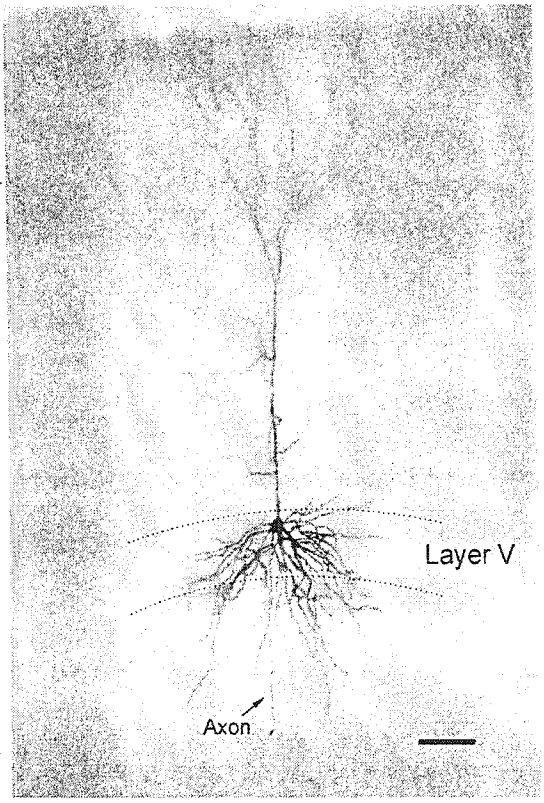

B

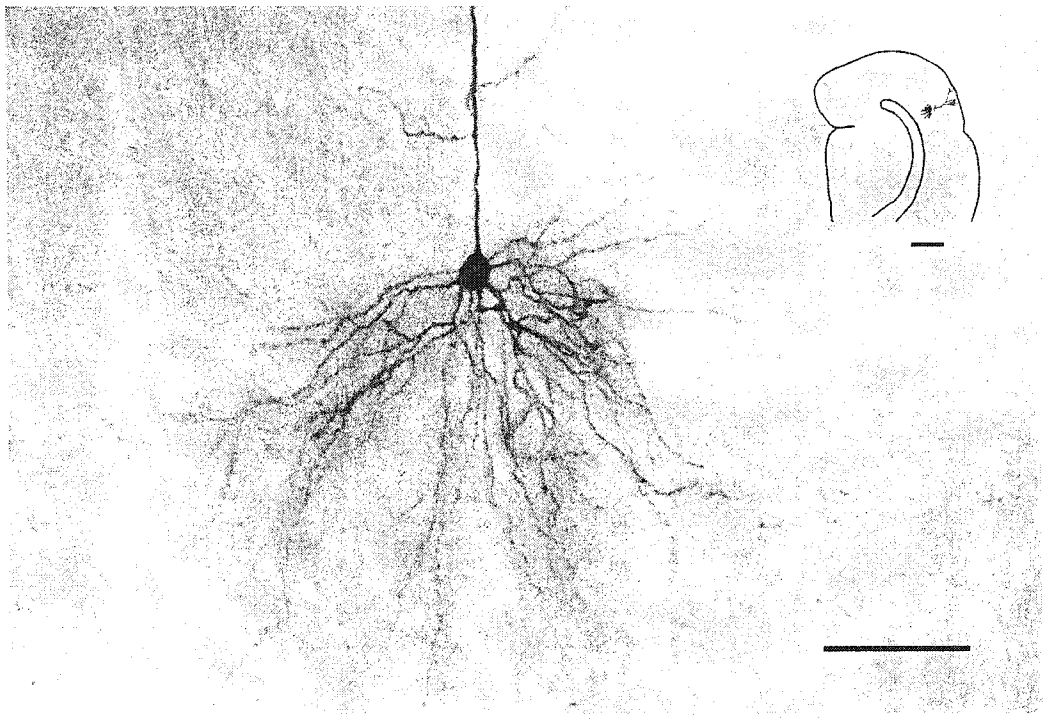

Fig 3: Some pyramidal neurons display instantaneous inward rectification along with subthreshold membrane potential oscillations and spike frequency adaptation. **A**: the current intensity/voltage response (I/V) plots for the same neuron as in figure 2. Note the absence of time-dependent inward rectification. Scale bars = 0.1 second, 1 nA and 20 mV; Resting membrane potential (Vr) = -62 mV. The inset displays an action potential with a monophasic after-hyperpolarizing potential (AHP). Scale bars = 0.02 second and 10 mV. **B**: plot of the I/V relation in A. Note the upward bending in the curve indicating inward rectification. **C**: voltage response to a 4 second positive current pulse application demonstrating pronounced spike frequency adaptation and cluster firing pattern. Scale bars = 1 second, 0.5 nA and 20 mV; Vr = -67 mV. **D**: (upper panel) in the same neuron, long-lasting trace demonstrating the emergence of subthreshold oscillations (reflected as an increase in the voltage trace noise) as the cell is progressively depolarized from its resting level by d.c. current injection. Scale bars = 20 second, 0.5 nA and 20 mV; Vr = -70 mV. The lower right panel illustrates the squared segment from the upper trace at an expanded time and voltage scale. Note the robust rhythmic subthreshold oscillations at a frequency of about 9.1 Hz as demonstrated by the power spectrum and autocorrelation function on the right panel. Scale bars = 1 second, 10 mV and (inset) 0.2 second.

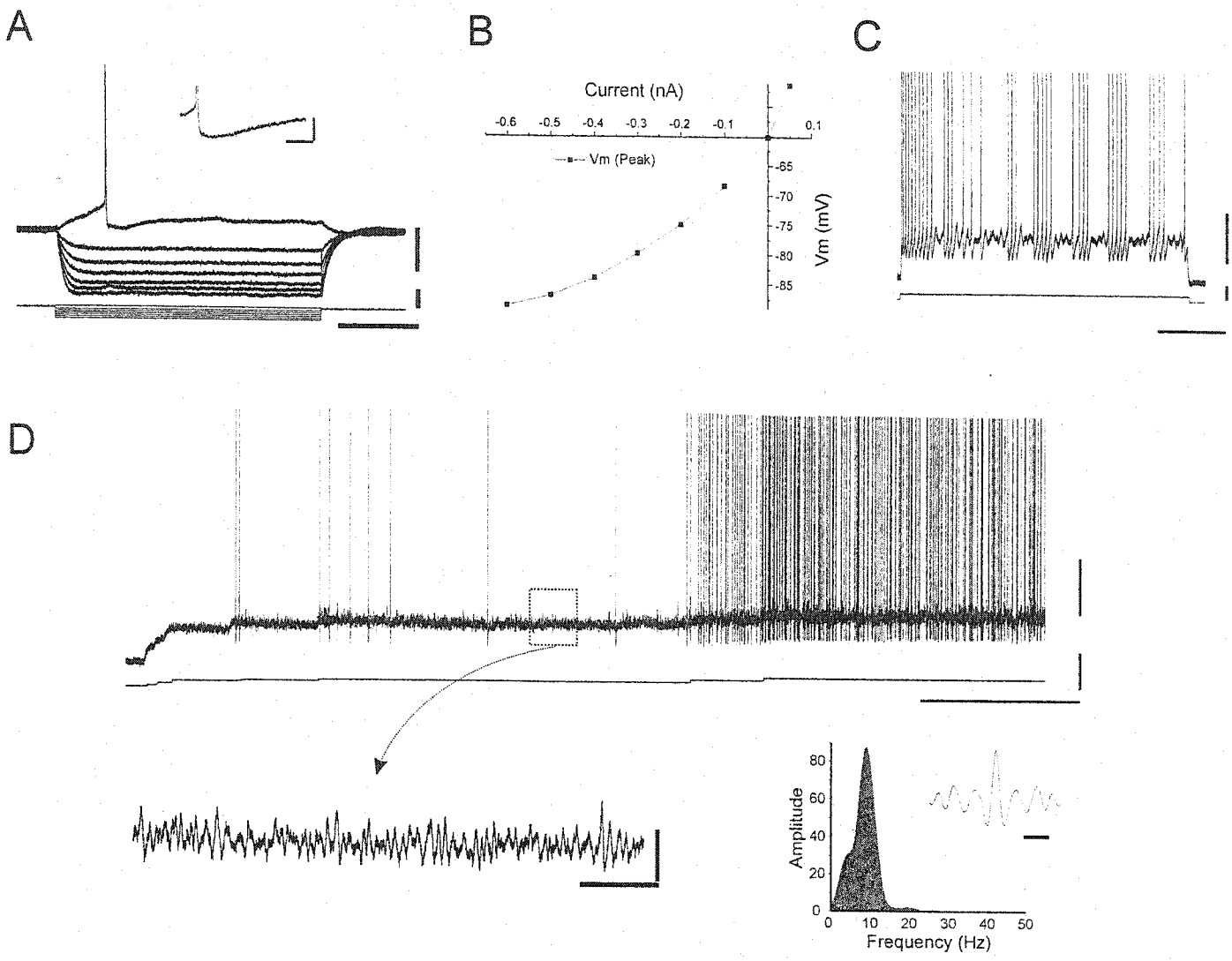
A
B
C
D
Current (nA)
-0.6
-0.5
-0.4
-0.3
-0.2
-0.1
0.1
Vm (Peak)
-65
-70
-75
-80
-85
Vm (mV)
Amplitude
80
60
40
20
0
0
10
20
30
40
50
Frequency (Hz)

Fig. 4: Some pyramidal neurons display time dependent inward rectification. **A**: low power photomicrograph of a pyramidal neuron with a small size soma. Scale bars = 100 μm. The inset indicates the position of the neuron in the horizontal slice. Scale bars = 1 mm. **B**: the digital reconstruction of the neuron in A. Scale bar = 100 μm. **C** and **D**: the I/V relation and the corresponding I/V plot, respectively, for the neuron in A. Note that this neuron displays time-dependent inward rectification as evident by the difference in the voltage level from the early response (peak; square) to the steady state level (circle). Scale bars = 0.1 second, 1 nA and 10 mV; Vr = -70 mV. The inset in C illustrates that this neuron's spike displayed a biphasic AHP. Scale bars = 0.02 second and 10 mV. **E**: voltage response to low intensity depolarizing current pulses in a different pyramidal neuron. Note that this neuron displayed an early response consisting of a spike doublet riding on a depolarizing envelope. Scale bars = 0.1 second, 1 nA and 10 mV; Vr = -79 mV. **F**: this neuron responded to a long-lasting suprathreshold current pulse with minimal spike frequency adaptation. Scale bars = 1 second, 1 nA and 10 mV; Vr = -73 mV.

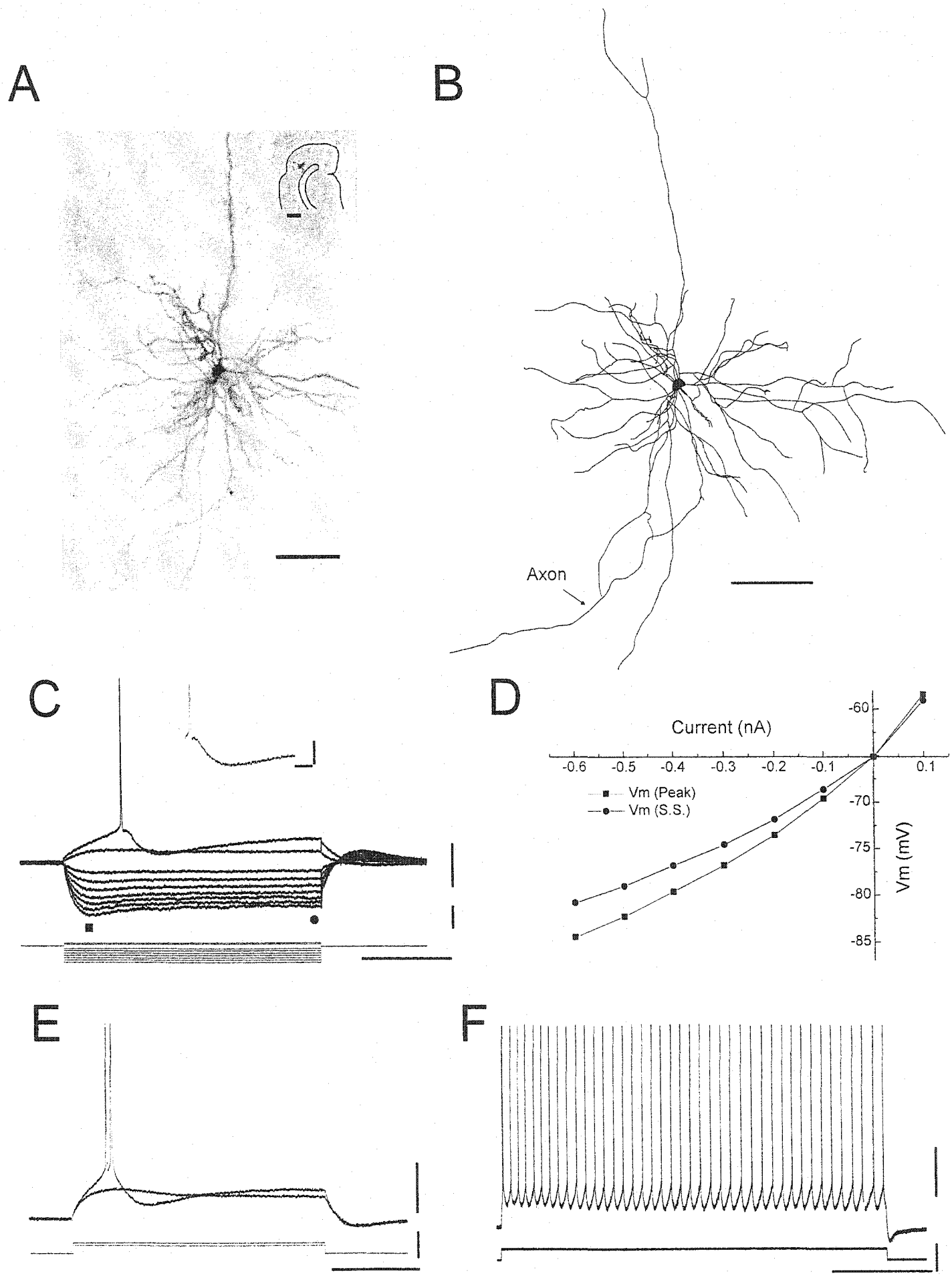
A
B
Axon
C
D
Current (nA)
-0.6
-0.5
-0.4
-0.3
-0.2
-0.1
0.1
Vm (Peak)
Vm (S.S.)
-60
-70
-75
-80
-85
Vm (mV)
E
F

Fig. 5: Some pyramidal neurons have star-shaped soma. **A**: photomicrograph depicting a typical pyramidal neuron that had a star like cell body. Scale bar = 100 μm. The inset indicates the position of the neuron in the slice. Scale bar = 1 mm. **B**: 3-D reconstruction of the neuron in A. The inset is an expansion of the somatic area showing in detail the star like morphology of the cell body. Scale bars = 100 μm and (inset) 20 μm. **C** and **D**: the I/V relation and the corresponding plot, respectively, demonstrating the presence of both fast and time dependent inward rectification. Scale bars = 0.1 second, 1 nA and 20 mV; Vr = -67 mV. **E**: in response to a long step depolarization this neuron responded with an initial rapidly adapting train of action potentials followed by a regular discharge at slow frequency. Scale bars = 1 second, 1 nA and 20 mV; Vr = -71 mV.

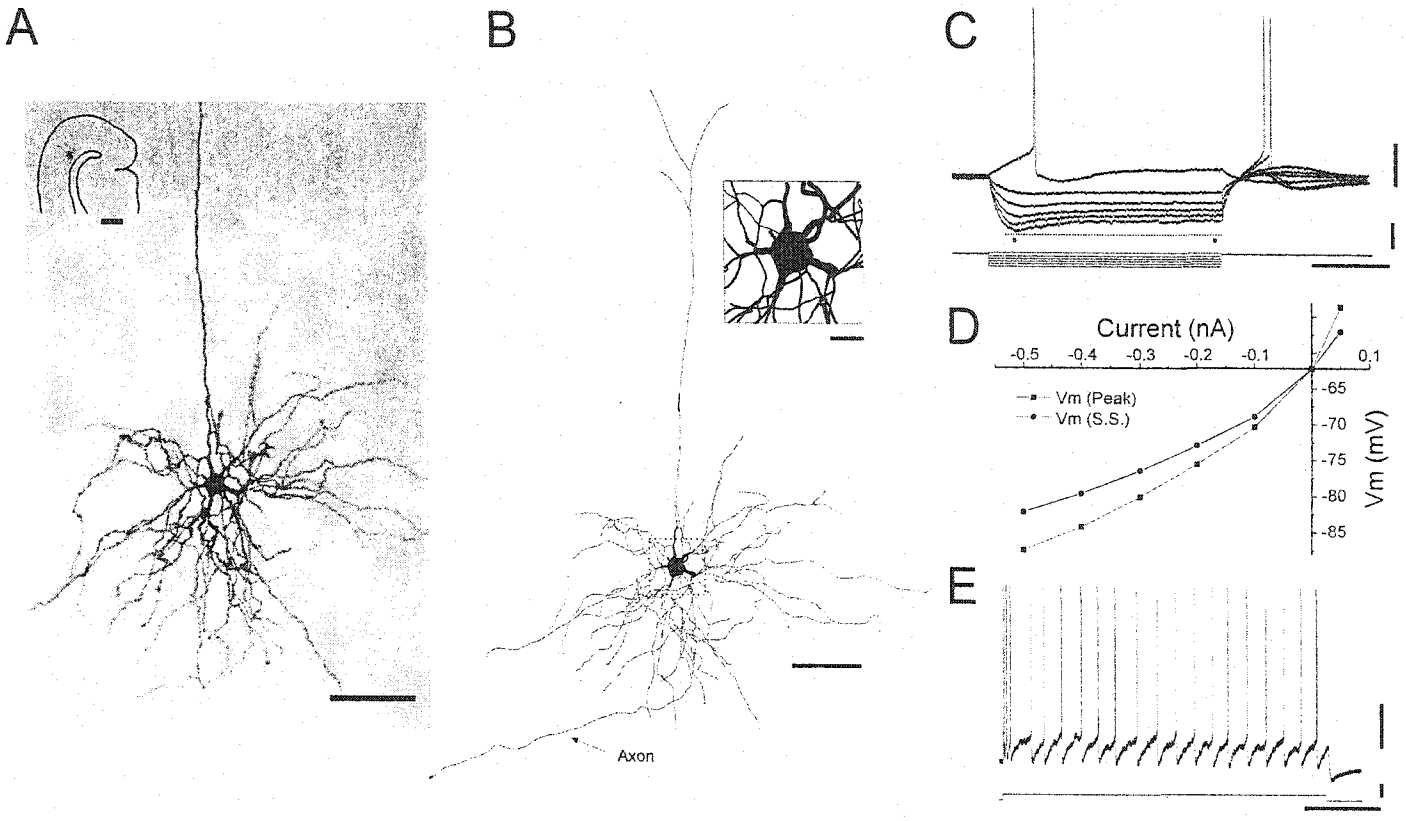
A
B
C
D
E
Axon
Current (nA)
-0.5
-0.4
-0.3
-0.2
-0.1
0.1
Vm (Peak)
Vm (S.S.)
-65
-70
-75
-80
-85
Vm (mV)

Fig. 6: A typical horizontal neuron in layer V of the LEA. The left panel composite illustrates the full extent of the neuron with the inset indicating the position of this neuron in the slice. Scale bars = 100 μm and (inset) 1 mm. The right panel shows high magnification images of different sections of the dendritic tree as indicated in the left panel. Note the dendritic spines and branches of the axon (**a**, **b**, **c**, **d** and **e**, respectively). Scale bar = 10 μm.

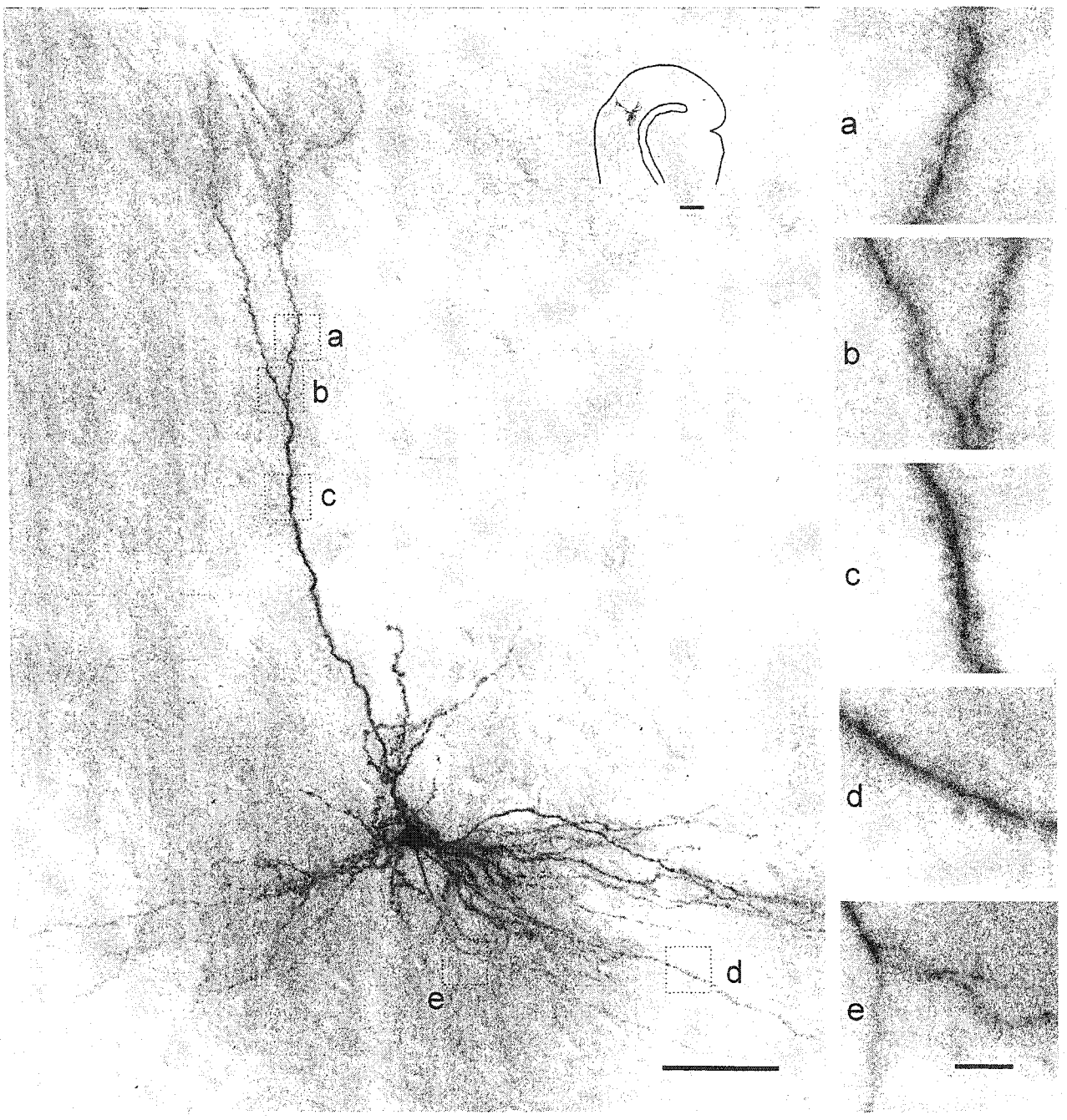
a
b
c
d
e
a
b
c
d
e

Fig. 7: Electrophysiological attributes of the horizontal neuron depicted figure 6. **A** and **B**: I/V relation and I/V plot, respectively, demonstrating the presence of instantaneous and time dependent inward rectification. Scale bars = 0.1 second, 1 nA and 20 mV; Vm = -65 mV. **C**: response of the cell to close to threshold depolarizing pulses from a hyperpolarized level (Vm = -90 mV). Scale bars = 0.1 second, 1 nA and 20 mV. The inset shows a typical bi-physic spike AHP with a small depolarizing after potential. Scale bars = 0.02 second and 10 mV. **D**: moderate spike frequency adaptation and cluster firing seen in the same neuron. Scale bars = 1 second, 1 nA and 20 mV; Vr = -70 mV.

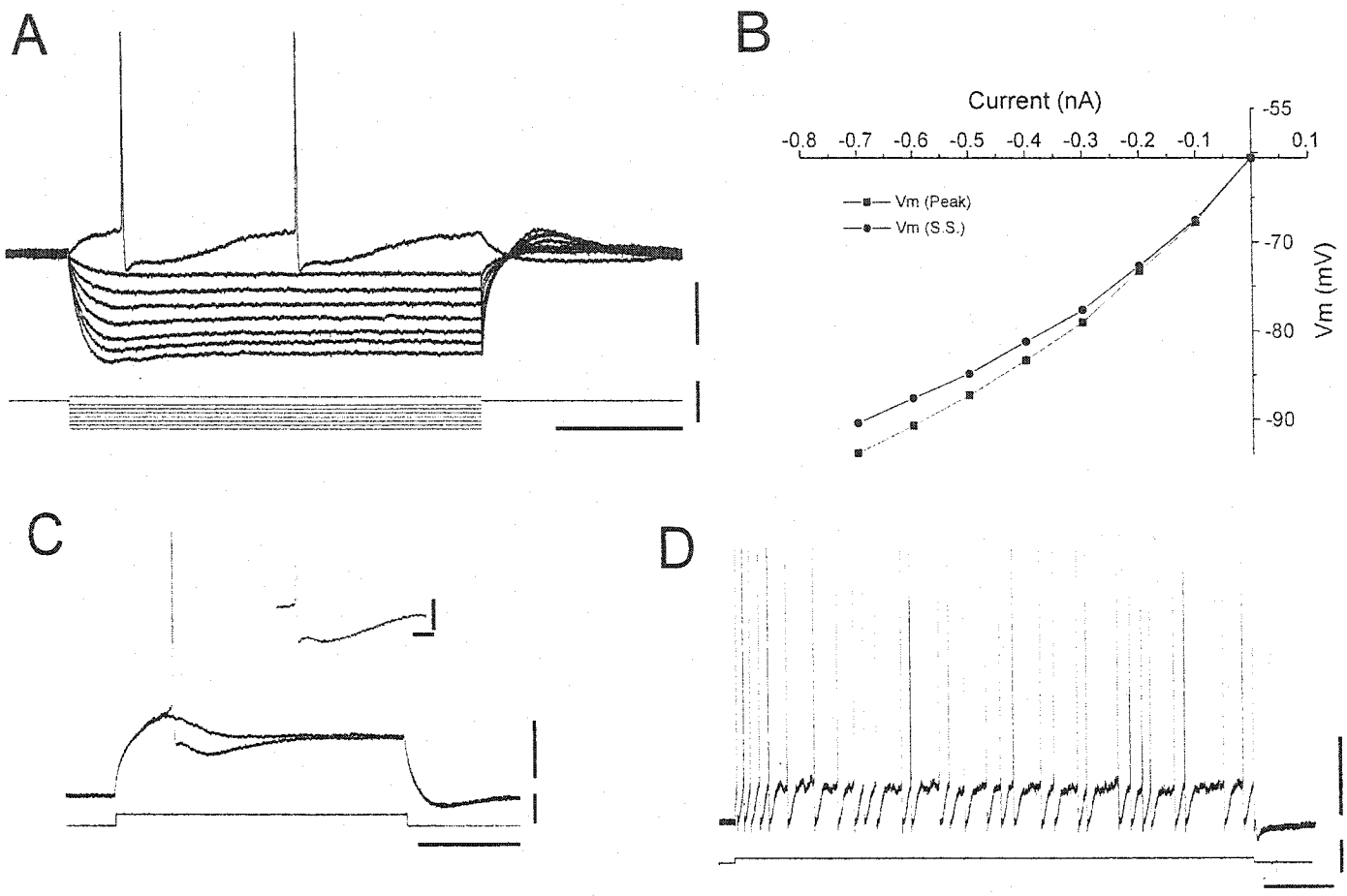
A
B
Current (nA)
-0.8
-0.7
-0.6
-0.5
-0.4
-0.3
-0.2
-0.1
0.1
-55
-70
-80
-90
Vm (mV)
Vm (Peak)
Vm (S.S.)
C
D

Fig. 8: Two examples of polymorphic neurons. **A**: a photomicrograph depicting a typical polymorphic neuron. Scale bar = 100 μm. **B**: the digitally reconstructed drawing of the same neuron is shown. Note the axon crossing into the lateral aspect of the angular bundle. The inset indicates the position of this neuron in the slice. Scale bars = 100 μm and (inset) 1 mm **C**: another photomicrograph depicting the polymorphic neuron in figure 1. Scale bars = 100 μm and (inset) 1 mm.

A

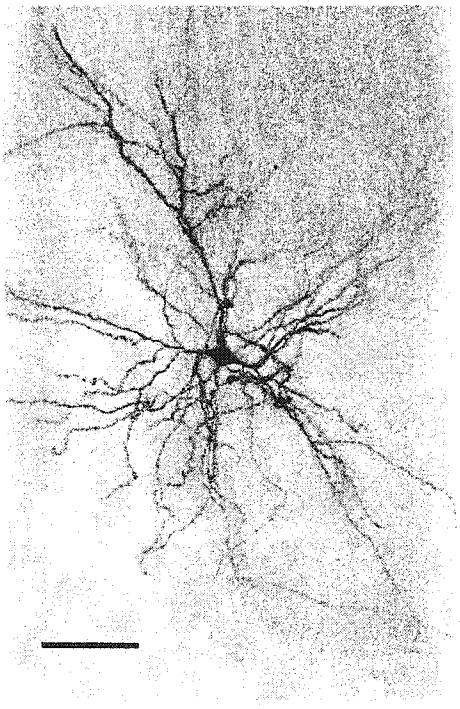

B

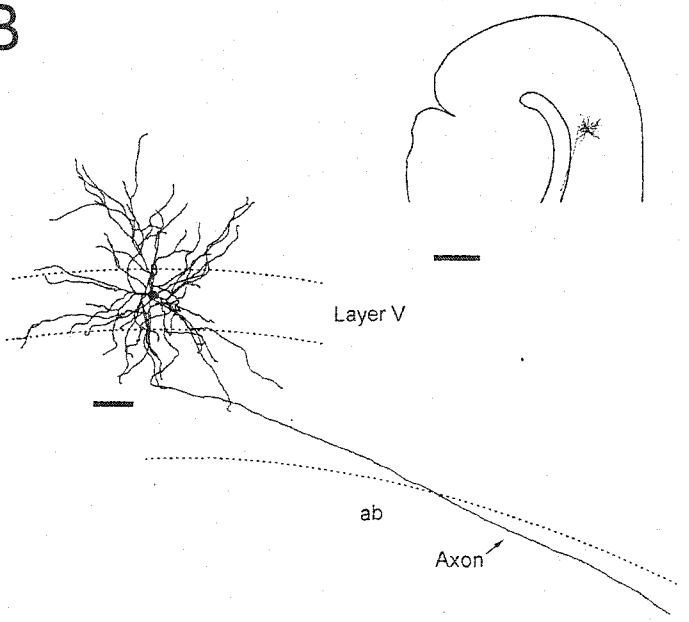

C

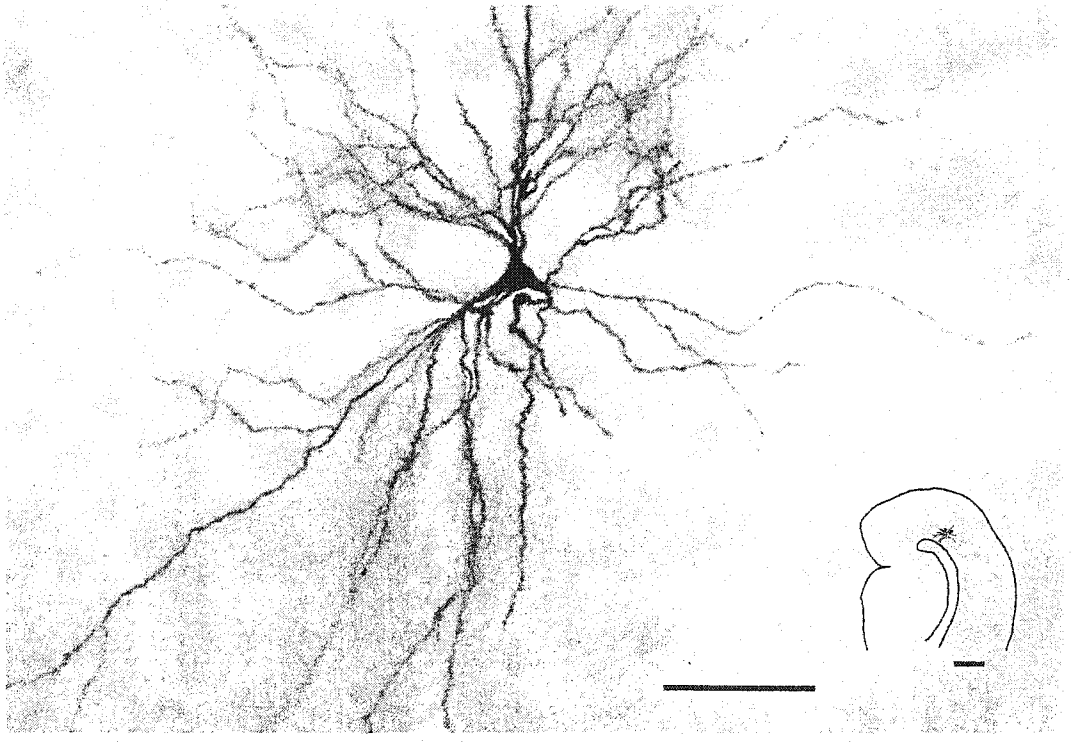

Fig. 9: Diversity of electrophysiological attributes of polymorphic neurons. The left (**A**) and right (**B**) panels raw correspond to the same neurons as in Fig. 8 A and C, respectively. $\mathbf{A_{1,2}}$ and $\mathbf{B_{1,2}}$: the I/V relation and plot, respectively, for each neuron. Note that cell A displays both instantaneous as well as time-dependent inward rectification. Scale bars = 0.1 second, 1 nA and 20 mV; Vr = -67 and -73 mV for cell A and B, respectively. The inset in panel 1 demonstrates a biphasic and a monophasic spike AHP for cells A and B, respectively. Scale bars = 0.02 second and 10 mV. $\mathbf{A_3}$, $\mathbf{B_3}$: voltage responses to a suprathreshold depolarizing current step. Note that while cell A shows minimal spike adaptation cell B displays robust adaptation. Scale bars = 1 second, 1 nA and 20 mV; Vr = -66 mV (A3) and -67 mV (B3).

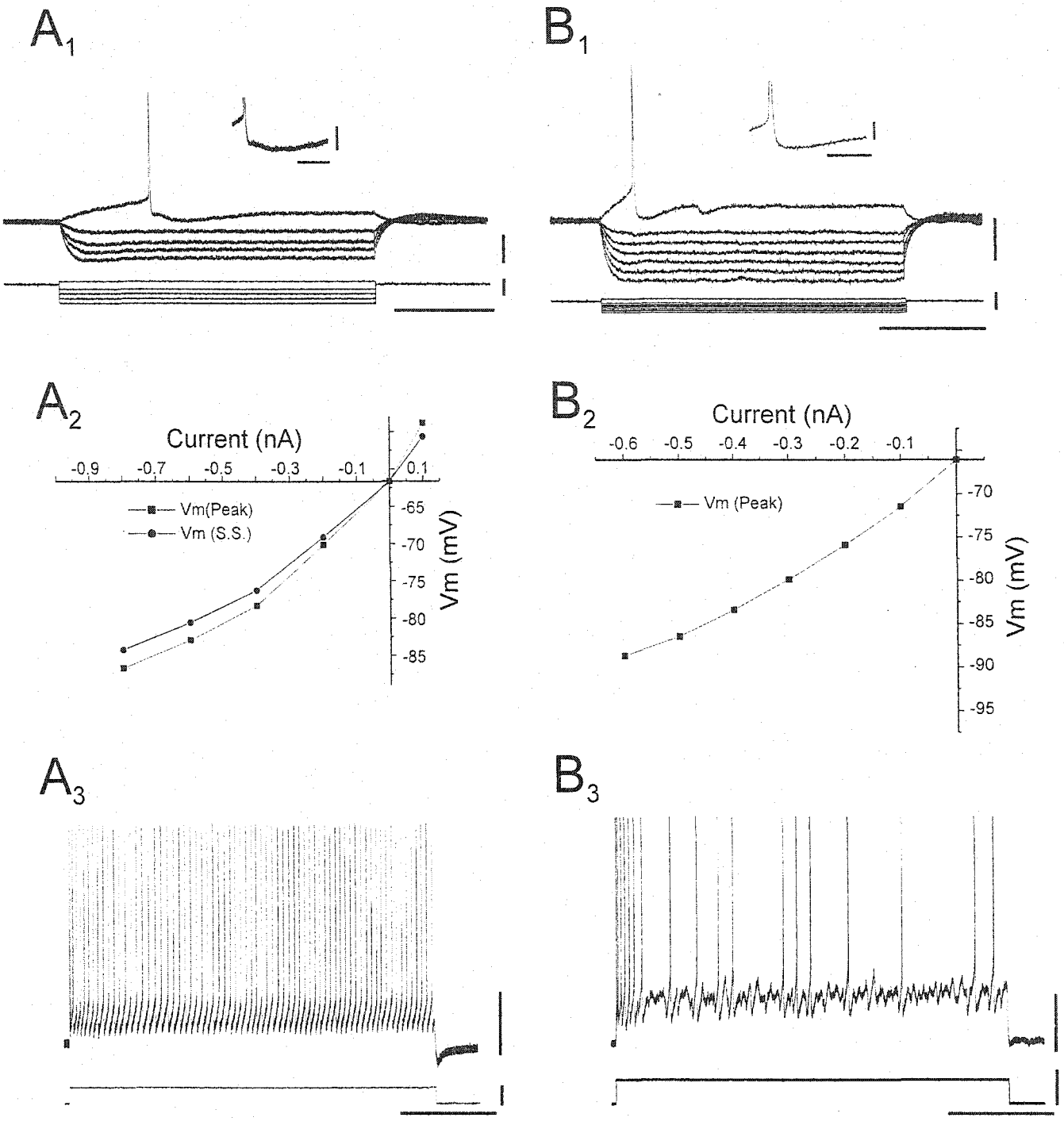
A1
B1
A2
Current (nA)
-0.9
-0.7
-0.5
-0.3
-0.1
0.1
Vm(Peak)
Vm (S.S.)
-65
-70
-75
-80
-85
Vm (mV)
B2
Current (nA)
-0.6
-0.5
-0.4
-0.3
-0.2
-0.1
Vm (Peak)
-70
-75
-80
-85
-90
-95
Vm (mV)
A3
B3

Fig. 10: Extracellular stimulation could induce excitatory or a sequence of excitatory and inhibitory postsynaptic response. **A**: schematic drawing illustrating the slice preparation with the intracellular recording electrode (right) and the stimulating electrode (left). **B**, response to extracellular stimulation in the polymorphic neuron depicted in figure 8A consisting of an epsp/ipsp sequence. Scale bars = 0.02 second and 20 mV; stimulation intensity = 500 μA. **C**: response to synaptic stimulation in the horizontal neuron in figure 6 and 7 showing only an epsp. Scale bars = 0.02 second and 20 mV; stimulation intensities at resting level (-67 mV) = 150, 250, 300 and 350 μA.

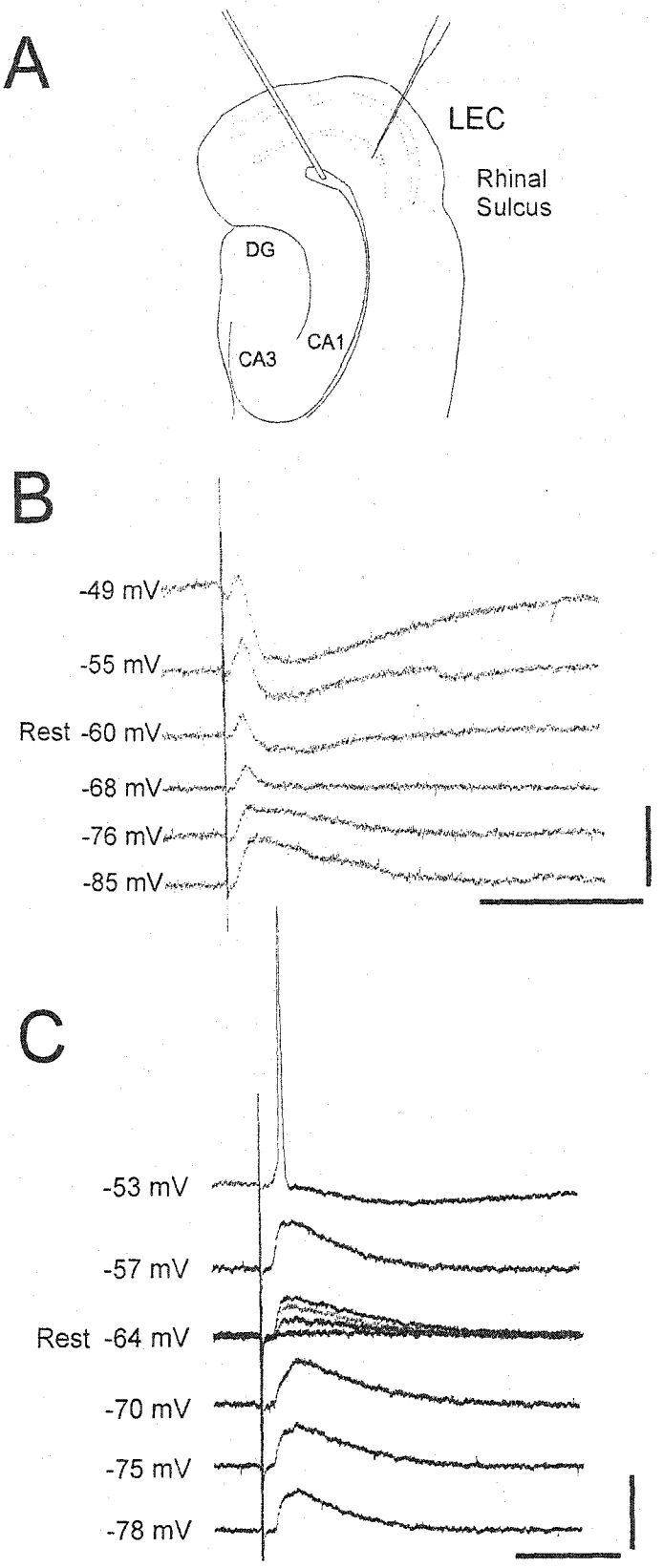
A
LEC
Rhinal
Sulcus
DG
CA1
CA3
B
-49 mV
-55 mV
Rest -60 mV
-68 mV
-76 mV
-85 mV
C
-53 mV
-57 mV
Rest -64 mV
-70 mV
-75 mV
-78 mV

Chapter Five

5. Persistent Sodium Channel Activity Mediates Subthreshold Membrane Potential Oscillations and Low-Threshold Spikes in Entorhinal Cortex Layer V Neurons

5.1 Preface

The main conclusions so far from the previous work is that layer V neurons of the entorhinal cortex are made up of three distinct morphological subtypes with similar electrophysiological properties and that these neurons are similar in the MEA and LEA. Also, contrary to neocortical layer V, these neurons lack cells with typical bursting properties that are usually associated with network rhythmicity. Instead, cells of all types displayed the described intrinsic subthreshold oscillatory behaviour that is characteristic of entorhinal layer II stellate cells. However, contrary to the latter, I_h does not seem to be a factor in the generation of the oscillatory activity in layer V. This study came to verify whether oscillations in layer V cells, similar to layer II, are dependent on persistent sodium activity and to describe the details relating to this current. Cells in the MEA were chosen for this study since the relevant data on this area is more abundant.

5.2 Abstract

Entorhinal cortex layer V occupies a critical position in temporal lobe circuitry since, on the one hand, it serves as the main conduit for the flow of information out of the hippocampal formation back to the neocortex and, on the other, it closes a hippocampal-entorhinal loop by projecting upon the superficial cell layers that give rise to the perforant path. Recent *in vitro* electrophysiological studies have shown that entorhinal cortex layer V cells have a rich subthreshold electrogenesis that includes their ability to generate subthreshold oscillations and all-or-none, low-threshold depolarizing potentials. In the present study, by applying current clamp, voltage clamp, and single-channel recording techniques in slices and dissociated neurons, we investigated whether entorhinal cortex layer V cells express a persistent sodium current and sustained sodium channel activity to evaluate the contribution of this activity to the electrogenic behavior of the cells. Sharp-electrode recording in slices demonstrated that layer V cells display tetrodotoxin-sensitive inward rectification in the depolarizing direction, suggesting that a persistent sodium current is present in the cells. Subthreshold oscillations and low-threshold regenerative events were also abolished by tetrodotoxin suggesting that their generation also requires the activation of such a low-threshold sodium current. The presence of a persistent sodium current was confirmed in whole-cell voltage clamp experiments which revealed that its activation "threshold" was negative by about 10 mV to that of the transient sodium current. Furthermore, stationary noise analysis and cell-attached, patch clamp recordings indicated that whole-cell persistent sodium currents were mediated by persistent sodium-channel activity, consisting of relatively high-conductance (~18 pS) sustained openings. The presence of a persistent sodium current in entorhinal cortex layer

V cells can cause the generation of oscillatory behavior, bursting activity and sustained discharge; this might be implicated in the encoding of memories in which the entorhinal cortex participates but, under pathological situations, may also contribute to epileptogenesis and neurodegeneration.

5.3 Introduction

Numerous anatomical and electrophysiological studies have demonstrated that the EC occupies a crucial position in temporal lobe circuitry since it acts as an "interface" between the hippocampus and the rest of the cortical mantle (Van Hoesen and Pandya, 1975; Swanson and Kohler, 1986; Insausti et al., 1987; Witter et al., 1989; Bear et al., 1996). While neocortical information converges onto the superficial cell layers (II and III) of the EC, from where it is transmitted into the hippocampus *via* the perforant path (Ramon y Cajal, 1902; Witter and Amaral, 1991; Alonso and Klink, 1993; Bear et al., 1996), the hippocampus feeds back in a topographically organized manner onto the deep layers (V-VI) of the EC (Swanson and Cowan, 1977; Sorensen and Shipley, 1979; Naber and Witter, 1998; Naber et al., 2000) that, in turn, give rise to long-range neocortical projections which thereby reciprocate the cortical input channels (Insausti et al., 1997; Swanson and Kohler, 1986). In addition to closing a long-range neocortical-hippocampal loop, EC layer V also sends robust local ascending projections onto the superficial cell layers thereby closing a nested entorhinal-hippocampal loop (Kohler, 1986; Dolorfo and Amaral, 1998).

Numerous studies in neuropsychology and neuroimaging in humans have now well established that the hippocampal-entorhinal network plays a critical role in the formation of episodic memory representations and the consolidation of these representations into long-term memory stored in neocortical circuits (Scoville and Milner, 1957; Owen et al., 1996; Corkin et al., 1997; Squire, 1998). Moreover, recording studies in animals indicate that entorhinal neuronal activity has the capacity to hold stimulus representations (Suzuki et al., 1997). It has also been recently suggested that oscillatory

bursts of activity ("ripples") by layer V neurons may be the mechanism by which encoded memory representations are transmitted to the neocortex (Buzsaki, 1996; Chrobak and Buzsaki, 1996). It is also becoming evident that, because of its specific intrinsic organization and extensive extrinsic connectivity, the EC may be an important locus for the generation and/or transmission of epileptic activity in the temporal lobe (Jones and Lambert, 1990; Dreier and Heinemann, 1991; Stringer and Lothman, 1992; Bear et al., 1996). In this respect, *in vitro* electrophysiological and imaging investigations have shown that EC layer V acts as a robust pacemaker for the generation of epileptiform events that can propagate throughout the EC-hippocampal loop (Heineman et al., 1993; Iijima et al., 1996; Nagao et al., 1996; Dickson and Alonso, 1997; Calcagnotto et al., 2000).

Recent studies of the morphological and electrophysiological properties of EC layer V neurons in slices (Schmitz et al., 1998; Hamam et al., 2000) have shown that a large proportion of these neurons display rhythmic, subthreshold membrane potential oscillations in the theta-frequency range which are similar to those typical of the EC layer II stellate cells (Alonso and Llinas, 1989; Alonso and Klink, 1993; van der Linden and Lopes da Silva, 1998). In addition, many of the layer V principal neurons also display a low-threshold discharge characterized by a spike-doublet riding on a slowly depolarizing potential (Hamam et al., 2000) Previous current and voltage clamp studies have shown that, in EC layer II neurons, similar forms of low-threshold electrogenesis are dependent on the activation of a TTX-sensitive, low-threshold persistent sodium current generated by a ~20-pS sustained sodium-channel activity (Alonso and Llinas, 1989; Klink and Alonso, 1993; Magistretti and Alonso, 1999; Magistretti et al., 1999). The biophysical

properties of this "persistent" sodium-channel activity are such that, in combination with other conductances, it can endow the cells with the ability to generate subthreshold oscillations, low-threshold burst discharge, and pacemaker potentials that sustain repetitive discharge. These single-cell intrinsic properties may be important for the normal memory operations of the entorhinal network (Dickson et al., 2000) but under pathological circumstances may also destabilize the system into promoting hyperexcitability and epileptogenesis (Taylor, 1993; Crill, 1996; Ragsdale and Avoli, 1998).

In the present study, by applying current clamp, voltage clamp and single-channel recording techniques in slices and dissociated neurons, we investigated whether EC layer V neurons express a persistent sodium current and sustained sodium-channel activity similar to that previously found in EC layer II cells. Our results demonstrate that EC layer V neurons do in fact express such a distinct sustained sodium-channel activity and that the current, which this activity generates, causes inward rectification in the depolarizing direction and is necessary for the generation of subthreshold oscillations and low-threshold discharge by the neurons.

5.4 Experimental Procedures

Slice Preparation

The procedures for slice preparation and intracellular recording were followed according to previously published procedures (Alonso and Klink, 1993). All efforts were made to minimize both the suffering and the number of animals used, and all the experiments were carried out in accordance with the Canadian Council on Animal Care

guidelines on the ethical use of animals. Briefly, young-adult male Long-Evans rats (P35-50) were decapitated, the brains were removed and a block of tissue containing the parahippocampal region was placed in ice-cold oxygenated Ringer solution (in mM: 124 NaCl, 5 KCl, 1.25 NaH_2PO_4, 2 $MgSO_4$, 26 $NaHCO_3$, 2 $CaCl_2$, and 10 D-glucose) maintained at pH 7.4 by saturation with 95% O_2 / 5% CO_2. Four-hundred micron thick horizontal slices from the retrohippocampal region were cut with a vibratome (Pelco, Redding CA), incubated at room temperature for at least two hours, and then transferred to an interface chamber maintained at 34 ± 1 °C and superfused at a rate of 1-2 ml/min.

Intracellular Recordings

Intracellular recording electrodes were pulled from borosilicate glass (WPI, Sarasota, FL) using a P87 puller (Sutter Instruments Co., Novato, CA). The electrodes were filled with 1.5 M K-acetate and had tip resistances of 90-120 MΩ. Signals were amplified using an Axoclamp 2A amplifier (Axon Instruments Co., Foster City, CA), visualized on-line using a digital oscilloscope, and stored on VHS tape for analysis. Entorhinal cortex layer V was identified as previously described (Hamam et al., 2000). The border with the more superficial layers was indicated by the *lamina dissecans*, a narrow fiber-rich, relatively acellular layer. The border with layer VI was indicated by a change to smaller, more densely packed cells.

Acute Dissociation of Layer V Neurons

The procedure for cell dissociation has been previously described (Magistretti et al., 1999; Magistretti et al., 1999). Briefly, entorhinal cortex layer V was microdissected from

400 to 500-μM thick brain slices, transferred to dissociation buffer (in mM: 115 NaCl, 3 KCl, 3 $MgCl_2$, 0.2 $CaCl_2$, 20 PIPES, and 25 D-glucose, pH 7.4 with NaOH) containing 1 mg/ml protease type XIV (Sigma-Aldrich, Oakville, Ontario, Canada), and incubated for 15 minutes at 32 °C. The tissue was then washed with fresh, enzyme-free dissociation buffer, left at room temperature for 1 hr, and then dissociated by trituration through Pasteur pipettes with fire-polished tips of progressively smaller inner diameter. Suspensions of dissociated cells were transferred to a recording chamber placed on the stage of an Axiovert 10 inverted microscope (Zeiss, Oberkochen, Germany) for patch clamp experiments.

Whole-Cell, Voltage Clamp Recordings

Persistent sodium currents were examined using the patch clamp technique in the whole-cell and cell-attached configurations (Hamill et al., 1981). In whole-cell experiments, transient sodium currents were examined using a low-sodium bath solution containing (in mM): 20 NaCl, 130 TEA-Cl, 2 $CaCl_2$, 3 $MgCl_2$, 0.2 $CdCl_2$, 5 4-aminopyridine, 10 HEPES, and 25 D-glucose, pH 7.4 with TEA-OH. Persistent sodium currents were studied using a bath solution consisting of (in mM): 100 NaCl, 40 TEA-Cl, 2 $CaCl_2$, 3 $MgCl_2$, 0.2 $CdCl_2$, 5 4-aminopyridine, 10 HEPES, and 25 D-glucose, pH 7.4 with NaOH. The intracellular pipette solution in whole-cell recordings contained 110 CsF, 10 HEPES-Na, 11 EGTA, and 2 $MgCl_2$, pH 7.4 with CsOH. Recordings were obtained using an Axopatch 200B amplifier and pCLAMP software (Axon Instruments). Experiments were performed at room temperature (~25 °C). Series resistance (typically 2-7 MΩ) was compensated by 60-80% using the amplifier's built-in clamp circuitry.

Currents were elicited, using either voltage steps or voltage ramps, from a holding potential of –80 mV. For step protocols, data were filtered at 1-5 kHz and sampled at 10 kHz. For ramp protocols, data were filtered at 1 kHz and sampled at 10 kHz. In all cases, currents were elicited first in control and then in 1-μM TTX (Sigma Chemical Co., St. Louis, MO). TTX-sensitive sodium currents were isolated off-line by subtracting TTX traces from control traces.

For transient sodium currents, the voltage-dependence of activation was determined by applying depolarizing steps to a range of test potentials, from a holding potential of –80 mV. Peak current amplitude (I_{peak}) was measured at each test potential and converted to conductance (G) according to the extended Ohm's law: $G = I_{peak} / (V_{test} - V_{rev})$, where V_{test} is the test potential and V_{rev} is the theoretical Nernst reversal potential for sodium currents (+58.2 mV). For persistent currents (I_{NaP}), current-voltage relationships were derived using either step protocols or slow voltage ramps. For steps, the average amplitude of the persistent component of TTX-subtracted currents was measured at each test potential, over the last 100 ms of 500-ms depolarizing step pulses and current values were converted to conductance as described above. For ramps, continuous conductance-voltage relationships were generated from ramp-evoked, TTX-subtracted currents, again by applying the extended Ohm's law. In both cases, plots were normalized with respect to the maximal conductance level. Activation curves were fitted with Boltzmann functions in the form: $1/(1 + \exp((V_{test}-V_{½})/k))$, where $V_{½}$ is the half-activation voltage and k is a slope factor. Steady-state inactivation of transient currents was assessed by applying 100-ms prepulses to a range of conditioning potentials, followed by a test pulse to –10 mV. The peak amplitude of currents evoked by the test pulses were normalized with respect to

the largest current and plotted as a function of prepulse potential, and the Boltzmann function in the above form was used for fitting to data points. The plot of I_{NaP} amplitude as a function of the inverse of depolarizing ramp slope (see Results) was fitted with the exponential function: $I_{NaP} = A \cdot \exp(-\alpha/r) + C$, where r is the ramp slope and α is a "slope constant" (both in V/s).

Stationary Noise Analysis

An estimation of the elementary conductance of single-channel openings generating whole-cell I_{NaP}s was obtained by performing stationary noise analysis of step-evoked currents. This analysis was limited to the sustained sodium-current component observed over the last 100 ms of 500-ms depolarizing pulses. According to the binomial distribution of channel opening probability and assuming a homogeneous behavior of the single channels under study, average current amplitude (I_{ave}) and current variance (σ^2_I) over the selected trace region can be expressed as: $I_{ave} = n \cdot i \cdot P_0$, and: $\sigma^2_I = n \cdot i^2 \cdot P_0 \cdot (1 - P_0)$, where n is the number of channels, i is the elementary current, and P_0 is the single-channel opening probability. This yields: $\sigma^2_I / I_{ave} = g \cdot (V - V_{rev}) \cdot (1 - P_0)$, where g is the single-channel conductance and V_{rev} is the theoretical Nernst reversal potential for sodium currents. According to the Boltzmann probability function, P_0 can be further expressed as a function of voltage as $P_0 = P_{0max} / (1 + \exp((V - V_{½})/k))$, where P_{0max} is the maximal single-channel opening probability, and $V_{½}$ and k have their usual meanings (see above).

We measured I_{ave} in TTX-subtracted traces, and current variance in both control (σ^2_{Icont}) and TTX (σ^2_{ITTX}) traces. The actual current variance due to single sodium-channel activity was derived as $\sigma^2_I = \sigma^2_{Icont} - \sigma^2_{ITTX}$. The ratio σ^2_I / I_{ave} was then calculated

in individual cells for each test potential and plotted as a function of voltage. The function $\sigma^2_I/I_{ave}(V) = g\cdot(V - V_{rev})\cdot(1 - P_{0max} / (1 + \exp((V - V_{½})/k)))$ was used to obtain fittings of data points. $V_{½}$ and k were kept fixed to the values returned by Boltzmann fitting of the average activation plot derived from step protocols (see Results). Fittings with the above function returned estimates of the two remaining free parameters, g and P_{0max}.

Cell-Attached, Patch Clamp Recordings

For cell-attached, patch clamp recordings, the cells were initially immersed in a bath solution containing (in mM): 140 NaCl, 5 KCl, 2 $CaCl_2$, 2 $MgCl_2$, 10 HEPES, and 25 D-glucose, pH 7.4 with NaOH. The recording pipettes were filled with the same solution and typically had input resistances of 10-30 MΩ. After obtaining the cell-attached configuration, a high-potassium extracellular solution (in mM: 140 K-acetate, 5 NaCl, 4 $MgCl_2$, 0.2 $CdCl_2$, 10 HEPES, and 25 D-glucose, pH 7.4 with KOH) was superfused into the bath to bring the cell membrane potential close to 0 mV. Single-channel currents were elicited by voltage steps applied from holding potentials of –100 to –120 mV. The data were low-pass filtered at 1 kHz and sampled at 10 kHz. Voltage steps were delivered every 5 s to prevent cumulative voltage-dependent inactivation of the persistent sodium channel activity. Capacity transients were partially nullified with the amplifier's built-in compensation circuitry. Remaining transients and leak currents were off-line subtracted from fits of averaged blank traces.

Because of the large number of channels in macropatch experiments, it was not possible to unequivocally determine the number of channels that contributed to persistent activity in a given sweep, or whether the number of functionally active persistent

channels changed from one sweep to the next. Therefore, to assess the level of persistent activity per sweep we used the parameter nP_0, which corresponds to the product of the single-channel opening probability (P_0) and the number of persistent channels in the patch (n). nP_0 values were determined for each sweep according to $nP_0 = I_{ave}/i$, in which I_{ave} is the average current level over the last 470 ms of 500-ms test pulses, and i is the single-channel amplitude.

5.5 Results

Current Clamp Analysis of Low-Threshold, TTX-Sensitive Responses in EC Layer V Neurons

In a recent study we have shown that although principal neurons in layer V of the medial entorhinal cortex (EC) can be grouped into three distinct morphological categories, the three categories of cells share a number of electrophysiological attributes. The latter include inward rectification in the depolarizing direction and the ability of many of the cells to generate rhythmic, subthreshold membrane potential oscillations and/or slow low-threshold depolarizing potentials that can trigger spike doublets (Hamam et al., 2000).

It has been previously shown that in many brain neurons inward rectification in the depolarizing direction (depolarizing IR) can be selectively abolished with TTX (Hoston et al., 1979; Stafstrom et al., 1982); this property is typically interpreted as indicative of the presence of a distinct low-threshold persistent sodium current (I_{NaP}). We thus first explored whether the depolarizing IR displayed by layer V neurons in slices was sensitive to TTX (1 μM). Membrane input resistance (R_{in}) was assessed by applying 100-

pA hyperpolarizing current pulses and plotted as a function of membrane potential in the subthreshold voltage range, both in control conditions and in the presence of TTX. As in the case illustrated in Fig. 1, in control conditions (●), all of the neurons tested displayed a marked, apparent increase in R_{in} with membrane depolarization particularly at potentials positive to about –60 mV. The effect of TTX (△) was always to selectively abolish this R_{in} increase at potentials positive to approximately –65 mV ($n = 5$).

Since the above data suggest that EC layer V neurons posses a low-threshold persistent sodium current, we next tested whether the low-threshold slowly depolarizing potentials, which can be triggered in many layer V neurons, could also be abolished by TTX. The left-hand panels of Fig. 2A and B (control) show typical examples of this response in two different layer V cells. Note that a small depolarizing current step resulted in a membrane response with a smooth trajectory (lower trace in Figs. 2A and B), suggesting little or no activation of voltage-dependent ionic conductances. However, somewhat larger current injections elicited in both cases an all-or-none slow regenerative response that culminated in the firing of a single spike (cell in panel A) and in a high-frequency spike doublet (cell in panel B). As demonstrated in the middle (TTX) and right-hand panel (superimposed) of Fig. 2, TTX completely abolished the low-threshold regenerative potential, indicating that, like depolarizing IR, this slow potential results from the activation of voltage-gated sodium channels.

A large percentage of EC layer V neurons also express another type of low-threshold intrinsic activity consisting of low amplitude rhythmic membrane potential oscillations at a frequency of ~4-14 Hz (Schmitz et al., 1998; Hamam et al., 2000). This type of oscillatory activity is voltage-dependent and develops in a ~10 mV voltage range

below firing threshold (about –42 mV) (Hamam et al., 2000), which is the voltage range where TTX-sensitive depolarizing IR also becomes most manifest. As is the case of EC layer II stellate cells (Klink and Alonso, 1993), subthreshold oscillations in EC layer V neurons were also abolished by TTX (Fig. 3, lower trace), suggesting that they also depend on the activation of a voltage-gated sodium conductance.

Whole-Cell, Voltage Clamp Analysis of I_{NaP} in EC Layer V Neurons

The aforementioned intracellular sharp-electrode experiments in slices suggest that depolarizing IR, slow low-threshold regenerative potentials and subthreshold oscillations expressed by EC layer V neurons are dependent on the activation of a low voltage-activated persistent sodium current. To confirm the presence of I_{NaP} in EC layer V neurons and to analyze its biophysical properties as compared to those of the I_{NaP} expressed by layer II cells (Magistretti and Alonso, 1999; Magistretti et al., 1999), we performed whole-cell and single-channel patch clamp recordings from acutely dissociated EC layer V neurons. Fig. 4A shows whole-cell sodium currents, elicited by step depolarizations to –60, –40, and –20 mV, in a dissociated layer V cell. The predominant TTX-sensitive current was a transient sodium current (I_{Na}) which rose rapidly to a peak and then decayed to near baseline within a few milliseconds. In addition to I_{Na}, we observed a smaller, TTX-sensitive sustained sodium current (I_{NaP}) that persisted throughout 500-ms long membrane depolarizations (Fig. 4B). The peak amplitude of I_{NaP} was small compared to the maximum transient current (~1% at –20 mV; note different scale bars in Fig. 4A and 4B). However, the relative degree of activation of I_{NaP} appeared still considerable at sub- or near-threshold membrane voltage levels (–60 to –40 mV). The

voltage-dependence of activation of I_{NaP} was analyzed in more detail by measuring, at each test potential, the average amplitude of the sustained current component over the last 100 ms of the 500-ms depolarizing steps and by deriving values for the underlying conductance (G_{NaP}) as explained in the Experimental Procedures. The average plot of G_{NaP} as a function of voltage, obtained from seven neurons, is shown in Fig. 4B, inset. The Boltzmann fitting of this plot returned a half-activation voltage, $V_{½}$, of –33.7 mV and a slope factor, k, of –8.9 mV.

To further characterize I_{NaP} and quickly explore its whole voltage range of activation without interference from the much larger transient current, we employed ramp protocols that gradually depolarized the membrane at a rate of 50 mV/s, since they allowed full inactivation of the fast decaying sodium current. TTX subtraction returned a continuous *I-V* relationship for I_{NaP} which, as in the representative case illustrated in Fig. 4C, had a threshold at about –60 mV and peaked at about –30 mV. The average peak amplitude of I_{NaP} recorded in this manner was –4.1 ± 0.7 pA/pF (n = 7). The ramp-derived *I-V*s from seven neurons were then converted to continuous G_{NaP}-voltage relationships (Fig. 4D). Boltzmann fitting to the G_{NaP} average activation curve returned a $V_{½}$ of –36.8 mV and a slope factor of –7.8 mV. As shown in Fig. 4D, G_{NaP} reached maximal activation at about –10 mV and displayed only a minor decay at more positive voltages.

The fact that the G_{NaP} voltage-dependence plot is not bell-shaped indicates that I_{NaP} cannot be attributed to a "window" sodium current (I_{NaW}) generated by the overlap of the activation and steady-state inactivation curves of the transient sodium current (Hodgkin and Huxley, 1952). To further clarify this point, the activation and steady-state

inactivation properties of I_{Na} were also characterized as illustrated in Fig. 5A. As expected from the observations described above, I_{Na} activation occurred at voltages more positive as compared to I_{NaP} and the I_{Na} activation and inactivation curves displayed only a limited overlap (Fig. 5B). Boltzmann fitting of the mean activation curve of I_{Na} (n = 4) returned a $V_{½}$ of –30.7 mV and a slope factor of –3.8 mV (which is less than half the k value for G_{NaP}). The predicted conductance-voltage relationship for I_{NaW} was determined from the product of the activation and steady-state inactivation curves for I_{Na}. The conductance underlying I_{NaW} rose to a maximum level at about –30 mV but then dropped off quickly at more positive potentials (Fig. 5, dotted, normalized line). This is in contrast to the activation of I_{NaP} which followed a sigmoidal curve approaching an asymptotic value of ~ –15 mV (Fig. 4D). These data suggest that I_{NaW} is not the main biophysical mechanism for I_{NaP} generation at most membrane potentials.

Persistent sodium currents in layer V cells showed little decay during 500-ms test pulses. Nevertheless, these currents did display inactivation with longer depolarizations. To assess the time course of this slowly developing inactivation, we examined the effects of depolarization speed on the amplitude of the I_{NaP}s elicited by voltage ramp protocols (Fleidervish and Gutnick, 1996; Magistretti and Alonso, 1999). At progressively slower rates of membrane depolarization, the amplitude of I_{NaP} was progressively lower, approaching asymptotic minima at a ramp slope of 25 mV/s (Fig. 6A). Fig. 6B plots the mean peak amplitude of I_{NaP} as a function of the inverse of ramp slope. The smooth line is an exponential fit to the data points, with a "slope constant" (α, see Experimental Procedures) of ~90.9 mV/s (n = 4). This value is of the same order as those found in EC layer II principal neurons (Magistretti and Alonso, 1999), where I_{NaP} inactivation takes

place with time constants between 2.6 and 6.8 s depending on membrane voltage. Therefore, the above-illustrated decrease of I_{NaP} amplitude with increasingly slower depolarizations reflects an I_{NaP} inactivation process that takes place on a time scale of a few seconds.

Noise Analysis of I_{NaP} in EC Layer V Neurons

It becomes apparent from the traces of I_{NaP}, such as those illustrated in Fig. 4B and C, that the activation of this current was accompanied by a substantial increase in current noise as compared to the baseline level. This suggests that in the neurons under study I_{NaP} is sustained by the opening of relatively high-conductance channels, similar to what has been previously demonstrated for principal cells of EC layer II (White et al., 1998). We therefore estimated the elementary conductance of the single-channel openings responsible for I_{NaP} by performing stationary noise analysis of step-evoked I_{NaP}s. The technique, described in the Experimental Procedures, allowed us to obtain reliable estimations of the current's variance-to-mean ratio (σ^2_I/I_{ave}) in the voltage range from –35 to +15 mV, due to the small values of σ^2_I and I_{ave} at more negative voltages. Fig. 7 shows the plot of σ^2_I/I_{ave} as a function of voltage obtained in a representative neuron. Data points were fitted with the $\sigma^2_I/I_{ave}(V)$ function described in the Experimental Procedures. In the cell illustrated, the fitting returned a single-channel conductance (g) value of 17.9 pS. An average in three cells gave $g = 17.5 \pm 3.6$ pS.

Single-Channel Analysis of I_{NaP} in EC Layer V Neurons

We then investigated directly the properties of the channels responsible for I_{NaP} in layer V neurons in cell-attached, patch clamp recordings from acutely dissociated cells. Because of the high sodium channel density, most patches contained greater than 10 channels. Fig. 8A shows sodium channel activity elicited by a 500-ms depolarization to –20 mV in one of these "macropatch" experiments. The test pulse initially elicited a large inward current that decayed back to near baseline within a few milliseconds. This transient current was caused by rapid activation and inactivation of transient sodium channels in the membrane patch. In addition to this transient channel activity, one channel in the patch remained open throughout almost the entire 500-ms sweep. Similar persistent channel activity was observed in most sweeps in this experiment (Fig. 8B). We propose that this persistent sodium channel activity is responsible for I_{NaP}, whereas the transient activity is responsible for I_{Na}. Consistent with this hypothesis, the average of many sweeps gave an ensemble current with transient and persistent components that closely resembled the transient and persistent components of whole-cell sodium currents, both in terms of time course and relative amplitude (Fig. 8C).

To quantify persistent activity in macropatch experiments, we determined nP_0, a measure of channel open probability (see Experimental Procedures). Because we wanted to examine only persistent activity, we assessed nP_0 over just the last 470 ms of each sweep (Fig. 9, the bracketed regions of the current traces). The graph in Fig. 9 shows a diary plot of nP_0 per sweep for a typical experiment (a different macropatch than in Fig. 8). The nP_0 values for most sweeps are high, indicating that there was substantial persistent channel activity throughout the entire course of the experiment. The plot also

suggests that nP_0 values were highest with strong depolarizations. This is also apparent in the example traces above the plot, which show that persistent activity consisted of brief, flickery openings with moderate depolarizations, whereas with stronger depolarizations it was characterized by long openings that sometimes lasted throughout the entire test pulse.

We have previously shown that, in EC layer II neurons, the single-channel conductance of persistent sodium channel activity is significantly higher (~20 pS) than that of transient channel activity (~16 pS) (Magistretti et al., 1999). Persistent activity in layer V neurons also had a high single-channel conductance. Fig. 10 shows a single-channel current-voltage relationship from a typical experiment. The straight line is a linear fit of the data points with a slope of 18.9 pS. The mean conductance of persistent openings in 6 experiments was 18.7 ± 1.0 pS, a value that compares favorably with the estimated single-channel conductance extracted from noise analysis of step-evoked, whole-cell I_{NaP}s (see above). This finding further confirms that the channel activity under examination indeed accounts for the macroscopic I_{NaP} expressed by EC layer V neurons.

5.6 Discussion

The results of the present study demonstrate that the subthreshold intrinsic excitability of entorhinal cortex layer V neurons is largely dominated by a low-threshold sustained sodium current (I_{NaP}) which appears to be mainly due to "persistent" sodium-channel activity similar to that previously described in entorhinal cortex layer II principal cells (Magistretti et al., 1999). Under current clamp conditions this voltage-gated "persistent" sodium-channel activity causes pronounced inward rectification in the

depolarizing direction and is necessary for the generation of theta-like subthreshold oscillations as well as slow low-threshold regenerative events.

Properties of I_{NaP} in EC Layer V Neurons

The properties of the I_{NaP} revealed by whole-cell, voltage clamp analysis are similar in several respects to those of persistent sodium currents that have been previously described in other brain regions (Stafstrom et al., 1985; French et al., 1990; Kay et al., 1998; Magistretti and Alonso, 1999). Firstly, I_{NaP} is very small as compared to the peak amplitude of the transient sodium current, I_{Na}. Secondly, the contribution of I_{NaP} is, nonetheless, considerable at relatively negative voltages. Indeed, the conductance-voltage relationship for I_{NaP} revealed a half-activation level, $V_{½}$, more negative than that of I_{Na} by ~3 to 6 mV. In addition, the slope factor, k, of the same relationship was higher than that found for I_{Na} by more than two times. As a consequence, the conductance-voltage relationship for I_{NaP} was much more extended towards negative potentials compared to I_{Na}, and, at subthreshold voltage levels (–60 to –40 mV), the relative degree of I_{NaP} activation was much higher. Overall, the activation "threshold" of I_{NaP} was negative to that of I_{Na} by approximately 10 mV. It should be noted, however, that the $V_{½}$ of I_{NaP} appeared to be considerably more positive in EC layer V cells than previously reported for EC layer II cells (–44.4 mV) (Magistretti and Alonso, 1999). Interestingly, although in both layer V and layer II cells I_{NaP}-dependent subthreshold oscillations develop 5-10 mV negative to spike threshold, the latter is found at significantly more positive levels in layer V than in layer II cells (about –42 mV *vs.* –51 mV) (Alonso and Klink, 1993; Hamam et al., 2000). The observation that the voltage range of I_{NaP} activation is shifted rightwards in

layer V cells as compared to layer II cells is thus consistent with the occurrence of subthreshold oscillations at more positive potentials in layer V than in layer II cells.

Using ramps of varying slope, we also demonstrated that I_{NaP} in layer V shows time-dependent decay, with time constants in the order of a few seconds (Fleidervish and Gutnick, 1996). This slow current decay could enable the rate and/or duration of membrane depolarization to influence the contribution of I_{NaP} to membrane voltage dynamics. Time-dependent attenuation of I_{NaP} may also be important for limiting abnormally large influx of sodium ions, which has been proposed to contribute to cell death during prolonged membrane depolarizations associated with seizures or ischemia (Taylor and Meldrum, 1995).

Biophysical and Molecular Bases for Persistent Sodium Channels

The stationary noise analysis we carried out on depolarizing step-evoked I_{NaP}s in layer V neurons allowed us to make predictions on the biophysical properties of the underlying elementary events. Our estimations returned, for the channel activity generating I_{NaP}, a predicted single-channel conductance of about 17.5 pS. (White et al., 1998)

A correlate of this expected single-channel activity was then directly looked for with single-channel experiments. Indeed, cell-attached, patch clamp recordings revealed a robust, persistent sodium-channel activity during the late phases of prolonged depolarizing pulses which was able to produce sizeable, sustained currents in ensemble-averaged traces. The single-channel conductance for these sustained channel openings averaged 18.7 pS. This measure compares favorably with the estimate obtained from

noise analysis. Our experimental approach, therefore, enabled us to establish a direct link between the sustained, sodium-dependent single-channel activity that can be found in layer V neurons and the macroscopic I_{NaP}s expressed by the same cells.

The molecular mechanisms that cause these persistent openings are not well understood. One hypothesis is that persistent activity results from periodic transition of conventional transient sodium channels to a persistent gating mode (Alzheimer et al., 1993; Crill, 1996). This switch from transient to persistent gating may be a random process, or it may be due to a more regulated modulation of function, resulting, for example, from phosphorylation (Numann et al., 1991) or G-protein interaction (Ma et al., 1997). The molecular diversity of brain sodium channels may also play a role in determining whether channels exhibit transient or persistent gating. The main structural component of the voltage-gated sodium channel is the 260 kDa α subunit. The brain expresses multiple α subtypes, and some of these are likely to be more biased toward persistent gating than others (Patton et al., 1994; Meadows et al., 1997; Smith et al., 1998; Smith and Goldin, 1998). Furthermore, brain α subunits associate with several different types of auxiliary subunits (Isom et al., 1992; Isom et al., 1995; Kazen-Gillespie et al., 2000; Morgan et al., 2000) which provide an additional mechanism for modulating channel kinetics. If in fact some channels are more inclined than others towards persistent gating, then this should be evident in single-channel recordings. However, in the experiments presented here, the patches contained so many channels that it was not possible to unequivocally determine the properties of any individual channel. Nevertheless, it is interesting that the level of persistent activity was fairly consistent from one depolarization to the next, as would be expected if persistent openings were mediated by a distinct subset of channels that were

strongly biased toward persistent gating. Indeed, in a previous study in layer II neurons, in which we were able to obtain membrane patches containing just a few sodium channels, we showed that individual channels could exhibit high levels of persistent gating over hundreds of depolarizations in experiments lasting from 10 to 20 minutes (Magistretti and Alonso, 1999; Magistretti et al., 1999). Based on this observation, we have suggested that there may be a distinct persistent sodium channel in entorhinal cortex neurons. We are currently combining various molecular and biophysical approaches to explore this hypothesis.

Functional Implications

The presence of I_{NaP} in a particular neuron may have a diversity of influences on its particular electroresponsiviness depending on the specific channel density and somatodendritic distribution as well as on its interactions with other active and passive properties of the cell. Because of its particular gating properties, I_{NaP} causes an apparent increase in input resistance in the subthreshold range (Hoston et al., 1979; Klink and Alonso, 1993; Stuart, 1999), thereby, effectively acting as an "amplifier" for other slower voltage-gated or synaptic membrane currents. For this reason, I_{NaP}, interacting primarily with I_h, as in the case of the EC layer II stellate cells (Dickson et al., 2000), or with low-threshold K^+ conductances, as it is likely for some neocortical pyramidal cells (Gutfreund et al., 1995) and amygdala neurons (Pape and Driesang, 1998), plays a critical role in the generation of subthreshold oscillatory activity. In addition, I_{NaP} has also been shown to enhance the effects of the T current and contribute to low-threshold bursting in thalamic neurons (Parri and Crunelli, 1998). Some EC layer V cells also display slow low-

threshold spikes (Hamam et al., 2000) but, as shown in the present study, the main driving force for this type of regenerative event appears to be I_{NaP}. A similar role for I_{NaP} has been recently described in frontal cortical neurons where I_{NaP} appears to be selectively inhibited by dopamine (Geijo-Barrientos, 2000).

Because of its very slow inactivating kinetics, I_{NaP} can also contribute to the generation of plateau potentials and act as a pacemaker current for the generation of repetitive discharge. As for EC layer V, the sustained firing activity towards which I_{NaP} can contribute may participate in holding information and, thus, be influential in the memory function of the EC. Importantly, it has recently been shown that the activity of NMDA-receptor channels tracks changes in intracellular sodium ion concentration, $[Na^+]_i$, so that raising $[Na^+]_i$ selectively increases glutamatergic NMDA-receptor mediated synaptic response (Yu and Salter, 1998). This mechanism may also have important consequences in memory function; however, it may also contribute to hyperexcitability and neurodegeneration, pathological processes that are prone to take place in entorhinal cortex layer V in diseases such as epilepsy or Alzheimer's.

5.7 References

Alonso A. and Klink R. 1993. Differential electroresponsiveness of stellate and pyramidal-like cells of medial entorhinal cortex layer II. J. Neurophysiol. 70: 128-143.

Alonso A. and Llinas R. R. 1989. Subthreshold Na^+-dependent theta-like rhythmicity in stellate cells of entorhinal cortex layer II. Nature 342: 175-177.

Alzheimer C., Schwindt P. C. and Crill W. E. 1993. Modal gating of Na^+ channels as a mechanism of persistent Na^+ current in pyramidal neurons from rat and cat sensorimotor cortex. J. Neurosci. 13: 660-673.

Bear J., Fountain N. B. and Lothman E. W. 1996. Responses of the superficial entorhinal cortex in vitro in slices from naive and chronically epileptic rats. J. Neurophysiol. 76: 2928-2940.

Burwell R. D. and Amaral D. G. 1998. Cortical afferents of the perirhinal, postrhinal, and entorhinal cortices of the rat. J. comp. Neurol. 398: 179-205.

Buzsaki G. 1996. The hippocampo-neocortical dialogue. Cereb. Cortex 6: 81-92.

Calcagnotto M. E., Barbarosie M. and Avoli M. 2000. Hippocampus-entorhinal cortex loop and seizure generation in the young rodent limbic system. J. Neurophysiol. 83: 3183-3187.

Chrobak J. J. and Buzsaki G. 1996. High-frequency oscillations in the output networks of the hippocampal-entorhinal axis of the freely behaving rat. J. Neurosci. 16: 3056-3066.

Corkin S., Amaral D. G., Gonzalez R. G., Johnson K. A. and Hyman B. T. 1997. H.M.'s medial temporal lobe: findings from magnetic resonance imaging. J. Neurosci. 17: 3964-3979.

Crill W. E. 1996. Persistent sodium current in mammalian central neurons. Annu. Rev. Physiol. 58: 349-362.

Dickson C. T. and Alonso A. 1997. Muscarinic induction of synchronous population activity in the entorhinal cortex. J. Neurosci. 17: 6729-6744.

Dickson C. T., Magistretti J., Shalinsky M. H., Fransen E., Hasselmo M. E. and Alonso A. 2000. Properties and role of I(h) in the pacing of subthreshold oscillations in entorhinal cortex layer II neurons. J. Neurophysiol. 83: 2562-2579.

Dolorfo C. L. and Amaral D. G. 1998. Entorhinal cortex of the rat: organization of intrinsic connections. J. comp. Neurol. 398: 49-82.

Dolorfo C. L. and Amaral D. G. 1998. Entorhinal cortex of the rat: topographic organization of the cells of origin of the perforant path projection to the dentate gyrus. J comp Neurol 398: 25-48.

Dreier J. P. and Heinemann U. 1991. Regional and time dependent variations of low Mg2+ induced epileptiform activity in rat temporal cortex slices. Exp. Brain Res. 87: 581-596.

Fleidervish I. A. and Gutnick M. J. 1996. Kinetics of slow inactivation of persistent sodium current in layer V neurons of mouse neocortical slices. J. Neurophysiol. 76: 2125-2130.

French C. R., Sah P., Buckett K. J. and Gage P. W. 1990. A voltage-dependent persistent sodium current in mammalian hippocampal neurons. J. Gen. Physiol. 95: 1139-1157.

Geijo-Barrientos E. 2000. Subthreshold inward membrane currents in guinea-pig frontal cortex neurons. Neuroscience 95: 965-972.

Gutfreund Y., Yarom Y. and Segev I. 1995. Subthreshold oscillations and resonant frequency in guinea-pig cortical neurons: physiology and modeling. J. Physiol. (Lond.) 483: 621-640.

Hamam B. N., Kennedy T. E., Alonso A. and Amaral D. G. 2000. Morphological and electrophysiological characteristics of layer V neurons of the rat medial entorhinal cortex. J. comp. Neurol. 418: 457-472.

Hamill O. P., Marty A., Neher E., Sakmann B. and Sigworth F. J. 1981. Improved patch-clamp techniques for high-resolution current recording from cells and cell-free membrane patches. Pflugers Arch. 391: 85-100.

Heineman U., Zhang C. L. and Eder C. 1993. Entorhinal cortex-hippocampal interactions in normal and epileptic temporal lobe. Hippocampus 3: 88-98.

Hodgkin A. L. and Huxley A. F. 1952 A quantitative description of membrane current and its application to conduction and excitation in nerve. J. Physiol. (Lond.) 117: 500-544.

Hoston J. R., Prince D. A. and Schwartzkroin P. A. 1979. Anomalous inward rectification in hippocampal neurons. J. Neurophysiol. 42: 889-895.

Iijima T., Witter M. P., Ichikawa M., Tominaga T., Kajiwara R. and Matsumoto G. 1996. Entorhinal-hippocampal interactions revealed by real-time imaging. Science 172: 1176-1179.

Insausti R., Amaral D. G. and Cowan W. M. 1987. The entorhinal cortex of the monkey: II. Cortical afferents. J. comp. Neurol. 264: 356-395.

Insausti R., Herrero M. T. and Witter M. P. 1997. Entorhinal cortex of the rat: cytoarchitectonic subdivisions and the origin and distribution of cortical efferents. Hippocampus 7: 146-183.

Isom L. L., De Jongh K. S., Patton D. E., Reber B. F., Offord J., Charbonneau H., Walsh K., Goldin A. L. and Catterall W. A. 1992. Primary structure and functional expression of the beta 1 subunit of the rat brain sodium channel. Science 256: 839-842.

Isom L. L., Ragsdale D. S., De Jongh K. S., Westenbroek R. E., Reber B. F., Scheuer T. and Catterall W. A. 1995. Structure and function of the beta 2 subunit of brain sodium channels, a transmembrane glycoprotein with a CAM motif. Cell 83: 433-442.

Jones R. S. G. and Lambert J. D. C. 1990. Synchronous discharges in the rat entorhinal cortex *in vitro*: site of initiation and the role of excitatory amino acid receptors. Neuroscience 34: 657-670.

Kay A. R., Sugimori M. and Llinas R. 1998. Kinetic and Stochastic Properties of a Persistent Sodium Current in Mature Guinea Pig Cerebellar Purkinje Cells. J. Neurophysiol. 80: 1167-1179.

Kazen-Gillespie K. A., Ragsdale D. S., D'Andrea M. R., Mattei L. N., Rogers K. E. and Isom L. L. 2000. Cloning, localization, and functional expression of sodium channel beta1A subunits. J. Biol. Chem. 275: 1079-1088.

Klink R. and Alonso A. 1993. Ionic mechanisms for the subthreshold oscillations and differential electroresponsiveness of medial entorhinal cortex layer II neurons. J. Neurophysiol. 70: 144-157.

Kohler C. 1986. Intrinsic connections of the retrohippocampal region in the rat brain. II. The medial entorhinal area. J. comp. Neurol. 246: 149-169.

Ma J. Y., Catterall W. A. and Scheuer T. 1997. Persistent sodium currents through brain sodium channels induced by G protein betagamma subunits. Neuron 19: 443-452.

Magistretti J. and Alonso A. 1999. Biophysical Properties and Slow Voltage-dependent Inactivation of a Sustained Sodium Current in Entorhinal Cortex Layer-II Principal Neurons. A whole-cell and single-channel study. J. Gen. Physiol. 114: 491-509.

Magistretti J., Brevi S. and de Curtis M. 1999: Biophysical and pharmacological diversity of high-voltage-activated calcium currents in layer II neurones of guinea-pig piriform cortex. J. Physiol. (Lond.) 518: 705-720.

Magistretti J., Ragsdale D. S. and Alonso A. 1999. High conductance sustained single-channel activity responsible for the low-threshold persistent Na(+) current in entorhinal cortex neurons. J. Neurosci. 19: 7334-7341.

Meadows L., Stetzer A., Isom L. L. and Ragsdale D. S. 1997. Modulation of rat brain type III sodium channel function by auxiliary b1 and b2 subunits. Soc. Neurosci. Abstr. 23: 1472.

Morgan K., Stevens E. B., Shah B., Cox P. J., Dixon A. K., Lee K., Pinnock R. D., Hughes J., Richardson P. J., Mizuguchi K. and Jackson A. P. 2000. beta 3: an additional auxiliary subunit of the voltage-sensitive sodium channel that modulates channel gating with distinct kinetics. Proc. natl. Acad. Sci. U.S.A. 97: 2308-2313.

Naber P. A. and Witter M. P. 1998. Subicular efferents are organized mostly as parallel projections: a double-labeling, retrograde-tracing study in the rat. J. comp. Neurol. 393: 284-297.

Naber P. A., Witter M. P. and Lopes da Silva F. H. 2001. Reciprocal connections between the entorhinal cortex and hippocampal fields CA1 and the subiculum are in register with the projections from CA1 to the subiculum. Hippocampus 11: 99-104.

Nagao T., Alonso A. and Avoli M. 1996. Epileptiform activity induced by pilocarpine in the rat hippocamapal-entorhinal slice preparation. Neuroscience 72: 399-408.

Numann R., Catterall W. A. and Scheuer T. 1991. Functional modulation of brain sodium channels by protein kinase C phosphorylation. Science 254: 115-118.

Owen A. M., Milner B., Petrides M. and Evans A. C. 1996. A specific role for the right parahippocampal gyrus in the retrieval of object-location: a positron emission tomography study. J. Cogn. Neurosci. 8: 603-625.

Pape H. C. and Driesang R. B. 1998. Ionic mechanisms of intrinsic oscillations in neurons of the basolateral amygdaloid complex. J. Neurophysiol. 79: 217-226.

Parri H. R. and Crunelli V. 1998. Sodium current in rat and cat thalamocortical neurons: role of a non-inactivating component of tonic and burst firing. J. Neurosci. 18: 854-867.

Patton D. E., Isom L. L., Catterall W. A. and Goldin A. L. 1994. The adult rat brain beta 1 subunit modifies activation and inactivation gating of multiple sodium channel alpha subunits. J. Biol. Chem. 269: 17649-17655.

Ragsdale D. S. and Avoli M. 1998. Sodium channels as molecular targets for antiepileptic drugs. Brain Res. Rev. 26: 16-28.

Ramon y Cajal S. 1902. Sobre un ganglio especial de la corteza esfeno-occipital. Trab. del Lab. de invest. Biol. Univ. Madrid 1: 189-201.

Schmitz D., Gloveli T., Behr J., Dugladze T. and Heinemann U. 1998. Subthreshold membrane potential oscillations in neurons of deep layers of the entorhinal cortex. Neuroscience 85: 999-1004.

Scoville W. B. and Milner B. 1957. Loss of recent memory after bilateral hippocampal lesions. J. Neurol. Neurosurg. Psychiat. 20: 11-21.

Smith M. R., Smith R. D., Plummer N. W., Meisler M. H. and Goldin A. L. 1998. Functional analysis of the mouse scn8a sodium channel. J. Neurosci. 18: 6093-6102.

Smith R. D. and Goldin A. L. 1998. Functional analysis of the rat I sodium channel in xenopus oocytes. J. Neurosci. 18: 811-820.

Sorensen K. E. and Shipley M. T. 1979. Projections from the subiculum to the deep layers of the ipsilateral presubicular and entorhinal cortices in the guinea pig. J. comp. Neurol. 188: 313-334.

Squire L. R. 1998. Memory systems. C. R. Acad. Sci. III 321: 153-156.

Stafstrom C. E., Schwindt P. and Crill W. E. 1982. Negative slope conductance due to a persistent subthreshold sodium current in cat neocortical neurons in vitro. Brain Res. 236, 221-226.

Stafstrom C. E., Schwindt P. C., Chubb M. C. and Crill W. E. 1985. Properties of persistent sodium conductance and calcium conductance of layer V neurons from cat sensorimotor cortex in vitro. J. Neurophysiol. 53: 153-170.

Stringer J. L. and Lothman E. W. 1992. Reverberatory seizure discharges in hippocampal-parahippocampal circuits. Exp. Neurol. 116: 198-203.

Stuart G. 1999 Voltage-activated sodium channels amplify inhibition in neocortical pyramidal neurons. Nat. Neurosci. 2: 144-150.

Suzuki W. A., Miller E. K. and Desimone R. 1997. Object and place memory in the macaque entorhinal cortex. J. Neurophysiol. 78: 1062-1081.

Swanson L. W. and Cowan W. M. 1977. An autoradiographic study of the organization of the efferent connections of the hippocampal formation in the rat. J. comp. Neurol. 172: 49-84.

Swanson L. W. and Kohler C. 1986. Anatomical evidence for direct projections from the entorhinal area to the entire cortical mantle in the rat. J. Neurosci. 6: 3010-3023.

Taylor C. P. 1993. Na+ currents that fail to inactivate. Trends Neurosci. 16: 455-460.

Taylor C. P. and Meldrum B. S. 1995. Na+ channels as targets for neuroprotective drugs. Trends Pharmacol. Sci. 16: 309-316.

van der Linden S. and Lopes da Silva F. H. 1998. Comparison of the electrophysiology and morphology of layers III and II neurons of the rat medial entorhinal cortex in vitro. Eur. J. Neurosci. 10: 1479-1489.

Van Hoesen G. W. and Pandya D. N. 1975. Some connections of the entorhinal (area 28) and perirhinal (area 35) cortices of the rhesus monkey. III. Efferent connections. Brain Res. 95: 39-59.

White J. A., Klink R., Alonso A. and Kay A. R. 1998. Noise from voltage-gated ion channels may influence neuronal dynamics in the entorhinal cortex. J. Neurophysiol. 80: 262-269.

Witter M. P. and Amaral D. G. 1991. Entorhinal cortex of the monkey: V. Projections to the dentate gyrus, hippocampus, and subicular complex. J. comp. Neurol. 307: 437-459.

Witter M. P., Groenewegen H. J., Lopes da Silva F. H. and Lohman A. H. M. 1989. Functional organization of the extrinsic and intrinsic circuitry of the parahippocampal region. Prog. Neurobiol. 33: 161-253.

Yu X. M. and Salter M. W. 1998. Gain control of NMDA-receptor currents by intracellular sodium. Nature 396: 469-474.

5.8 Figures

Fig. 1: Membrane input resistance in a typical layer V neuron plotted as a function of membrane holding potential in control (●) and 1-μM TTX (△). The inward rectification observed at voltage levels positive to about –63 mV was completely abolished by TTX, whereas the *V-I* relationship was nearly unaffected by TTX at more negative voltages. The inset shows membrane voltage responses to small hyperpolarizing current steps, applied from a holding potential of –54 mV, both in control conditions and after application of TTX.

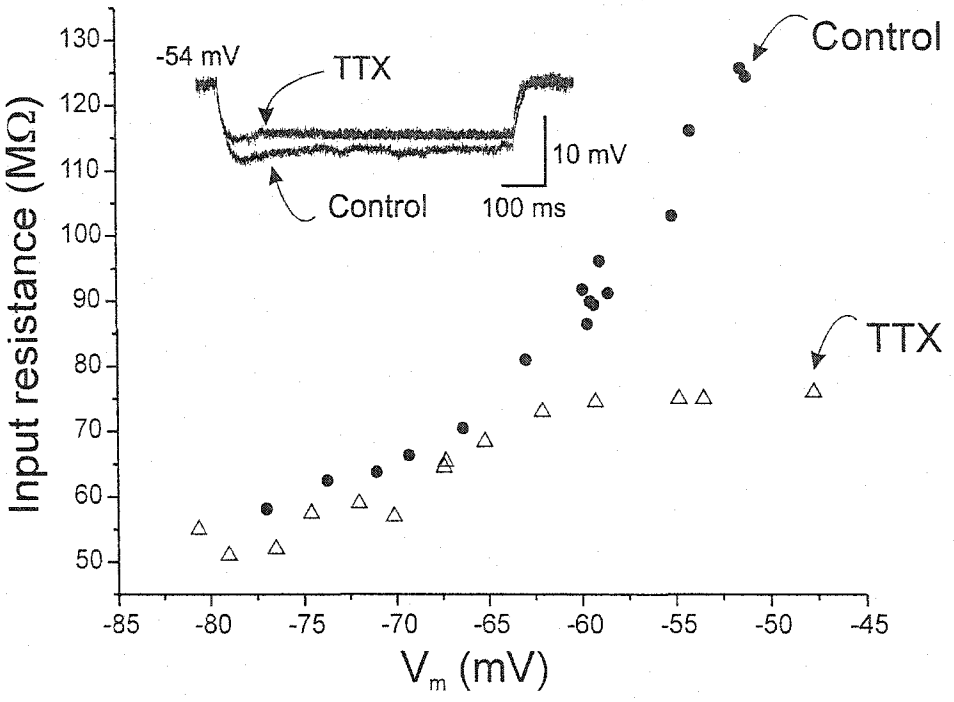
Input resistance (MΩ)
130
120
110
100
90
80
70
60
50
-85
-80
-75
-70
-65
-60
-55
-50
-45
V_m (mV)
-54 mV
TTX
Control
10 mV
100 ms
Control
TTX

Fig. 2: Neurons from layer V of entorhinal cortex exhibit a low-threshold depolarizing response. (A, B) The left panels (Control) illustrate the responses elicited in two different layer V cells by depolarizing current pulses applied from a holding potential of –70 mV (A) or –75 mV (B). Note in the cell in A that a 0.1 nA depolarizing current pulse resulted in a passive response (lower trace), while a slightly larger pulse (0.11 nA) triggered a slow regenerative potential (upper traces) that could culminate with fast action potential. Similarly, in the cell in B, a 0.1 nA depolarizing current pulse triggers a passive response while a 0.2 nA pulse elicits a slow regenerative response that culminates with a spike-doublet. The traces in the middle panels (TTX) demonstrate that in both cells the slow low-threshold regenerative responses were fully abolished by TTX (1 μM). In the right panels (Superimposed) the largest amplitude traces from control (left) and TTX (middle) have been superimposed.

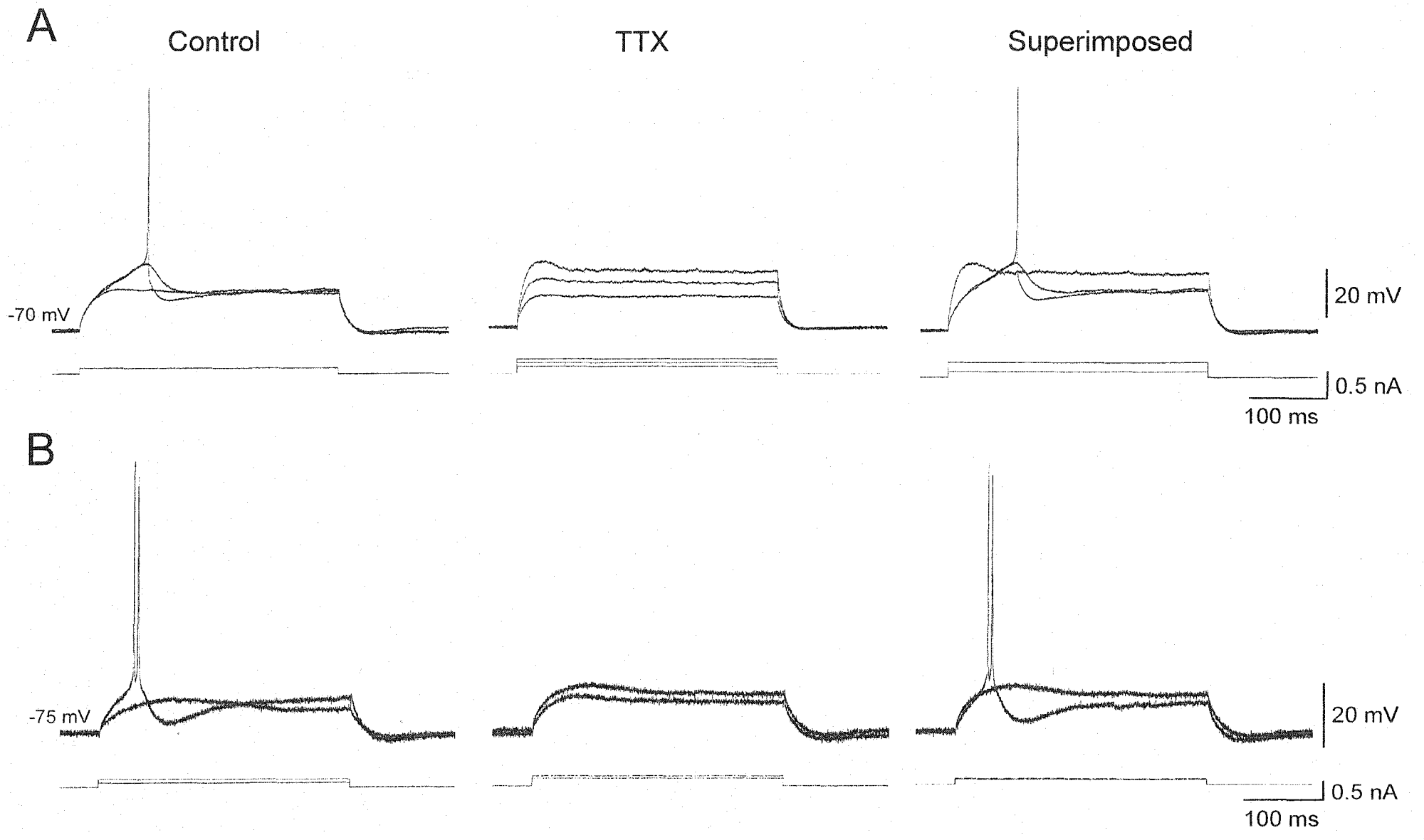
A
Control
TTX
Superimposed
-70 mV
20 mV
0.5 nA
100 ms
B
-75 mV
20 mV
0.5 nA
100 ms

Fig. 3: Layer V neurons show subthreshold oscillations in membrane potential. The top (control) trace shows oscillatory activity in a typical layer V cell held at –48 mV by injection of steady depolarizing current. In the bottom trace, these oscillations were completely blocked by 1-μM TTX.

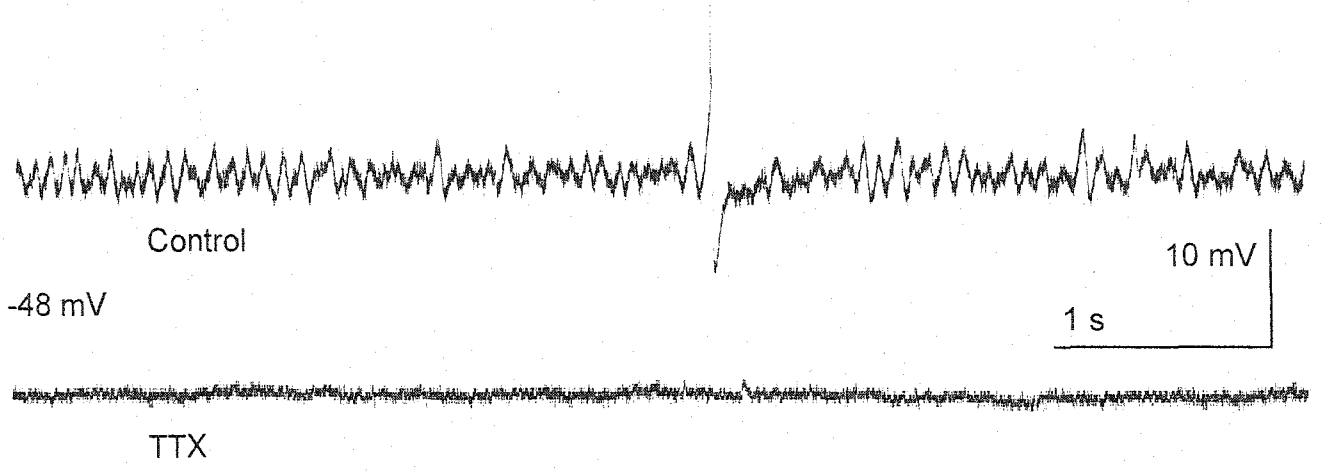
Control
10 mV
-48 mV
1 s
TTX

Fig. 4: Transient and persistent sodium currents recorded by whole-cell voltage clamp in acutely dissociated entorhinal cortex layer V neurons. (A) I_{Na} in a representative neuron. The currents were elicited by 70-ms step depolarizations to –60, –40 and –20 mV, from a holding potential of –80 mV. (B) I_{NaP} in a different neuron. The currents were evoked by 500-ms depolarizing test pulses (only steps to –50 and –20 mV are shown). The traces shown are TTX-subtracted and are displayed at a much higher gain than in panel A to reveal the small persistent current components. The inset in B shows the average, normalized conductance-voltage relationship (●) for I_{NaP}, derived from step protocols and best fitted with a Boltzmann function (smooth line) as described in the Experimental Procedures (data are from seven neurons). The Boltzmann fitting returned $V_{½}$ = –33.7 mV and k = –8.9 mV. In this and subsequent figures, error bars indicate SEMs. (C) I_{NaP} current-voltage relationship determined by applying a 50 mV/s ramp depolarization from –80 mV to +20 mV. Ramps were applied first in control conditions and then in 1-μM TTX (inset). The main panel shows the difference between control and TTX traces. (D) Average conductance-voltage relationship for I_{NaP} as obtained from ramp protocols. Current-voltage data like that shown in panel C were converted to normalized conductance-voltage relationships also as described in the Experimental Procedures. The noisy trace shows the mean from seven cells. The smooth line through the data is the best Boltzmann fit to the experimental data (see Experimental Procedures), with $V_{½}$ = –37.6 mV and k = –7.4 mV.

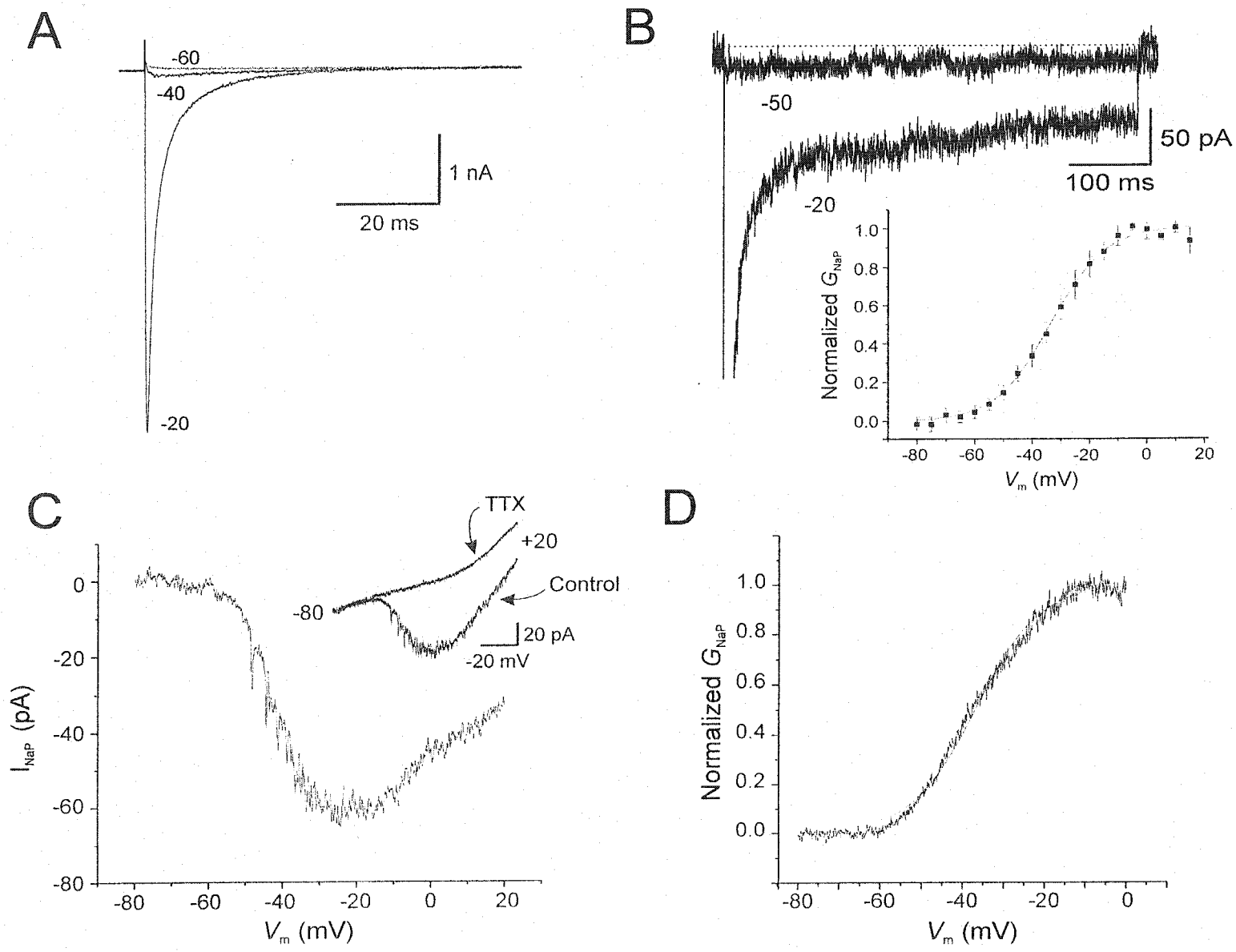
A
-60
-40
1 nA
20 ms
-20
B
-50
50 pA
100 ms
-20
Normalized G_{NaP}
1.0
0.8
0.6
0.4
0.2
0.0
-80
-60
-40
-20
0
20
V_m (mV)
C
TTX
+20
Control
-80
20 pA
-20 mV
I_{NaP} (pA)
0
-20
-40
-60
-80
-80
-60
-40
-20
0
20
V_m (mV)
D
Normalized G_{NaP}
1.0
0.8
0.6
0.4
0.2
0.0
-80
-60
-40
-20
0
V_m (mV)

Fig. 5: Activation and steady-state inactivation properties of the transient sodium current, I_{Na}. (A) The voltage protocol used for studying I_{Na} activation and steady-state inactivation (above) and sodium-current traces obtained in a representative neuron (below). (B) Average activation (■) and steady-state inactivation (●) curves for I_{Na}. Data are from 4 neurons. Activation and inactivation curves were generated as described in the Experimental Procedures. The smooth lines are best Boltzmann fits to data points, with the following values for half-activation voltage and the slope factor: activation, $V_{½}$ = –30.0 mV, k = –4.0 mV; inactivation, $V_{½}$ = –57.9 mV, k = –7.7 mV. The dotted line represents the predicted conductance-voltage curve for the conductance underlying I_{NaW}, determined from the product of the fits of the transient current activation and inactivation curves.

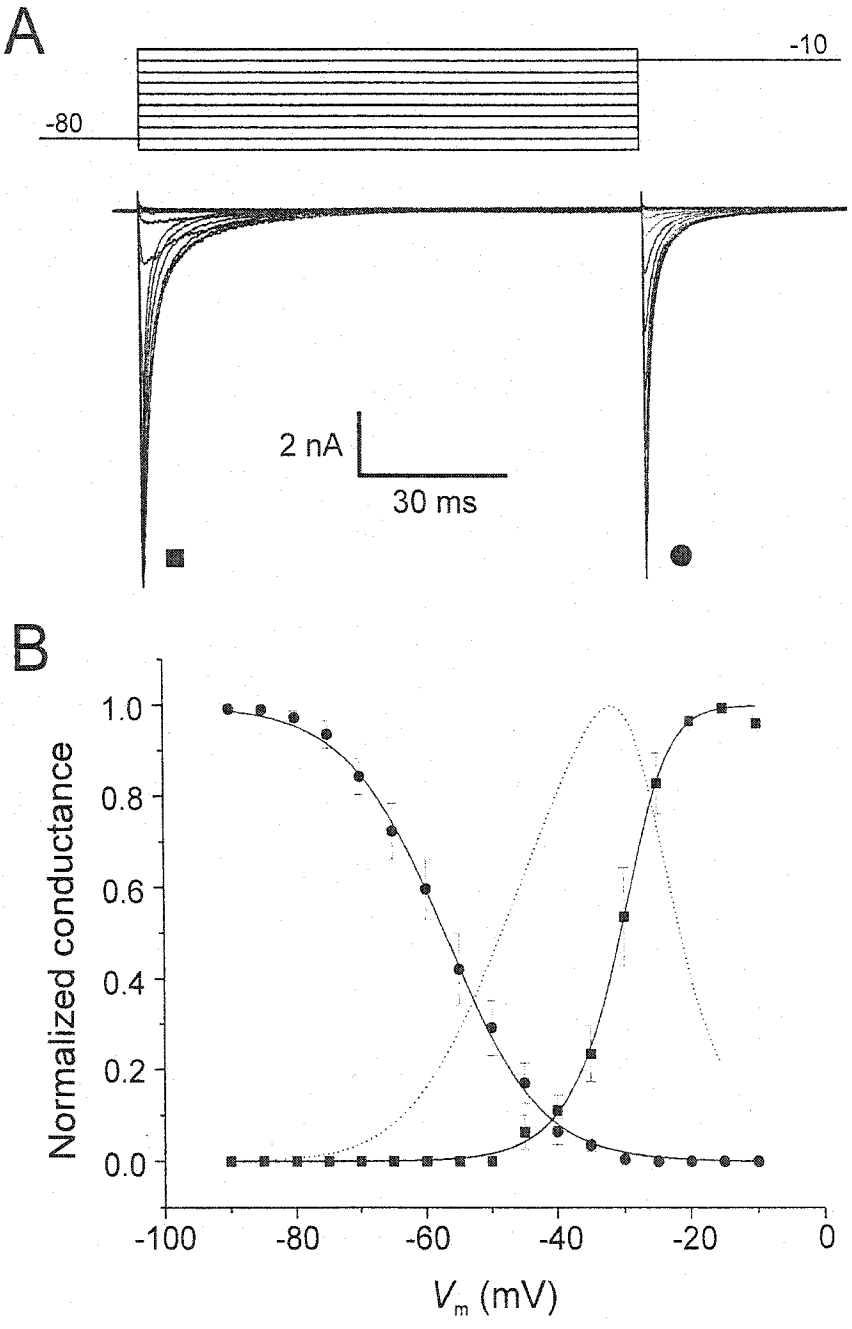
A
-10
-80
2 nA
30 ms
B
Normalized conductance
1.0
0.8
0.6
0.4
0.2
0.0
-100
-80
-60
-40
-20
0
V_m (mV)

Fig. 6: Dependence of I_{NaP} amplitude on the rate of membrane depolarization. (A) Persistent sodium currents elicited in an exemplary dissociated layer V neuron by application of ramps of variable slope (200, 66.7, and 25 mV/s). (B) Average, normalized peak amplitude of I_{NaP} in four experiments, plotted as a function of the inverse of ramp slope. The smooth line is an exponential fit with a "slope constant" of 90.9 mV/s.

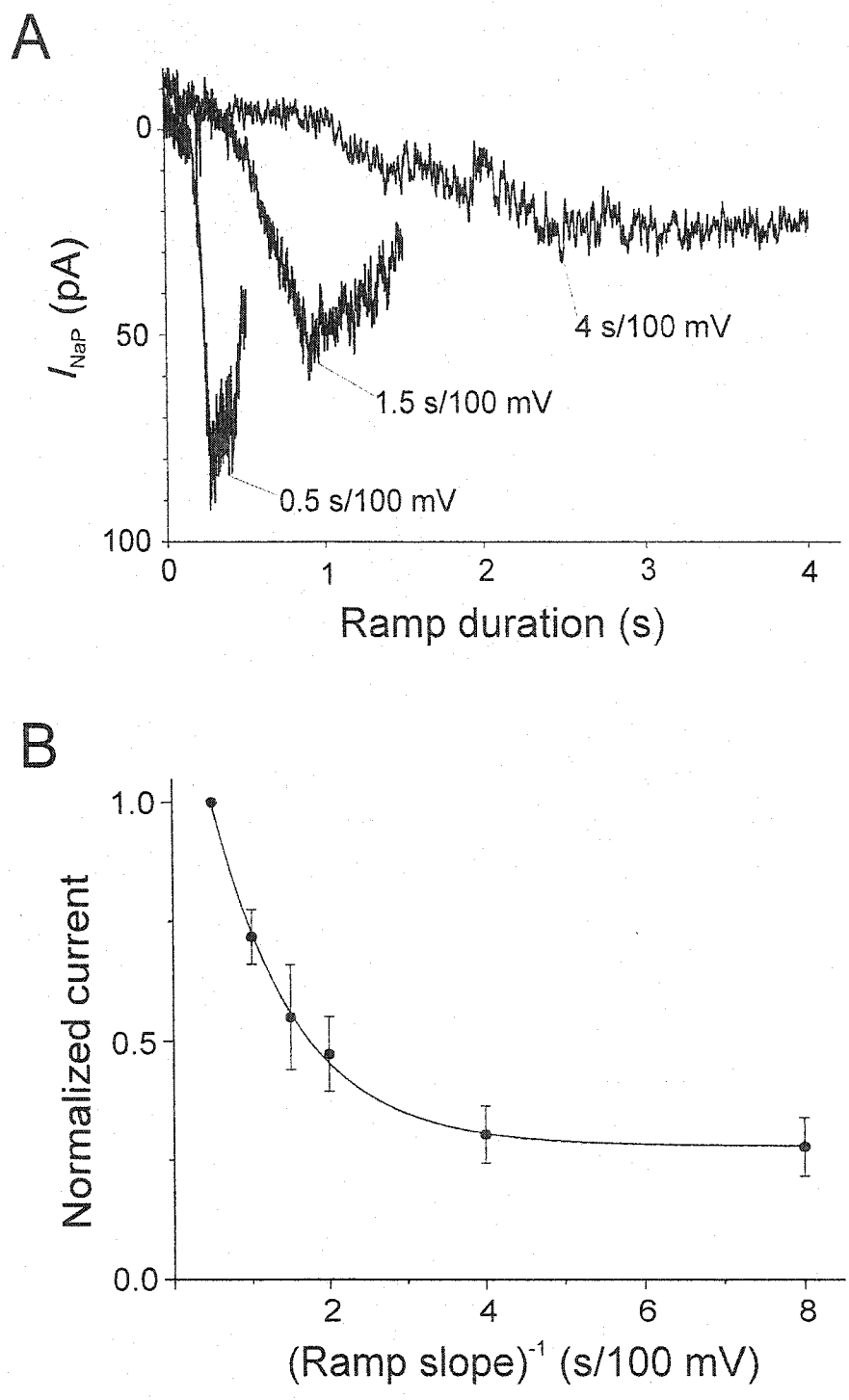
A
0
50
100
I_{NaP} (pA)
4 s/100 mV
1.5 s/100 mV
0.5 s/100 mV
0
1
2
3
4
Ramp duration (s)
B
1.0
0.5
0.0
Normalized current
2
4
6
8
(Ramp slope)$^{-1}$ (s/100 mV)

Fig 7: Plot of the variance-to-mean persistent current ratio, σ^2_I/I_{ave}, as a function of test potential, in an exemplary neuron (■). The smooth line is a fit of the data points using the equation described in the section on stationary noise analysis of the Experimental Procedures. The fit returned a single-channel conductance (g) value of 17.9 pS for this cell. An average $g = 17.5 \pm 3.6$ pS was obtained from three cells.

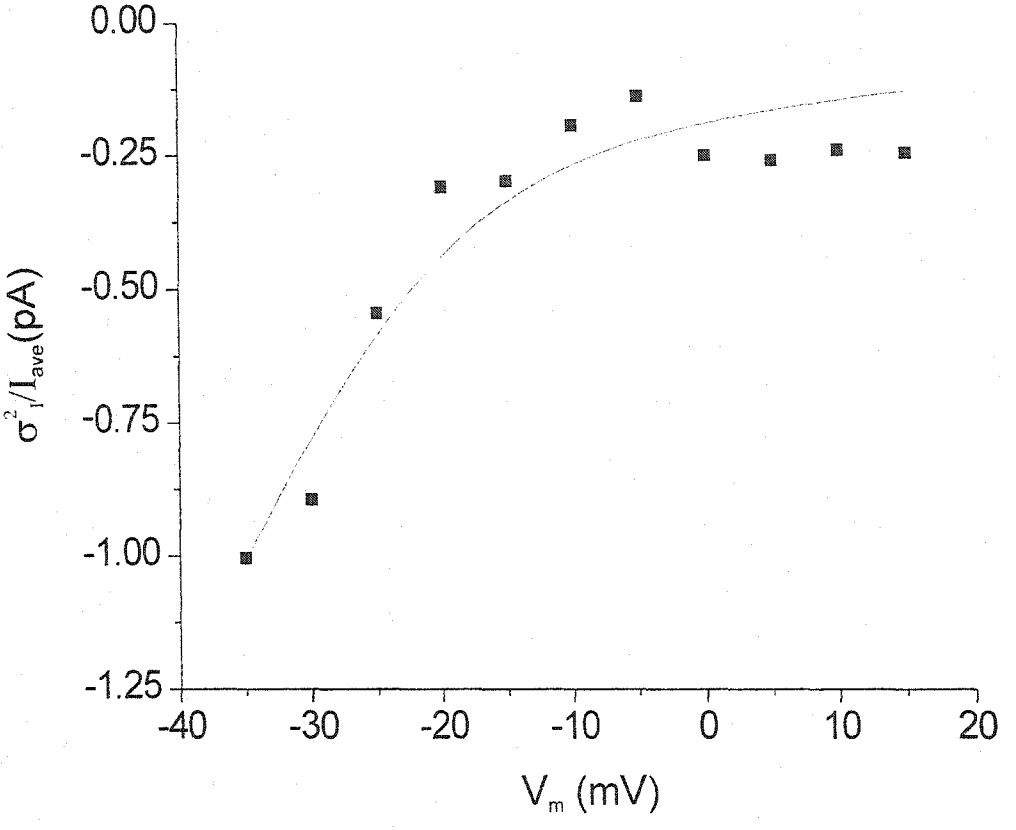
0.00
-0.25
-0.50
-0.75
-1.00
-1.25
σ^2_I/I_{ave}(pA)
-40
-30
-20
-10
0
10
20
V_m (mV)

Fig. 8: Transient and persistent sodium channel activity recorded in a cell-attached patch from a dissociated layer V neuron. (A) A typical trace elicited by step depolarization to –20 mV, from a holding potential of –100 mV. (B) Eighteen consecutive traces recorded in the same cell as in panel A. The break marks indicate that the transient current has been cut off in these traces. (C) The ensemble-average current generated by averaging the traces in panel B. The inset shows the persistent component of current at a higher gain.

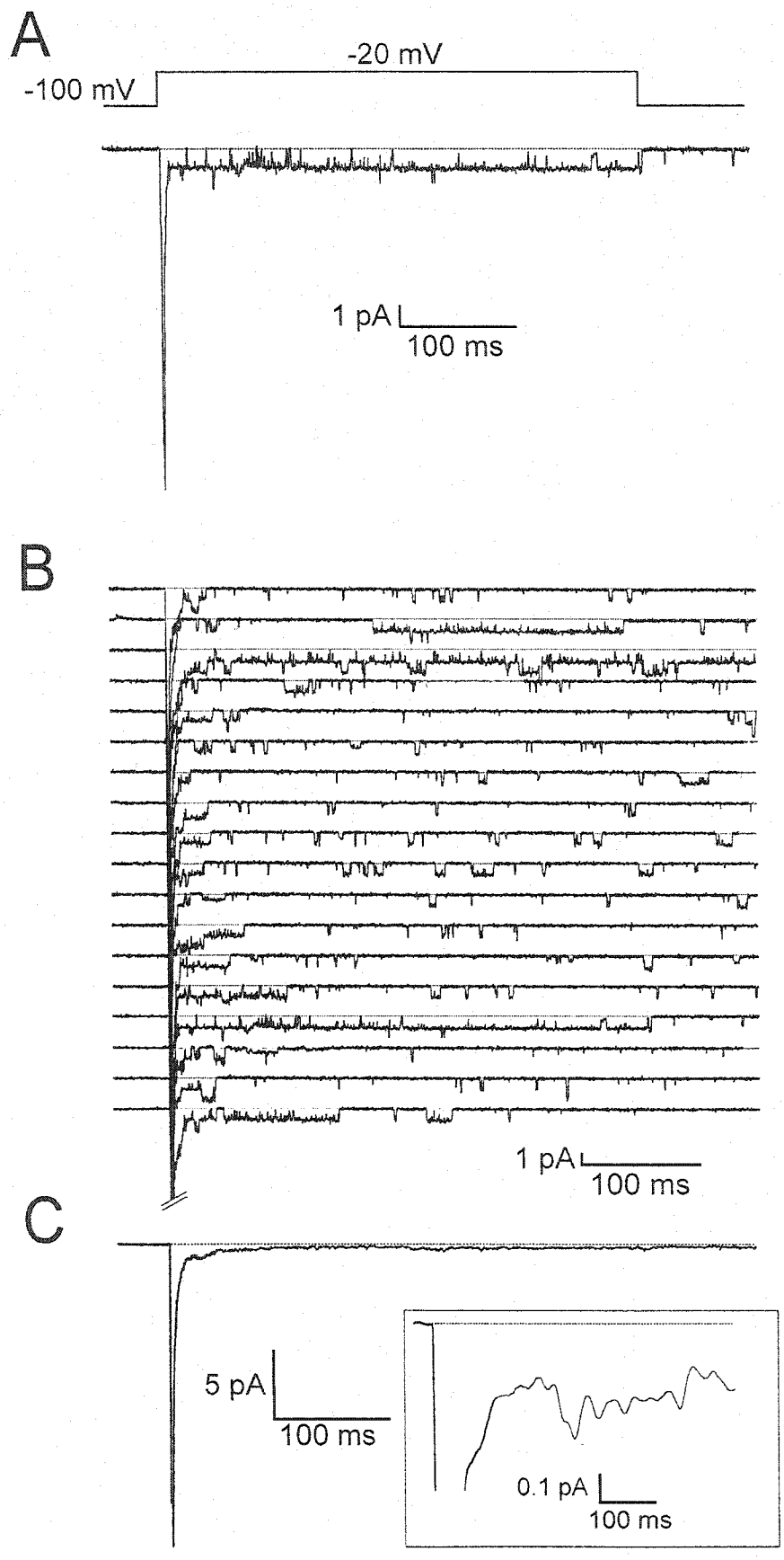
A
-20 mV
-100 mV
1 pA
100 ms
B
1 pA
100 ms
C
5 pA
100 ms
0.1 pA
100 ms

Fig. 9: A diary plot of persistent channel open probability for consecutive sweeps throughout an 8-min macropatch experiment. Each bar shows nP_0 (see Experimental Procedures) for an individual sweep. The test-potential levels are shown above the plot. Example sweeps at –30 mV and +20 mV are shown at the top of the figure.

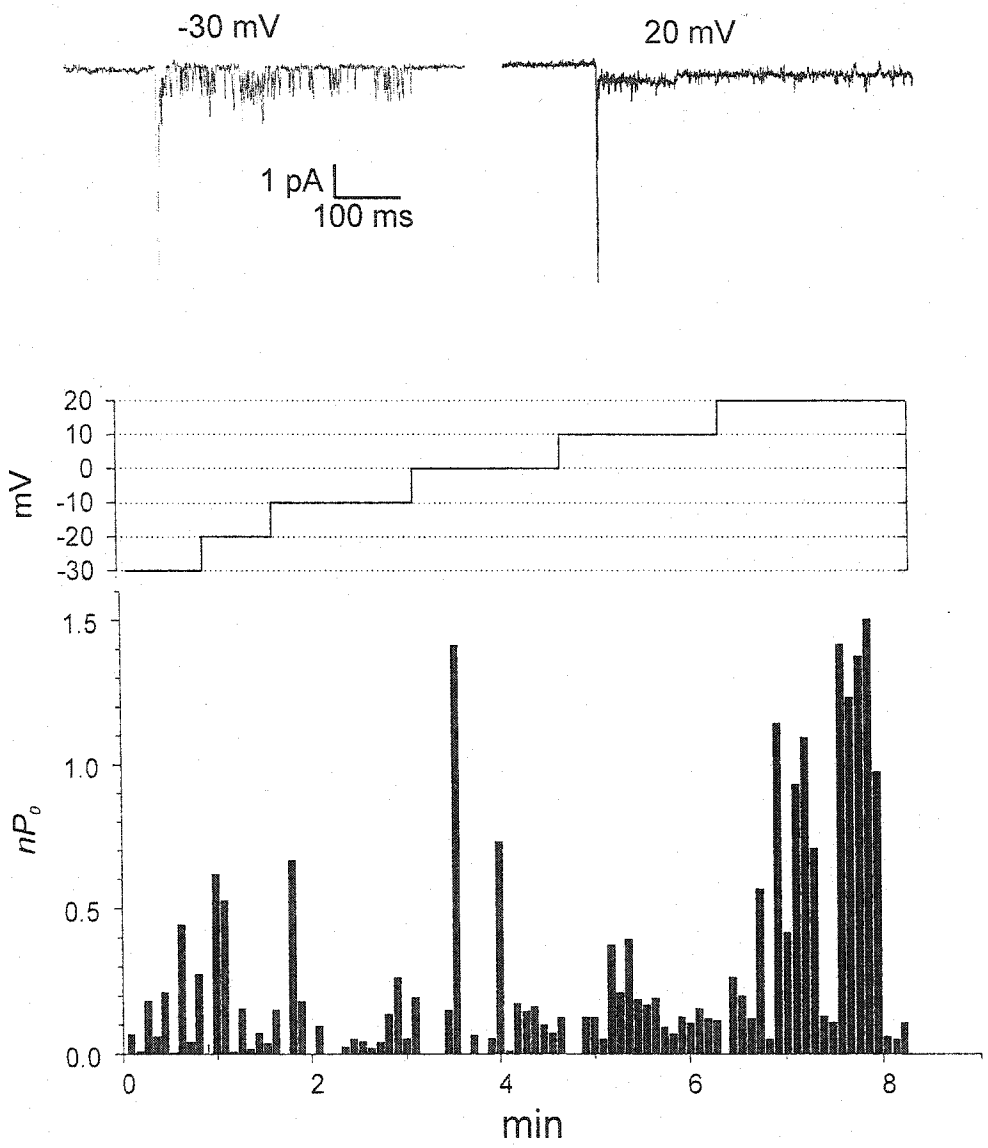
-30 mV
20 mV
1 pA
100 ms
mV
20
10
0
-10
-20
-30
nP_o
1.5
1.0
0.5
0.0
0
2
4
6
8
min

Fig. 10: Voltage-dependence of the amplitude of persistent single-channel sodium currents in a representative experiment. The straight line through the data is a linear fit with a slope of 18.9 pS.

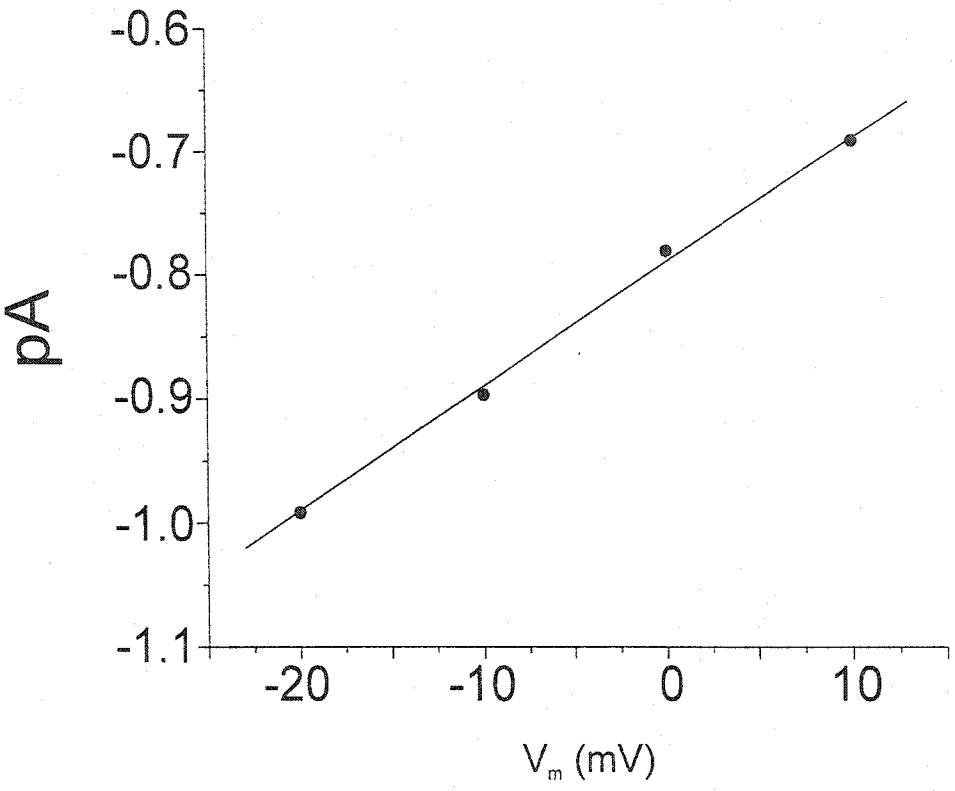
-0.6
-0.7
-0.8
-0.9
-1.0
-1.1
pA
-20
-10
0
10
V_m (mV)

Chapter Six

6. General Discussion and Conclusions

The objective of the work included in this thesis was to carry out an extensive investigation of the electroresponsive properties of neurons in the medial and lateral subdivisions of the entorhinal cortex and to attempt to establish a correlation between the electrophysiological properties of the cells and their morphological attributes. We wanted to mainly establish whether entorhinal cortex layer V neurons could follow into similar categories as those applied for the neocortex, and whether the functional differences that exist between the medial and lateral entorhinal cortex are reflected at the level of layer V cellular properties. In addition, while carrying out the morphological analysis, we adapted a technique used for processing intact embryos for whole-mount imunohistochemistry

(Kennedy et al., 1994), to avoid resectioning of the tissue during the biocytin histochemical processing procedure and therefore improve the morphological analysis of the cells. Finally, we also investigated the contribution of subthreshold Na^+ conductances to the electroresponsive behaviour of the recorded cells. Three main conclusions could be reached from the present work. First, principal cells in both the medial and lateral subdivisions of the entorhinal cortex have very similar morphological attributes and we could distinguish three main subtypes: pyramidal, horizontal and polymorphic cells. Second, each morphological principal cell subtype is comprised by an electrophysiologically heterogeneous group of cells and no major electrophysiological differences exist among the different morphological subtypes. Third, while layer V of the entorhinal cortex appears devoid of intrinsically rhythmic bursting neurons, many entorhinal layer V cells from all morphological subtypes generate rhythmic subthreshold membrane potential oscillations and a low threshold discharge which is based primarily on the presence of a "persistent" Na^+ current similar to that previously described in entorhinal cortex layer II cells.

6.1 Modified Histochemical Processing

The whole-mount histochemical technique that we adapted proved to be very helpful in carrying out the electrophysiological and morphological characterization of individual neurons. The whole-mount histochemical processing was possible because of improvement in the permeabilization steps and blocking of unspecific reactions. This made possible the clear visualization of the entire somato-dendritic structure of the cells, which, before that, was only obtained by resectioning the tissue. Most *in vitro*

electrophysiological studies make use of tissue samples around 400 μm thick. Labelling neurons in such a thick section always meant that resectioning the original sample into much thinner sections (40 - 80 μm) was important for sufficient substrate penetration during histochemical processing. This resulted in having the target cell scattered along multiple sections, which made the reconstruction and the analysis of that structure both time consuming and inaccurate. The application of the technique we used here increased the time efficiency as well as the accuracy of the acquired somatodendritic structure of the cells.

6.2 Complexity of Entorhinal Cortex Layer V Cells

The results of this study indicate that layer V of the entorhinal cortex is divided into three basic morphological principal cell types: pyramidal cells, which could also be divided into cells with large, small and star-like soma (the latter being specific only to the lateral entorhinal area), horizontal cells and polymorphic cells. Pyramidal cells had a typical pyramidal appearance with a basal dendritic tree projecting in layers V & VI and an apical dendrite projecting to and branching in layers II & I. Horizontal cells also had an apical dendrite, but it typically started bifurcating deeper in layer II than that of the pyramidal cells, and a characteristic horizontally oriented basal dendritic plexus that ran parallel to the borders of this layer. Polymorphic cells lacked a prominent dendrite that travelled into the superficial layers where it could bifurcate; instead, they were characterized by multiple equally prominent dendrites that could extend into any orientation, travel for long distances and bifurcated profusely. In this particular group,

frequently cells had dendrites that reached the angular bundle and, in some cases, even extending into the subiculum.

This clear-cut difference between the different morphological subtypes, however, did not correlate with a clear differentiation based on the electroresponsive properties we tested in these cells. Hence, cells from all morphological groups shared a number of electrophysiological properties. It has been previously shown that layer V cells in the neocortex with distinct morphologies typically displayed distinct electrophysiological characteristics (Chagnac-Amitai et al., 1990; Connors and Gutnick, 1990). Our results indicate that this is not the case for cells in layer V of the entorhinal cortex. A similar finding, i.e. cells with different morphological attributes sharing similar electrophysiological properties, has been recently reported for cells in the perirhinal cortex (Faulkner and Brown, 1999; McGann et al., 2001). In this line, it has been shown that the total functional output of a certain neuron is a function of the geometry it has along with the type, amount and distribution of ionic channels it possesses (Llinas, 1988; Mainen and Sejnowski, 1996; Johnston et al., 2000). Hence, cells with different geometry might still have similar electrophysiological profiles if they also have a differential distribution of ion channels.

The observation that EC layer V neurons with similar morphologies have quite different electrophysiological characteristics suggests that there are within the same pathway (i.e. the same cell group) multiple processing venues. If this hypothesis is correct, it would make layer V of the entorhinal cortex much more complex that previously appreciated. However, in our study, we can't rule out the possibility of further

electrophysiological segregation based on parameters we failed to distinguish. Further studies are needed to resolve this issue.

6.3 Low Threshold Firing Mechanism "Bursting" in Layer V Cells

Preliminary investigations by others (Jones and Heinemann, 1988) suggested that a subset of EC layer V neurons were rhythmically bursting cells similar to those previously observed in the neocortex (Connors et al., 1982; Connors and Gutnick, 1990) or in the hippocampal CA3 subfield (Kandel and Spencer, 1961). Neocortical layer V as well as the hippocampal CA3 subfield have been shown to be able to act as "pacemakers" for the generation of epileptogenic activity (Wong and Traub, 1983; Silva et al., 1991). It has also been postulated that intrinsic bursting activity of neocortical layer V or hippocampal CA3 neurons might be a mechanism leading to hypersynchronicity and epilepsy (Connors et al., 1982, Gutnick et al., 1982; Traub and Wong, 1982; Connors, 1984; Wong et al., 1986). Similar to neocortical layer V, entorhinal layer V is also highly epileptogenic (Jones and Heinemann, 1988; Jones and Lambert, 1990; Bragin et al., 1997; Dickson and Alonso, 1997). However, we did not find intrinsically bursting neurons as those of the neocortex or the hippocampal CA3 subfield. Nevertheless, we did find a substantial number of layer V cells that displayed a slow low-threshold firing mechanism that typically carried a single action potential or a non-repetitive spike-doublet. This type of non-repetitive "bursting" activity was the closest resemblance to what has been described for neocortical layer V cells. However, while calcium conductance has been implicated in neocortical and hippocampal intrinsic bursting (Wong and Prince, 1978;

Gutnick, 1982), the "bursting" phenomena that we encountered in EC layer V proved to be mostly sodium dependent.

6.4 Layer V Cells Posses Strong Intrinsic Rhythmic Properties

Our results indicate that layer V of the entorhinal cortex has a large number of cells that display subthreshold membrane potential oscillations in the "theta" rhythm frequency range. These oscillations were very similar to the ones previously described in layer II of this structure; however, in layer V oscillations had larger amplitude and occurred at a more positive membrane potential level than those in layer II cells (Klink and Alonso, 1993). In addition, while the voltage-sensitive persistent sodium current (I_{NAP}) and the hyperpolarization-induced depolarizing current (I_h) seem to interact to produce subthreshold oscillations in layer II (Alonso and Llinas, 1989; Dickson et al., 2000), only the former seems to play a role in the generation of oscillatory activity in layer V. Oscillations in layer V occur in cells that display moderate to little I_h and, in some cases, very strong oscillations could occur in layer V cells completely lacking I_h. It is likely that some other potassium dependent outward current is working in concert with I_{NAP} to produce the oscillatory activity in layer V. Hence, from this it seems that very similar intrinsic oscillations can be driven by different mechanisms in different neuronal populations of the same brain area.

An important issue is what might be the function of the layer V neurons subthreshold oscillations. In EC layer II cells intrinsic oscillatory activity appears clearly related to the genesis of theta rhythm (Alonso and Llinas, 1989, Dickson et al., 2000). Neurons in EC layer II are active during periods of theta rhythm, either during waking or

paradoxical sleep, and fire rhythmically and phase-locked to the "theta" waves (Mitchell and Ranck, 1980; Alonso and García-Austt, 1987). On the other hand, cells in layer V appear to be most active during slow wave activity and EC layer V generates high-frequency "ripples" in association with those of the hippocampus (Chrobak and Buzsaki, 1994; Chrobak and Buzsaki, 1996). The mechanism by which EC "ripples" are generated is not known. In the hippocampal CA1 subfield, sharp waves and their associated "ripple" activity are driven by population bursts of the CA3 pyramidal cells that cause depolarization of both CA1 pyramidal cells and interneurons that interact to generate the high-frequency "ripple" oscillation (Buzsaki, 1986; Buzsaki et al., 1992). It seems unlikely that the slow subthreshold oscillations we observed in layer V neurons may play a role in a similar high-frequency "ripple" event in the EC. In addition, as mentioned above, we did not encounter in EC layer V a subpopulation of bursting cells similar to those of CA3. It might be that the mechanism of "ripple" generation in EC layer V is quite different to that of the hippocampus and that it mostly relies on local circuit synaptic interactions. Then, the slow (theta-range) subthreshold oscillation of the layer V cells may be related (as that present in EC layer II cells) to theta-rhythm generation. In fact, a recent "in vivo" study has shown that some deep EC layer neurons (Frank et al., 2001) do fire rhythmically in association with theta rhythm activity. In addition, EC layer V is, similarly to EC layer II, densely innervated by inputs from the medial septal complex (Alonso and Kohler, 1984) which acts as a "master oscillator" for theta rhythm generation in limbic structures (Petsche et al., 1962; Andersen et al., 1979; Mitchell et al., 1982; Stewart and Fox, 1990). The intrinsic oscillations present both in EC layer II and layer V neurons may help the corresponding local networks to "resonate" to the theta rhythm

frequency commanded by the medial septum. The detailed circuit mechanisms of how this might be achieved remain to be elucidated.

6.5 Comparison Between the Medial and the Lateral Entorhinal Areas

It is well established that the entorhinal cortex is divided into a medial and lateral subdivision based on differences in cytoarchitectural and connectional distribution (reviewed in Amaral and Witter, 1995, and here in chapter one). Functional differences between the two areas have also recently been described. The microinjection of the cholinergic agonist carbachol induces fast oscillations in the MEA and not the LEA (van Der Linden et al., 1999). In addition, lesion in the medial component of the perforant path leads, in behaving rats, to impairments in place learning while lesioning the lateral component of the perforant path has no effect (Ferbinteanu et al., 1999). Our results do not reflect any major difference in terms of the intrinsic morphological and/or electrophysiological characteristics of cells within these two areas as far as layer V is concerned. The lateral entorhinal area had a new subtype ("star-like") of the pyramidal cell category, fewer cells belonging to the horizontal category and a larger abundance of cells expressing time dependent inward rectification, as compared to the medial entorhinal area. All the other morphological or electrophysiological parameters we investigated were very similar among cells in the two areas. This suggests that the differences between the two areas might be mostly related to the differences in their inputs (Burwell and Amaral, 1998) and to the operations carried out by the superficial cell layers (Blackstad, 1956; Haug, 1976; Steward, 1976; McNaughton, 1980; Witter, 1993).

6.6 Concluding remarks

The present study represents the first extensive investigation of the electrophysiological and morphological characteristics of neurons in layer V of the entorhinal cortex. We have shown that the electroresponsive properties of these cells do not fall into the same categorization as neocortical layer V cells. This is not surprising since, cytoarchitecturally, the EC is a specialized transitional cortex and this seems also reflected electrophysiologically. The main observation in this work has been that EC layer V principal neurons are nevertheless electrophysiologically quite heterogeneous and that there is no clear-cut correlation between the intrinsic electrophysiological and morphological attributes of the cells. While EC layer V has typically been considered as a relay station for the transfer of hippocampal output information to the neocortex, the complexity of its neurons suggests that more complex processing operations are conducted by the neurons in this layer. We also did not find any clear cellular electrophysiological characteristic that might explain the propensity of EC layer V to generate either the high-frequency "ripple" oscillations driven by this layer "in vivo" or the pronounced tendency towards epileptogenesis that it also displays. We suggest that this oscillatory behaviour might mostly rely on local synaptic interactions, which remain to be investigated. On the other hand, we propose that the subthreshold oscillations that we found in a large percentage of EC layer V neurons may contribute to the generation of theta-rhythm population oscillations and act as a timing device for the local processing of information.

6.7 References

Alonso A, García-Austt E. 1987. Neuronal sources of theta rhythm in the entorhinal cortex. I. Laminar distribution of theta field potentials. Exp. Brain Res. 67:493-501.

Alonso A, Kohler C. 1984. A study of the reciprocal connections between the septum and the entorhinal area using anterograde and retrograde axonal transport methods in the rat brain. J Comp Neurol 225:327-343.

Alonso A, Llinas RR. 1989. Subthreshold Na^+-dependent theta-like rhythmicity in stellate cells of entorhinal cortex layer II. Nature 342:175-177.

Amaral DG, Witter MP (1995) Hippocampal Formation. In: The rat nervous system, 2nd Edition (Paxinos G, ed): Academic Press Inc. London, pp 443-493.

Andersen P, Bland HB, Myhrer T, Schwartzkroin PA. 1979. Septo-hippocampal pathway necessary for dentate theta production. Brain Res 165:13-22.

Blackstad TW. 1956. Commissural connections of the hippocampal region in the rat, with special reference to their mode of termination. J. Comp. Neurol. 105:417-537.

Bragin A, Csicsvari J, Penttonen M, Buzsaki G. 1997. Epileptic afterdischarge in the hippocampal-entorhinal system: current source density and unit studies. Neuroscience 76:1187-1203.

Burwell RD, Amaral DG. 1998. Cortical afferents of the perirhinal, postrhinal, and entorhinal cortices of the rat. J Comp Neurol 398:179-205.

Buzsaki G. 1986. Hippocampal sharp waves: their origin and significance. Brain Res 398:242-252.

Buzsaki G, Horvath Z, Urioste R, Hetke J, Wise K. 1992. High-frequency network oscillation in the hippocampus. Science 256:1025-1027.

Chagnac-Amitai Y, Luhmann HJ, Prince DA. 1990. Burst generating and regular spiking layer 5 pyramidal neurons of rat neocortex have different morphological features. J Comp Neurol 296:598-613.

Chrobak JJ, Buzsaki G. 1994. Selective activation of deep layer (V-VI) retrohippocampal cortical neurons during hippocampal sharp waves in the behaving rat. J. Neurosci. 14:6160-6170.

Chrobak JJ, Buzsaki G. 1996. High-frequency oscillations in the output networks of the hippocampal-entorhinal axis of the freely behaving rat. J. Neurosci. 16:3056-3066.

Connors BW. 1984. Initiation of synchronized neuronal bursting in neocortex. Nature 310:685-687.

Connors BW, Gutnick MJ. 1990. Intrinsic firing patterns of diverse neocortical neurons. Trends Neurosci. 13:99-104.

Connors BW, Gutnick MJ, Prince DA. 1982. Electrophysiological properties of neocortical neurons in vitro. J Neurophysiol 48:1302-1320.

Dickson CT, Alonso A. 1997. Muscarinic induction of synchronous population activity in the entorhinal cortex. J. Neurosci. 17:6729-6744.

Dickson CT, Magistretti J, Shalinsky M, Hamam B, Alonso A. 2000. Oscillatory activity in entorhinal neurons and circuits. Mechanisms and function. Ann N Y Acad Sci 911:127-150.

Dickson CT, Magistretti J, Shalinsky MH, Fransen E, Hasselmo ME, Alonso A. 2000. Properties and role of I(h) in the pacing of subthreshold oscillations in entorhinal cortex layer II neurons. J Neurophysiol 83:2562-2579.

Faulkner B, Brown TH. 1999. Morphology and physiology of neurons in the rat perirhinal-lateral amygdala area. J Comp Neurol 411:613-642.

Ferbinteanu J, Holsinger RM, McDonald RJ. 1999. Lesions of the medial or lateral perforant path have different effects on hippocampal contributions to place learning and on fear conditioning to context. Behav Brain Res 101:65-84.

Frank LM, Brown EN, Wilson MA. 2001. A comparison of the firing properties of putative excitatory and inhibitory neurons from CA1 and the entorhinal cortex. J Neurophysiol 86:2029-2040.

Gutnick MJ, Connors, B.W. and Price, D. 1982. Mechanisms of neocortical epileptogenesis in vitro. J. Neurophysiol. 48:1321-1335.

Haug FM. 1976. Sulphide silver pattern and cytoarchitectonics of parahippocampal areas in the rat. Special reference to the subdivision of area entorhinalis (area 28) and its demarcation from the pyriform cortex. Adv Anat Embryol Cell Biol 52:3-73.

Johnston D, Hoffman DA, Magee JC, Poolos NP, Watanabe S, Colbert CM, Migliore M. 2000. Dendritic potassium channels in hippocampal pyramidal neurons. J Physiol 525 Pt 1:75-81.

Jones RSG, Heinemann V. 1988. Synaptic and intrinsic responses of medial entorhinal cortical cells in normal and magnesium-free medium "in vitro". J. Neurophysiol. 59:1476-1496.

Jones RSG, Lambert JDC. 1990. Synchronous discharges in the rat entorhinal cortex *in vitro*: site of initiation and the role of excitatory amino acid receptors. Neuroscience 34:657-670.

Kandel ER, Spencer WA. 1961. Electrophysiology of hippocampal neurons. II. After-potentials and repetitive firing. J. Neurophysiol. 24:243-259.

Kennedy TE, Serafini T, de la Torre JR, Tessier-Lavigne M. 1994. Netrins are diffusible chemotropic factors for commissural axons inthe embryonic spinal cord. Cell 78:425-435.

Klink R, Alonso A. 1993. Ionic mechanisms for the subthreshold oscillations and differential electroresponsiveness of medial entorhinal cortex layer II neurons. J. Neurophysiol. 70:144-157.

Llinas RR. 1988. The intrinsic electrophysiological properties of mammalian neurons: Insights into central nervous system function. Science 242:1654-1664.

Mainen ZF, Sejnowski TJ. 1996. Influence of dendritic structure on firing pattern in model neocortical neurons. Nature 282:363-366.

McGann JP, Moyer JR, Jr., Brown TH. 2001. Predominance of late-spiking neurons in layer VI of rat perirhinal cortex. J Neurosci 21:4969-4976.

McNaughton BL. 1980. Evidence for two physiologically distinct perforant pathways to the fascia dentata. Brain Res 199:1-19.

Mitchell SJ, Ranck JBJ. 1980. Generation of theta rhythm in medial entorhinal cortex of freely moving rats. Brain Res. 189:49-66.

Mitchell SJ, Rawlins JNP, Steward O, Olton DS. 1982. Medial septal area lesions disrupt theta rhythm and cholinergic staining in medial entorhinal cortex and produce impaired radial arm maze behavior in rats. J. Neurosci. 2:292-302.

Petsche H, Stumpf C, Gogolak G. 1962. The significance of the rabbit's septum as a rely station between the midbrain and the hippocampus. I. The control of hippocampus arousal activity by the septum cells. Electroenceph. Clin. Neurophysiol. 19:25-33.

Silva LR, Amitai Y, Connors BW. 1991. Intrinsic oscillations of neocortex generated by layer 5 pyramidal neurons. Science 251:432-435.

Steward O. 1976. Topographic organization of the projections from the entorhinal area to the hippocampal formation of the rat. J Comp Neurol 167:285-314.

Stewart M, Fox SE. 1990. Do septal neurons pace the hippocampal theta rhythm? Trends Neurosci. 13:163-168.

Traub RD, Wong RK. 1982. Cellular mechanism of neuronal synchronization in epilepsy. Science 216:745-747.

van Der Linden S, Panzica F, de Curtis M. 1999. Carbachol induces fast oscillations in the medial but not in the lateral entorhinal cortex of the isolated guinea pig brain. J Neurophysiol 82:2441-2450.

Witter MP. 1993. Organization of the entorhinal-hippocampal system: a review of current anatomical data. Hippocampus 3 Spec No:33-44.

Wong RK, Prince DA. 1978. Participation of calcium spikes during intrinsic burst firing in hippocampal neurons. Brain Res 159:385-390.

Wong RK, Traub RD. 1983. Synchronized burst discharge in disinhibited hippocampal slice. I. Initiation in CA2-CA3 region. J Neurophysiol 49:442-458.

Wong RK, Traub RD, Miles R. 1986. Cellular basis of neuronal synchrony in epilepsy. Adv Neurol 44:583-592.